Armi Tiihonen

The effect of electrolyte purification on performance and long-term stability of dye-sensitized solar cells

School of Science

Thesis submitted for examination for the degree of Master of Science in Technology.

Espoo 24.9.2013

Thesis supervisor:

Prof. Peter Lund

Thesis advisor:

D.Sc. (Tech.) Kati Miettunen

Aalto University
School of Science

AALTO UNIVERSITY
SCHOOL OF SCIENCE

ABSTRACT OF THE
MASTER'S THESIS

Author: Armi Tiihonen

Title: The effect of electrolyte purification on performance and long-term stability of dye-sensitized solar cells

Date: 24.9.2013 Language: English Number of pages:8+80

Department of Applied Physics

Professorship: Advanced Energy Systems Code: Tfy-56

Supervisor: Prof. Peter Lund

Advisor: D.Sc. (Tech.) Kati Miettunen

The two main objectives of this thesis were to study if performance or long-term stability of dye solar cells increase as a result of electrolyte material purification. Not only the combined effect of the purification of all the electrolyte materials has been examined but also the effect of the purification of each compound has been compared. Furthermore, the specific reasons for cell degradation have been investigated where possible.

The overall degradation rate of the test solar cells during the aging test was faster than expected and thus the origin of this fast aging formed as the third main research question. Ultraviolet light was detected to be a very likely reason for the fast degradation and thus, additionally the effect of ultraviolet light on the cell aging has been discussed.

The secondary object of this study was to determine the proper procedures for performing long aging studies in the future. This task included the assessment of useful tests and the effects of unavoidably varying light intensity during the aging tests. Also statistical tests were introduced to the analysis of the results of the aging studies.

This study showed that the purification of electrolyte solvent does not affect the initial performance of the dye solar cells but increases the cell lifetime. The other electrolyte components were not detected to have any statistically significant effect on either cell lifetime or initial performance. The aging mechanism was discovered to be electrolyte bleaching, i.e. the consumption of charge carrying iodine in the electrolyte. The bleaching was clearly fastest in the cells that contained unpurified electrolyte solvent but the mechanism was present in all the cells. Additionally, the exposure to even relatively small amounts of ultraviolet light seemed to affect detrimentally cell lifetime through accelerated bleaching.

Keywords: Dye solar cells, stability, electrolyte, electrolyte bleaching, UV light

AALTO-YLIOPISTO
PERUSTIETEIDEN KORKEAKOULU

DIPLOMITYÖN
TIIVISTELMÄ

Tekijä: Armi Tiihonen

Työn nimi: Elektrolyytin puhdistamisen vaikutukset väriaineaurinkokennojen suorituskykyyn ja pitkän aikavälin stabiiliuteen

Päivämäärä: 24.9.2013 Kieli: Englanti Sivumäärä:8+80

Teknillisen fysiikan laitos

Professuuri: Energiatieteet Koodi: Tfy-56

Valvoja: Prof. Peter Lund

Ohjaaja: TkT Kati Miettunen

Työn kahtena päätavoitteena oli selvittää, vaikuttaako väriaineaurinkokennon elektrolyytin materiaalien puhdistaminen myönteisesti väriaineaurinkokennon suorituskykyyn tai elinikään. Työssä ei tarkasteltu ainoastaan kaikkien elektrolyyttimateriaalien yhtäaikaisen puhdistamisen vaikutusta aurinkokennoihin, vaan eriteltiin myös yksittäisten elektrolyyttikomponenttien puhdistamisen vaikutukset. Lisäksi tutkittiin kennon ikääntymistä aiheuttavia tekijöitä.

Tutkimuksessa tehdyn ikääntymismittauksen aikana kaikki testikennot ikääntyivät odotettua nopeammin, minkä vuoksi työn kolmanneksi päätavoitteeksi muodostui havaitun nopean ikääntymisen aiheuttajan löytäminen. Lopulta ultraviolettivalon todettiin olevan erittäin todennäköinen syy ilmiölle. Siksi työssä on käsitelty myös ultraviolettivalon vaikutuksia väriaineaurinkokennojen ikääntymiseen.

Työn toissijaisena tavoitteena oli määrittää väriaineaurinkokennojen pitkäaikaisiin ikääntymistutkimuksiin soveltuvat menettelytavat. Työosuus sisälsi ikääntymistutkimuksiin soveltuvien mittausmenetelmien määrittämisen ja sen arvioimisen, missä määrin tutkimuksen aikana väistämättä jonkin verran vaihteleva valointensiteetti vaikuttaa tutkimustulokseen. Myös sopivia tapoja hyödyntää tilastollisia menetelmiä ikääntymistutkimuksen tulosten arvioimisessa on käsitelty.

Työssä havaittiin, että elektrolyytin liuottimen puhdistaminen ei vaikuta tuoreen kennon suorituskykyyn, mutta kasvattaa selvästi kennon elinikää. Muilla elektrolyytin ainesosilla ei havaittu olevan tilastollisesti merkittävää vaikutusta kennon elinikään eikä alkuperäiseen suorituskykyyn. Ikääntymisen havaittiin tapahtuvan elektrolyytin vaalentumisen, eli elektrolyytin varauksenkuljettajana toimivan jodin määrän pienenemisen, kautta. Vaalentuminen oli nopeinta oli puhdistamatonta elektrolyytin liotinta sisältävissä kennoissa, mutta havaittavissa kaikissa testikennoissa. Lisäksi ultraviolettivalon todettiin pieninäkin altistuksina nopeuttavan kennojen ikääntymistä.

Avainsanat: Väriaineaurinkokennot, stabiilisuus, elektrolyytti, elektrolyytin vaaleneminen, UV-valo

Preface

I wish to thank my instructor, D.Sc. Kati Miettunen, for inspiring ideas and numerous drawing sessions during the preparation of this thesis. I am also grateful to my supervisor, Prof. Peter Lund for the possibility to work at New Energy Technologies group at Aalto University. Working here has been interesting and teachful.

I thank also D.Sc. Denys Mavrynsky for purifying the electrolyte materials and advices regarding chemistry and laboratory work, M.Sc. Sabiner Rendon for her expertise in LC-MS measurements, Mr. Sampo Kaukonen for performing Raman measurements, and Lic.Sc. Eeva Vilkkumaa for kind advices regarding statistical analysis, Mr. Sami Jouttijärvi and Mr. Sampo Kaukonen are thanked for enabling my holidays by helping in weekly measurements, and D.Sc. Imran Asghar I thank for nice discussions.

MIDE (FerroPV) and Akademy of Finland (SOLID) made this project possible by offering the funding for the study.

Last but definitely not least, I thank my family and friends for support and taking care that I have also a lot of other nice things in my life than work. As the written part of this work was mainly put together during a short period of time, I address special thanks to Helmi for spurring me with supportive text messages, and to Antti for dinners and flowers brought to sweeten the long nights of writing.

Otaniemi, 24.9.2013

Armi Tiihonen

Contents

Abstract ii

Abstract (in Finnish) iii

Preface iv

Sisällysluettelo v

Symbols and abbreviations vii

1 Introduction 1

2 Background 3
2.1 Dye-sensitized solar cell . . . 3
2.2 Causes of degradation in dye-sensitized solar cells . . . 6
2.3 Measurement techniques . . . 8
2.3.1 IV measurements . . . 8
2.3.2 Incident-photon-to-collected-electron efficiency and transmittance tests . . . 10
2.3.3 Electrochemical impedance spectroscopy . . . 10
2.3.4 Liquid chromatography - mass spectrometry . . . 14
2.3.5 Raman spectroscopy . . . 15
2.3.6 Cell photographing . . . 16

3 Materials and methods 18
3.1 Material purification . . . 18
3.2 Cell preparation . . . 19
3.3 Aging tests . . . 21
3.4 Simple statistical methods in analysis of aging data . . . 24

4 Results 26
4.1 Cells . . . 26
4.2 Aging times and dates . . . 26
4.3 IV measurement results . . . 27
4.4 Transformation of IV curves during the aging . . . 31
4.5 IV measurements as a function of light intensity . . . 31
4.6 Results of impedance measurement results performed in dark . . . 33
4.7 Results of impedance measurements performed under illumination . . . 37
4.8 Quantum efficiency measurements . . . 42
4.9 Liquid chromatography - mass spectroscopy measurements . . . 45
4.10 Raman spectroscopy . . . 47
4.11 Cell photographing . . . 50
4.11.1 Connection of ultraviolet light and electrolyte bleaching . . . 52
4.11.2 Estimation of iodine concentration in the cells during the aging 52
4.11.3 Comparison of photographing results to IV aging data . . . 54

5 Summary **56**

References **58**

Appendices **64**

A Relative IV data during the aging **64**

B Illumination spectra of AM 1.5G and light soaking lamps **80**

Symbols and abbreviations

Symbols

β	Symmetry parameter depending on the catalyst
$c_{I_3^-,eq}$	Tri-iodide equilibrium concentration
$c_{I^-,eq}$	Iodide equilibrium concentration
$c_{I_3^-}$	Tri-iodide concentration
C_{CE}	Charge transfer capacitance at the counter electrode - electrolyte interface
C_{CO}	Contact capacitance
C_{μ}	Photoelectrode capacitance
C_{SU}	Charge transfer capacitance between the substrate and the electrolyte
d	Distance
$D_{I_3^-}$	Diffusion constant of I_3^-
f	Frequency
F	Faraday's constant
FF	Fill factor
E_0	Constant electric field
η	Cell efficiency
η_{COL}	Electron collection efficiency
η_{INJ}	Electron injection efficiency
η_{IPCE}	Incident-photon-to-collected-electron efficiency
η_{LH}	Light harvesting efficiency
η_{REG}	Dye regeneration effciency
ϵ_0	Permittivity
i_{AC}	alternating current
I_{lim}	Limiting current of the cell
I_{mpp}	Current of the maximum power point of the cell
I_{sc}	Short circuit current
k	Rate constant for the charge transfer reaction at the counter electrode
k_B	Boltzmann constant
χ	Susceptibility
m/z	Mass-charge ratio
ω	Angular frequency
ω_i	Frequency of the elementary excitation
ω_0	Angular frequency of incident light
P_{ideal}	Power of cell without any losses
P_{in}	Power of the incident light
P_{max}	Maximum power of the cell
P_s	Polarization
R_{CO}	Contact resistance
R_{CE}	Charge transfer resistance at the counter electrode - electrolyte interface
$R_{CE,0}$	Charge transfer resistance at the counter electrode - electrolyte interface at 0 V
R_D	Diffusion resistance of the electrolyte
R_s	Series resistance of the cell
R_T	Transport resistance in the semiconductor film
R_{PE}	Photoelectrode resistance
R_{REC}	Charge recombination resistance including the dark current
R_{SU}	Charge transfer resistance between the substrate and the electrolyte

t	time
T	Temperature
τ	Electron lifetime
U	Acceleration voltage
V_{AC}	Alternating current voltage component
V_{cell}	voltage over the cell
V_{DC}	Direct voltage component
V_{mpp}	Voltage of the maximum power point of the cell
V_{oc}	Open circuit voltage
V_{PE}	Voltage over the photoelectrode
Z	impedance of the cell
Z_D	Mass transport impedance at the counter electrode
X	Contribution of collective excitations to susceptibility

Abbreviations

ANOVA	one-way analysis of variances
CPE	Constant phase element
DSSC	Dye-sensitized solar cell
EIS	Electrochemical impedance spectroscopy
GuSCN	Guanidinium thiocyanate
HOMO level	Highest occupied molecule orbital energy level
IPCE	Incident-photon-to-collected-electron measurement
IV measurement	Current-voltage measurement
I_3^-	Tri-iodide
I^-	Iodide
I_2)	Iodine
LC-MS	Liquid chromatography - mass spectrometry
LUMO level	Lowest unoccupied molecule orbital level
MPN	3-methoxypropionitrile
NMBI	1-methyl-benzimidazole
N3	Cis-bis(isothiocyanato)-bis(2,20-bipyridyl-4,40-dicarboxylato)-ruthenium(II) dye
$TiCl_4$	Titanium tetrachloride
N719	Cis-bis(isothiocyanato)-bis(2,20-bipyridyl-4,40-dicarboxylato)-ruthenium(II)bis-tetrabutylammonium dye
PMII	1-propyl-3-methylimidazolium iodide
SCN	Thiocyanate
TBME	Tert-butyl methyl ether
TBP	4-tert butyl pyridine
TCO	Transparent conducting oxide
THF	Tetrahydrofuran
TiO_2	Titanium dioxide

1 Introduction

Solving the energy production problems is a debated subject at the moment. Resiling from the fossil fuels should be done quickly but totally satisfactory compensatory technologies are still missing. They should be safe, affordable, efficient, and clean, which is, after all, quite a lot of demands. Solar electricity is one of the promising options. The silicon solar cells are the most commonly used type of solar cells. However, the cost of silicon cells remains high mainly because the manufacturing process of the cells is energy-intensive and some relatively costly materials are needed in the process [1]. Also, recycling valuable or toxic panel materials increases the cost of silicon solar cells [2].

Dye-sensitized solar cells (DSSC) are hoped to solve these problems. They can be made of non-toxic materials which are easily recyclable, have wide application area and the large-scale production is quite profitable. They are also efficient: 14.14 % efficiency record for DSSCs has been achieved [3]. At the moment the main challenge is the cell stability. The structure of DSSC is quite complicated and unfortunately the components tend to age when the DSSC is exposed to light, humidity, and extreme temperatures [4–9]. Naturally, there are plenty of applications for solar cells and some of them only require lifetime of few years. Still, the ultimate goal of integration of dye solar cells into buildings requires that dye solar cells will stand 20 years of exposure to natural light without substantial aging.

Usage of highly pure materials are regarded as an essential step in preparation of most efficient cells [10]. Material purification has additionally been proposed to increase the stability of the cells [11]. The reported data related to the purity of materials is not, however, conclusive, in particular for individual materials. From industrial point of view, material purification increases production costs of the cells. Thus the necessity of material purification should be studied carefully, just like any step that increases the complexity of the production.

The main objective of this study is to investigate if cell stability and efficiency increase as a result of the electrolyte material purification. Not only the effect of purification of all the electrolyte materials has been studied but also the effect of each compound has been compared. Furthermore, the specific reasons for cell degradation have been investigated when possible.

Aging issues have been a target of intensive research in dye solar cell field lately. Test cells are usually prepared at least partly by handwork in laboratories. In aging studies, the aging process is often accelerated by continuous, sunlight-simulating illumination, elevated temperatures or high air humidity. Still, a typical duration

for an aging study is 1000 hours that corresponds to approximately 1 year operation in sun light in European latitudes [12]. Long duration makes it challenging to perform aging studies and treat the results because the effects of variations in test conditions accumulate during the whole test period. Asghar et al. noted in their review of stability studies on dye solar cells that the aging test procedures in the field of dye solar cell research vary a lot [13]. It is still quite common in the field to utilize quite few tests, mainly IV curve measurements in aging studies, or to test the cells only at the beginning and end of the aging [6–8, 14, 15]. Additionally, statistical treatment of the results is very rare.

Thus, the secondary object of this study is to determine the optimal way of performing long aging studies in the future, i.e. to investigate the effect of light intensity variation during the aging study, sufficient amount of test cells and aging tests that are useful from perspective of aging studies. In this study, the cells are analysed by a multitude of different tests: IV tests, impedance measurements, cell photographing, quantum efficiency tests, Raman spectroscopy and a combination of liquid chromatography and mass spectrometry. Automatic IV curve and impedance measurements are also performed continuously to monitor the trends in cell degradation. Additionally, statistical methods (Pierce's criterion, regression analysis and one-way analysis of variances) are utilized in analysis of the results.

2 Background

A dye-sensitized solar cell (DSSC) is a electrochemical device that converts sunlight to electricity. Next, the main principles of solar cell structure and operation, and the aging tests utilized in this thesis, are introduced.

2.1 Dye-sensitized solar cell

The schematic structure of a DSSC is shown in Fig. 1. As the picture shows, the photoelectrode is layered on top of the conducting substrate, typically glass with a transparent conductive oxide (TCO) layer. The photoelectrode consists of semiconductor nanoparticles, e.g. titanium dioxide (TiO_2), and dye that is adsorbed on the surface of the nanoparticles. The counter electrode consists of catalyst layer, here platinum (Pt), on top of another conducting substrate. Between the both electrodes is the electrolyte that is typically liquid containing I_3^-/I^- redox couple. The electrolyte is also adsorbed in the photoelectrode because the nanoparticle film is porous.

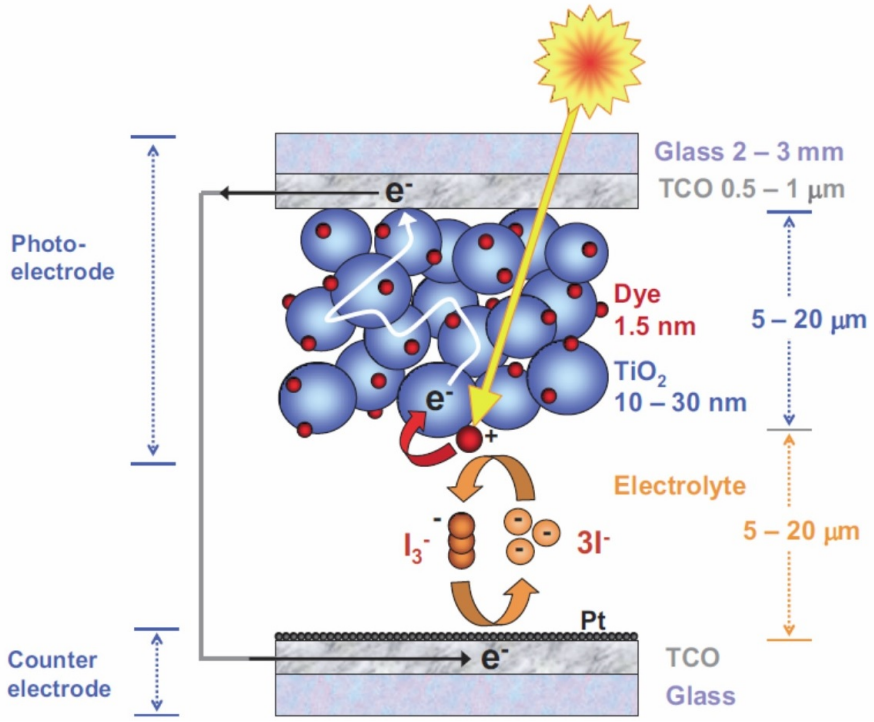

Figure 1: DSSC structure schematics [16].

The operating principle of the DSSC is shown in Fig. 2. Incoming photons are absorbed by the dye. Consequently, the dye is excited to a higher energy level.

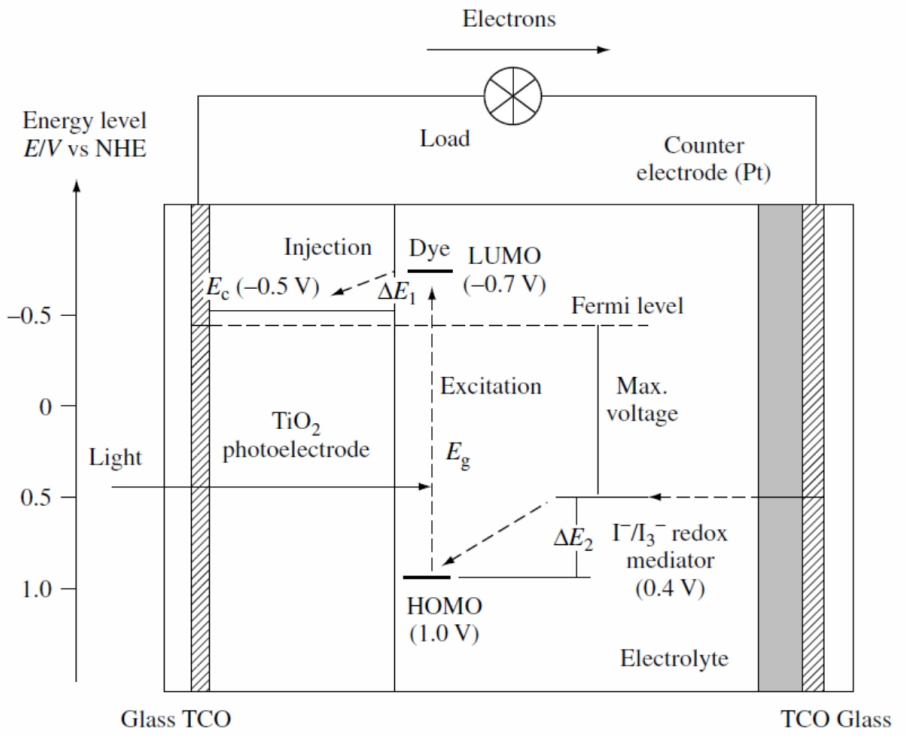

Figure 2: Energy level diagram of a DSSC [17].

The excited state of the dye is at higher energy level than the conduction band of TiO_2 so the excited electron moves into TiO_2 and is diffused to the outermost side of the photoelectrode. From there the electron is carried to the counter electrode through an external load. Meanwhile the dye which has become positively charged, recovers itself to the ground state by accepting an electron from the electrolyte. The oxidized electrolyte diffuses toward the counter electrode and recovers by accepting an electron that has arrived there from the photoelectrode through an external load. The mediators of this electrolyte redox reaction are usually I^- ions. They oxidize to I_3^- when they donate an electron to the dye. The reduction reaction back to I^- is catalyzed at the counter electrode [17]:

$$3I^- \leftrightarrow I_3^- + 2e^-. \tag{1}$$

The loop has finally closed and, in principle, no chemical transformation has happened. In practice some transformations occur and reduce the cell performance during the time. This is called the aging or degradation of the cell, that is discussed more comprehensively in chapter 2.2.

The DSSC operation is dependent of the energy level compatibility of the materials that are used. The band gap between the conductivity and ground level of

the semiconductor is so large that the incoming photons cannot lift electrons to the conductivity band. But, like Fig. 2 shows, the dye is normally selected so that the band gap between the ground state (HOMO, the highest occupied molecule orbital energy level) and the excited state (approximately the LUMO level, the lowest unoccupied molecule orbital level) is small enough for electron excitation by visible light. The efficiency of this mechanism is called light-harvesting efficiency η_{LH}. In principle, the photocurrent in the cell increases when the distance between HOMO and LUMO levels of the dye decreases because lower energy photons are also adsorbed. There is a second demand, though: the LUMO level of the dye must be sufficiently higher than the conductivity band of TiO_2 to make the electron drop swiftly into the conductivity band. Additionally, large enough difference between the dye ground level and semiconductor conductivity level ensures that the excited electron drops much more likely to the conduction band than relaxes back to the dye ground state. Again, the reason why the iodine donates an electron to the dye is the energy level difference. The dye ground state must be situated at the lower energy level than the iodine to force the electron to move readily into the dye. On the other hand, the energy level of electrolyte redox couple should be low in order to maximize the cell voltage. Maximum cell voltage (without losses from e.g. current collector resistivity) is determined by the energy level difference of TiO_2 Fermi level and the redox couple mediator energy level, like has been depicted in Fig. 2. Thus, the optimization of dye solar cell performance includes a trade-off between high voltage and high current.

In summary, the operation of the cell is thus described by three main kinetic charge transfer mechanisms: *electron injection* from dye HOMO level to semiconductor conductivity level, *charge transfer* towards cell contacts in the semiconductor and *dye regeneration* after oxidation [17]. The corresponding reaction efficiencies are η_{INJ}, η_{COL} and η_{REG}.

It must also be considered that the liquid electrolyte, TiO_2 and the dye are all mixed together in the cell. Thus also side-reactions occur in the cell. Two main negative charge transfer mechanisms in the cell are *charge recombination*, i.e. relaxation of excited electron to the dye ground state, and *dark current*, i.e. recombination between injected electrons and I_3^- ions [17]. These phenomena affect to cell performance especially by decreasing open circuit voltage of the cell, V_{oc}.

2.2 Causes of degradation in dye-sensitized solar cells

DSSC stability for approximately 20 years in outdoor conditions is an essential prerequisite for introduction of DSSCs into wide commercial market. At the moment, cell stabilities after thousands of hours of continuous illumination have been reported [18, 19] but Asghar et al. showed in their review of stability studies on DSSCs that the aging methods vary a lot and the whole field lacks the established practices for stability testing [13]. Additionally, the same study revealed that the degradation mechanisms themselves would need more consistent research because there are many unconfirmed assumptions and hypotheses about degradation mechanisms going around the field [13]. This is partly a chicken and egg situation: proper tests have to be determined to study the aging mechanisms of the cells but there has to be at least an idea of aging mechanisms to be able to determine the proper aging tests. Next, the main degradation mechanisms in the cells are introduced by cell components.

Conducting glass substrates are generally regarded as stable cell components although impurities can cause side-effects in the conducting layer just like impurities in any other component.

TiO_2 film and the conducting layer of the substrate can physically degrade so that electron transport resistance in the semiconductor film, R_T, or the contact resistance, R_{CO}, increases [13]. The other option is that detached counter electrode particles or electrolyte components attach to TiO_2 thus increasing recombination and decreasing electron lifetime in the conduction band of TiO_2, τ [20].

Naturally, also the catalytic activity of the counter electrode decreases if particles are detached from it although the above-mentioned counter electrode particle deposition on the photoelectrode is usually the more problematic phenomenon. Counter electrode particle detaching could happen e.g. because of impurities between TCO layer and Pt [13]. This could be seen as increased charge transfer resistance at the counter electrode/electrolyte interface, R_{CE}. R_{CE} can also increase as a result of plain electrolyte component deposition on the counter electrode surface [21], or as a result of some unwanted chemical reactions between the counter electrode and the electrolyte materials [22].

Dye can cause cell degradation through dye degradation or desorption. Dye desorption into electrolyte is a problem mainly at high temperatures, e.g. at 80 °C, and the dye partly adsorbs back to the photoelectrode when temperature decreases [8]. Dye desorption can clearly be observed as the reddish color of the electrolyte. There are some hypotheses about the reason of desorption. There might exist a reversible

chemical equilibrium between dissolved and absorbed dye that shifts because of increasing temperature [8] or water in the cell could react with hydrophilic TiO_2 and lead to dye desorption [23]. Also electrolyte has been blaimed: electrolyte decomposion products could adsorb onto TiO_2 or oxidiced dye and electrolyte radicals (e.g. iodine radicals) could react, thus leading to desorption of the dye [21]. Actual dye degradation has been suggested to happen through thiocyanate ligand (SCN) substitution with electrolyte materials, e.g. methoxypropionitrile (MPN) or 4-tert butyl pyridine (TBP) [24, 25]. MPN substitution has not reportedly been studied in whole DSSCs but 100 % substitution with TBP has been shown to halve cell efficiency through 30 nm blue shift in dye absorption spectrum, 14 % decrease in charge separation efficiency and increase in recombination that causes halving of electron diffusion length [26].

Chemical changes can degrade also the electrolyte. A typical sign of degradation is bleaching which indicates a decrease in I_3^- concentration, $c_{I_3^-}$. In case of I_3^-/I^- redox couple, the maximum current that the cell can produce, I_{lim}, is limited by ionic diffusion and is relative to $c_{I_3^-}$:

$$I_{lim} = \frac{4FD_{I_3^-}c_{I_3^-}}{d} \tag{2}$$

where F is Faraday's constant, $D_{I_3^-}$ is diffusion constant of I_3^- and d is the diffusion distance, i.e. approximately the distance of the electrodes [27]. Thus, bleaching decreases I_{lim} of the cell. Even the short circuit current of the cell can decrease if the concentration of charge carriers has decreased a lot. The other effect of bleaching on cell performance is increase in diffusion impedance of the electrolyte, R_D which leads to a decrease in the fill factor FF of the cell (assuming that the short circuit current has remained the same) [14]. There are several hypotheses for bleaching. Iodine sublimation caused by gelation of the ionic liquid or iodate-forming reactions with impurities like water or oxygen have been suggested [28]. It is known that UV light causes direct band excitations in TiO_2 which might lead to formation of radicals [29]. The radicals have been proposed to attack electrolyte as UV exposure causes bleaching of the electrolyte [29]. It is also known that electrolyte contact with the current collectors causes corrosion which destroys both components. It has been confirmed that bleaching is not detected in CE-CE cells but even in cells with undyed TiO_2 [30]. This supports the hypothesis that bleaching is not a result of reaction between the electrolyte and dye or counter electrode, but namely between the electrolyte and TiO_2. Bleaching and performance decrease caused by

high temperature are partly recovered in low temperatures, which indicates that a reversible temperature-dependent equilibrium reaction is related to cell bleaching [8, 30].

From the previous discussion it can be deduced that impurities and environmental conditions are important factors in cell degradation. High temperatures seem to degrade cells very efficiently [8]. It is also clear that UV light has a detrimental effect on cell stability [29], even when introduced to the cells in moderate temperatures [31]. Water is one of the main impurities that has been reported to cause cell degradation [9, 15] but also contradictory results have been got [32]. Thus, more research on the effects of water in the cells is needed. In this study, the focus is in the effects of impurities in the electrolyte, especially water as electrolyte adsorbs humidity quite readily.

2.3 Measurement techniques

One of the aims of this study was to determine the appropriate measurement techniques for long-term aging tests, where the applied tests have traditionally been limited to IV curve measurements. Thus, a large variety of different tests from standard methods to techniques that are quite new to DSSC aging studies were applied for the cells. Next, the techniques and the analysis methods are discussed.

2.3.1 IV measurements

IV curve of a cell (Fig. 3) is simply a result from a steady state current measurement as a function of voltage that is applied to the cell. Typically, two-way sweep is performed to reveal if the sweep speed is so high that it disturbs the steady state and creates hysteresis in the curve. The IV curve can be measured under illumination or in dark. The IV curve in Fig. 3 has been measured under illumination.

An IV curve measurement is a fast way to determine how well the cell works. The basic parameters that describe the cell performance can be determined easily from the IV curve if the illumination conditions are known [33]. Open circuit voltage V_{oc} and short circuit current I_{sc} can be determined from the intersections of the IV curve and the zero current or zero voltage lines of the graph, respectively. Fill factor FF describes the squareness of the IV curve and it can be determined as

$$FF = \frac{P_{max}}{P_{ideal}} = \frac{I_{mpp}V_{mpp}}{I_{sc}V_{oc}} \tag{3}$$

where P_{max} is the actual maximum output power of the cell P_{max} and P_{ideal} is the

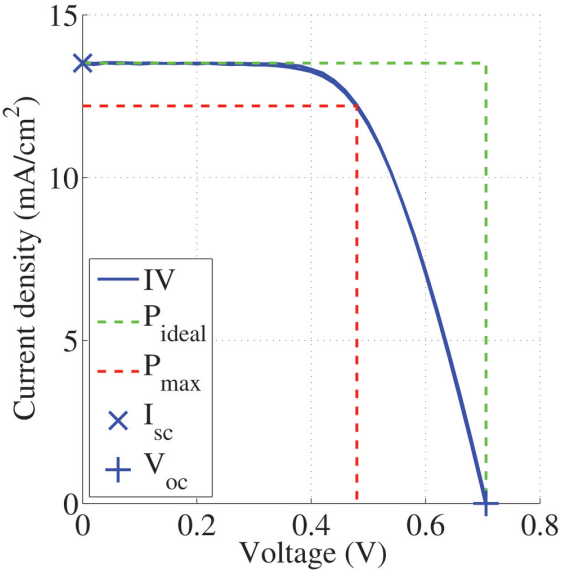

Figure 3: An IV curve of cell E4 that represents a typical cell in this study with 5.9 % efficiency. Main parameters, open circuit voltage V_{oc} and short circuit current I_{sc} are also marked to the graph, as well as tetragons which area represents the actual maximum power of the cell, P_{max}, and power of cell without any losses, P_{ideal}.

output power of cell in case that it does not suffer from any losses. Naturally, these powers can be expressed as a product of V_{oc} and I_{sc}, and voltage and current of the maximum power point, V_{mpp} and I_{mpp}.

Cell efficiency η is defined simply as

$$\eta = \frac{P_{max}}{P_{in}} \tag{4}$$

that is a ratio of maximum output power of the cell and the incident illumination power P_{in}. Cell performance can vary over varying illumination and temperature. Thus efficiency is measured in standard test conditions which are usually an illumination spectrum called Air Mass 1.5, P_{in} of 1000 Wm^{-2} and temperature of 25 °C [33], shortly referred as 1 sun illumination.

IV curve measurements can not be utilized just for cell performance determination but also for studying the reasons for weakened cell performance. In case of a well-working cell I_{sc} is almost linearly dependent on P_{in} over large scale of P_{in}. The linear relation is broken just when P_{in} increases so much that the limiting current density, I_{lim}, of the cell is reached. The reason for existence of I_{lim} is the finite number of charge carriers in the cell, especially the number of charge carriers in the electrolyte as described in Eq. 2. Sometimes a cell performs poorly in 1 sun condi-

tions but well in low illumination. This is caused by so low I_{lim} that it affects the cell output current even at 1 sun conditions. This problem is easily revealed by measuring multiple IV curves as a function of incident light intensity and determining $I_{sc}(P_{in})$.

2.3.2 Incident-photon-to-collected-electron efficiency and transmittance tests

Incident-photon-to-collected-electron efficiency, η_{IPCE}, describes the photocurrent generation properties of the cell. Assuming that the incident-photon-to-collected-electron (IPCE) measurement is done at conditions where there are no other current limiting factors, e.g. electrolyte mass transport limitations, η_{IPCE} is determined by four factors:

$$\eta_{IPCE} = \eta_{LH}\eta_{INJ}\eta_{REG}\eta_{COL} \tag{5}$$

where η_{INJ}, η_{REG} and η_{COL} are the kinetic charge transfer mechanisms described in chapter 2.1. η_{LH} is the light harvesting efficiency of the dye, i.e. the efficiency with which the dye adsorbs incident light. Different IPCE measurements can be combined in order to extract information about each factor of η_{IPCE} [16] yet in this study the analysis has been limited to simple low-intensity dye IPCE measurements from the photoelectrode side of the cell without any bias light due to time limitations. Next, the analysis of this kind of measurements will be introduced. The main focus in the analysis is the wavelength dependence of the changes in η_{IPCE}. Firstly, η_{INJ} can be approximated to be independent of light wavelength [16]. The effect of η_{REG} can not be separated from η_{INJ} by methods used in this study. η_{LH} is dependent on light wavelength because shorter wavelengths get absorbed into dye (or any other materia) easier than the long ones. Because of the same reason and the fact that successful diffusion of electrons to the cell contacts is dependent on the distance from the contacts, also η_{COL} is wavelength dependent [16]. The decrease in η_{COL} is visible especially at the longer wavelengths because the distance from injection point to the contacts is longer with long wavelengths than with short ones. From a practical point of view, η_{IPCE} should be plotted both as absolute and relative values because the wavelength dependence is best visible in relative graph.

2.3.3 Electrochemical impedance spectroscopy

Electrochemical impedance spectroscopy (EIS), is used for determining the electrical performance of different cell components. In EIS, voltage V that consists of a

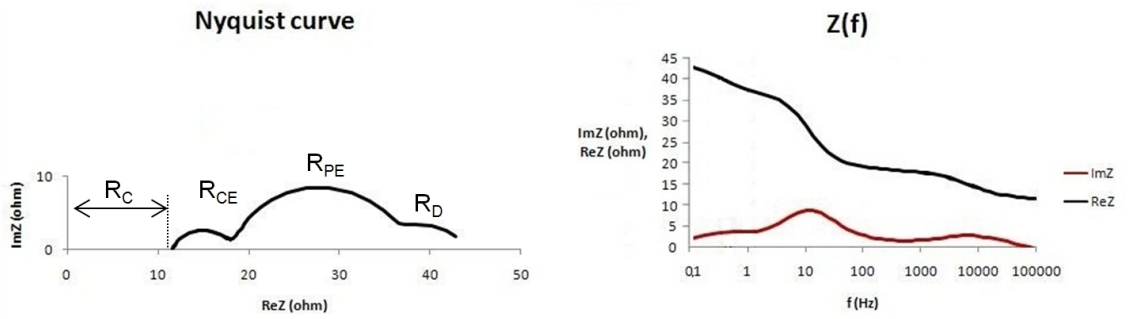

Figure 4: A typical impedance measurement result is shown as an Nyquist curve and as a function of frequency. Typically, the effects of resistive elements in the cell are seen as separate arcs in Nyquist plot. The elements marked to the Nyquist graph are related to series resistance of the cell (R_s), photoelectrode (R_{PE}), counter electrode (R_{CE}) and electrolyte (R_D).

sinusoidal component V_{AC} superimposed on a direct voltage component V_{DC}, is applied to the cell. The solar cell responses by producing alternating current i_{AC} that is measured. The amplitude of V_{AC} is small, usually around 10 mV, and V_{DC} is on the range of cell output voltages. The impedance of the cell, Z, can then be determined as a function of V_{DC}, time t and angular frequency ω:

$$Z = \frac{V_{AC}(\omega, t)}{i_{AC}(\omega, t, V_{DC})} \tag{6}$$

Also other operating conditions such as temperature and light intensity affect the response. The resulting data in EIS is the real and imaginary part of the impedance of the cell as a function of frequency of V_{AC}, f. The data can be visualized as a Nyquist curve, where the axes are the real and imaginary parts of the impedance. An example of EIS result is shown in Fig. 4.

The cell components can be distinguished from each other in EIS because they have different time constants and are thus visible at different frequencies, as has been illustrated in Fig. 4. EIS result can be further analyzed by fitting an equivalent circuit consisting of electronic components and describing solar cell physics to the resulting data. The equivalent circuits have been determined by studying the different charge transfer mechanisms in the cells. In this study, an equivalent circuit model described in literature [16] has been utilized for EIS analysis. The full model is illustrated in Fig. 5 and has been described more thoroughly in [16].

The circuit components in Fig. 5 are electron transport resistance of TiO_2 film (R_T), charge recombination resistance including also the dark current (R_{REC}), photoelectrode capacitance (C_μ), contact resistance (R_{CO}) and capacitance (C_{CO}),

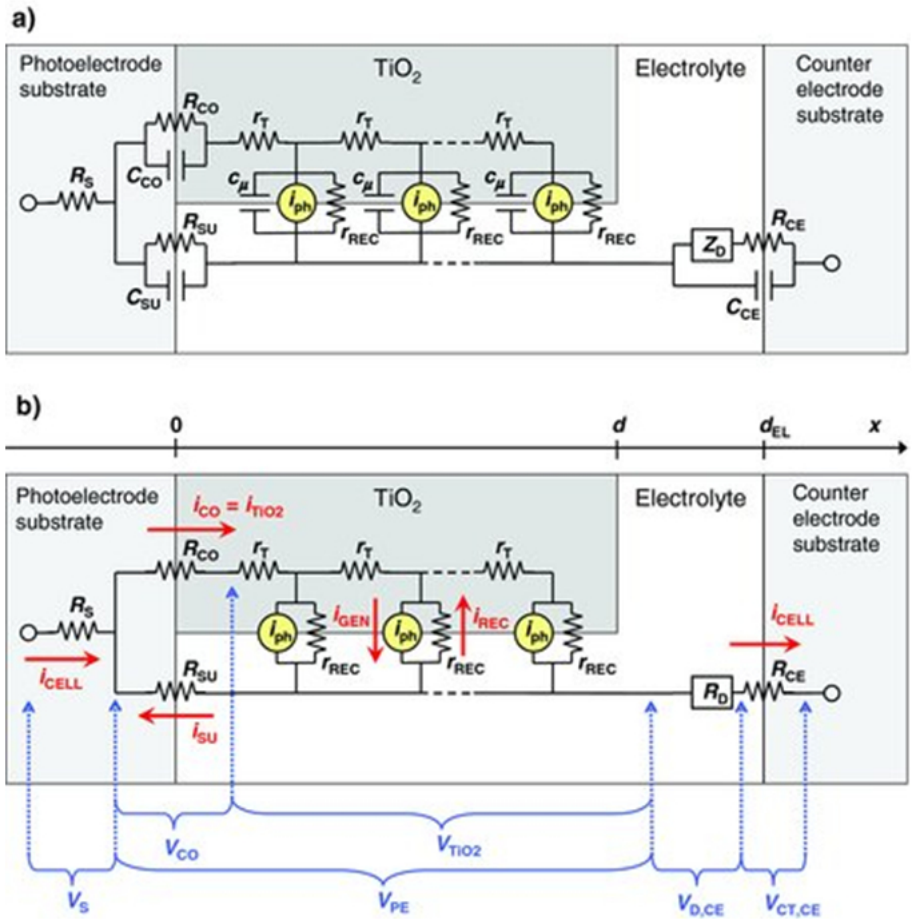

Figure 5: Equivalent circuit model of the dye solar cell. The figure is from [16].

charge transfer resistance and capacitance between the substrate and the electrolyte (R_{SU} and C_{SU}, correspondingly), charge transfer resistance and capacitance at the interface between counter electrode and electrolyte (R_{CE} and C_{CE}, correspondingly), mass transport impedance at the counter electrode (Z_D) and series resistance of the cell R_s [16]. The resistive components represent the resistances to charge transport in cell materials or at the interfaces between the cell components, and capacitors represent the charge accumulation at the interfaces [16]. The equivalent circuit model for the dye solar cells is quite comprehensive and takes into account the phenomena described thus far in chapters 2.1 and 2.2. The drawback is that the amount of parameters that are apparently free to change, is large and thus fitting the circuit to measurement data logically is difficult.

Fortunately, the model can be simplified to be suitable for most occasions quite easily. The first three components can be combined to one impedance regarding the TiO_2 layer, Z_{TiO_2} [16]. The amount of variables for the equivalent circuit seems still

large but can in most cases be simplified by assuming good substrates ($R_{SU} \to \infty$ and C_{SU}=0) and contacts (R_{CO}=0 and C_{CO}=0). The steady state (ω=0) of the cell is the most interesting state during the analysis as this is the operating state of the cell. Assumptions of good substrates and contacts lead to simplification of the expression for the whole photoelectrode in the steady state: R_{PE} reduces to R_{TiO_2}. As a result, only six components are left to be determined: R_{PE} and C_{PE}, R_{CE} and C_{CE}, R_s and R_D that is the steady state value of Z_D [16]. This amount of fitting parameters seems to be suitable as there are three arcs and an Ohmic resistance visible in Fig. 4. In reality, the RC-circuits of the cell are not ideal and this difference is often balanced by replacing the capacitances with constant phase elements (CPE) which have an ideality factor differing from value one [16].

In practice, all the parameters can not be determined simultaneously reliably from an EIS result because the simplifying assumptions are not valid at the same time in all the cell components. The steady state assumption for the photoelectrode is valid when the voltage over the photoelectrode (V_{PE}) is known, i.e. when the currents through the cell are very small. In these circumstances the resistive phenomena do not affect the voltage inside the cell and thus V_{PE} is same than the voltage over the cell (V_{cell}). In practice, photoelectrode properties of the cell are studied from impedance data that is measured in dark (the cell does not produce current) and with small voltages (the slope of the IV curve is small). For the counter electrode, the corresponding reliable state develops when the concentrations of electroactive species of the electrolyte (e.g. I_3^- and I^-) are in equilibrium near the counter electrode surface [16]. Thus, V_{oc} is a good state for the analysis of the counter electrode. This applies also for determination of R_D because R_D depends on cell current I_{cell}:

$$R_D = \frac{k_B T}{2q} \left(\frac{1}{I_{lim,I_3^-} - i_{cell}} + \frac{1}{I_{lim,I_3^-} - I_{cell}} \right) \tag{7}$$

where I_{lim,I_3^-} has been defined in Eq. 2 and similarly, I_{lim,I^-} is

$$I_{lim,I^-} = \frac{4FD_{I^-}c_{I^-}}{3d} \tag{8}$$

[16]. At zero polarization

$$R_{CE,0} = \frac{k_B T}{2Fkc_{I_3^-,eq}^{1-\beta/2} c_{I^-,eq}^{\beta/2}} \tag{9}$$

where k_B is Boltzmann constant, T is temperature, F is Faraday's constant, k is

the rate constant for the charge transfer reaction at the counter electrode, $c_{I_3^-,eq}$ is tri-iodide equilibrium concentration, $c_{I^-,eq}$ is iodide equilibrium concentration and β is a symmetry parameter depending on the catalyst [16]. Thus it can be calculated that R_{CE} that is related to the counter electrode - electrolyte interface depends not only on the counter electrode properties but also on the concentrations of iodide and tri-iodide [16]. As a result, based on EIS it is not possible to determine if the changes in R_{CE} result from changes in counter electrode or electrolyte.

As a final remark, electron lifetime in the photoelectrode, τ, can simply be calculated by [16]:

$$\tau = R_{REC}C_{\mu} \approx R_{PE}C_{PE} \tag{10}$$

when EIS has been measured in dark. Decreased electron lifetime indicates that cell performance has decreased because of increased recombination or dark current.

2.3.4 Liquid chromatography - mass spectrometry

Liquid chromatography - mass spectrometry (LC-MS) is a combination of two different techniques used for analyzing the compositions of unknown compounds.

The principle of liquid chromatography (LC) relies on different solubility of compounds in different materials [34]. In LC, the sample is first dissolved in a liquid (a mobile phase). Next, the liquid mixture is passed through a column containing another compound that is immobile and not miscible to the mobile phase (a stationary phase). The two phases are chosen in such way that the compounds in the sample have a different solubility in the two phases. Thus, the different compounds in the sample move through the column at different speeds depending on the relation of the solubility of the compound in the phases. The sample liquid that has passed through the column is separated into small portions that are analyzed in the mass spectrometer (MS).

In mass spectrometry, the main steps are samples vaporization, sample ionization, sorting by mass-charge ratio (m/z) and detection [35]. In this study, ionization technique has been electrospray ionization in which the pH of the dissolved sample is modified to ensure ionization. The ionized samples are categorized by the relation of their mass and charge. In this study, this is done by quadrupole-time-of-flight mass spectroscopy. In time-of-flight mass spectroscopy, the ions are all accelerated by the same electric field, and then the ions travel for a certain distance before hitting to a detector [36]. All the ions have gained the amount of kinetic energy that is relative to the charge of the ions. On the other hand, the velocity gained by the ions as a

result of acceleration is relative to both kinetic energy and mass of the ion. Thus, the ratio (m/z) can be calculated from the basic equations of kinetic energy and uniform electric field based on the travel time t of the ions:

$$\frac{m}{z} = \frac{2Ut^2}{d^2} \tag{11}$$

where U is the acceleration voltage and d is the distance.

2.3.5 Raman spectroscopy

Raman spectroscopy is an important method for investigating the elementary excitations, e.g. phonons and plasmons, of different materials. Raman theory is a wide subject and beyond the scope of this thesis. Thus, only the basic principles of the measurement technique are presented here.

The excitations are studied by illuminating the sample by high-intensity light of angular frequency ω_0, which leads to the scattering of light via the polarized valence electrons of the material [37]. Polarization is a function of the studied elementary excitations but also of other collective excitations, e.g. magnons. Both contributions can be taken into account in an serial expansion of susceptibility χ of form

$$\begin{aligned} \chi &= \chi^0 + (\partial\chi/\partial X)\, X \\ &\approx \chi^0 + (\partial\chi/\partial X)\, X_0 cos(\omega_i t) \end{aligned} \tag{12}$$

where terms marked by 0 are constants, X is the contribution of collective excitations, ω_i is the frequency of the elementary excitation that is the subject of interest, and t is time [37]. The wave vector of the scattering has been assumed to be small in the latter transition [37]. Thus, the polarization P_s becomes

$$\begin{aligned} P_s &= \epsilon_0 \chi E_0 cos(\omega_0 t) \\ &\approx \epsilon_0 E_0 \chi^0 cos(\omega_0 t) + \\ &\quad \frac{1}{2}\,(\partial\chi/\partial X)\, X_0 E_0\, (cos((\omega_0 + \omega_i)t) + cos((\omega_0 - \omega_i)t)) \end{aligned} \tag{13}$$

where ϵ_0 is permittivity and $E_0 cos(\omega_0 t)$ is the electric field of incident light [37]. The Poynting vector of the scattered light that describes the energy flux and direction of the flux, is a function of P_s [37]. Thus, it can be seen from Eq. 13 that the scattered light contains radiation both at the frequency of the incident light and at frequencies that differ from the frequency of the incident light by the

frequency of the studied excitation. Raman spectroscopy requires very high quality spectrometer and high intensity incident laser beam because the intensities of the studied side peaks are much lower than the intensity of the middle peak and the response frequencies of different excitations [37].

In practice, the locations of the peaks of each interesting compound is determined experimentally [38]. The peak intensity is directly proportional to the concentration of the material that the peak originates from [39]. Thus Raman measurement peak intensities of two different measurements can be directly compared if the intensity of the laser power and other frequency dependent factors remain constant [39]. The other option that can be used in aging studies is to relate the intensities of the studied peaks to one peak that stays constant during the aging. E.g. TiO_2 peak at 145 cm^{-1} should stay constant because the concentration of TiO_2 is not expected to change during the aging [38]. In this study, also I_3^- peak at 113 cm^{-1} and dicarboxibipyridine band at 1400-1700 cm^{-1}, which virtually originates from the dye, are studied [38].

2.3.6 Cell photographing

Cell photographing is a practical measurement technique that can be used for monitoring changes in e.g. electrolyte color over time. The changes can be evaluated quantitatively through RGB values of the pictures. In this thesis, cell photographing was performed by a method that is described in literature [30].

The electrolyte color is strongly dependent on the amount of iodine in electrolyte because the other electrolyte components are mostly transparent or almost transparent, and iodine is clearly yellowish. Blue is known to be the complementary color for yellow. Thus the changes in the darkness of the yellow color of the electrolyte are seen clearly as changes in the blue pixel value of photographs that have been taken of the electrolyte and saved in JPEG format that presents the images in RGB format. The blue pixel value of the electrolyte has been showed to correlate almost linearly with the concentration of iodine in the electrolyte over a wide concentration range of 0.025 - 0.1 M [30]. The resolution of the method has been calculated to be $7.35 \cdot 10^{-4}$ M per blue pixel value [30]. Cell photographing is also suitable for monitoring dye desorption to the electrolyte because desorption will increase the red pixel values of the cells [30].

The image processing method is easily affected by even minor changes in illumination level and settings of the camera that is used for taking the photographs. Thus, it essential that the illumination level is homogenized both between the photographed cells and different photographing times. This should be done in two ways:

by stabilizing the illumination level at the spot at which the photographs are taken and by using proper color calibration methods (white and color balance) to minimize the effect of still existing variations [30].

3 Materials and methods

The study consists of a long-term aging test series that had two objectives. The first, scientifically oriented objective was to study if cell lifetime or efficiency would benefit from purification of electrolyte materials. The second, metrologically oriented aim was to specify optimal long-term aging test procedures for the research group for future measurements and to introduce statistical methods into result analysis. Next, the practical matters of the test series are introduced.

The effects of electrolyte purification on cell performance were studied by laborious but essentially simple comparison tests. The first step was to determine the proper techniques for purification of electrolyte materials that is described in chapter 3.1. Several electrolytes were prepared to compare the effect of purification of each electrolyte material. The second step was to prepare cells from these electrolytes, which is described in chapter 3.2. The cells were composed and prepared in a uniform way except for the electrolyte that was used. Finally, cell performances were compared before, during and after the aging, which is described in chapter 3.3.

3.1 Material purification

Material purification part of the study was planned and performed by Dr. Denys Mavrynsky from Laboratory of Organic Chemistry at Åbo Akademi. The aim was to purify electrolyte components and all components of dye solution and especially to minimize absorbtion of humidity into materials. Thus, material purification was performed under an inert atmosphere either using standard Schlenk techniques and argon line or using a nitrogen-filled glovebox with oxygen and water content below 1ppm [40]. Additionally, all glassware was oven-dried at 150 °C overnight and cooled down in a dessicator over phosphorus pentoxide.

The electrolyte used in this study consisted of iodine (I_2), 1-methyl-benzimidazole (NMBI), 1-propyl-3-methylimidazolium iodide (PMII), guanidinium thiocyanate (GuSCN) and 3-methoxypropionitrile (MPN). Iodine was not purified because commercial grade "double sublimated" iodine (Merck, $\geq$ 99.5 %) was considered to be pure enough. Purification of the other materials required usage of few different purified solvents or reagents: tert-butyl methyl ether (TBME, Sigma-Aldrich), tetrahydrofuran (THF, Sigma-Aldrich), n-propyliodide (Sigma-Aldrich), N-methylimidazole (Sigma-Aldrich) and isopropanol (Sigma-Aldrich). The first two materials were purified by redistilling them over sodium benzophenone ketyl. N-propyliodide and N-methylimidazole were stirred overnight at 60 °C with calcium hydride and redis-

tilled at reduced pressure. Isopropanol was purified in a similar way but redistilled at atmospheric pressure. The actual electrolyte material purification was performed according to the following techniques: Commercially available NMBI (Sigma-Aldrich, 99 %) was recrystallized from hot TBME and isolated by filtration in a glovebox. PMII was prepared from n-propyliodide and N-methylimidazole according to [41]. Commercially available GuSCN (Sigma-Aldrich, $\geq$ 99 %) was recrystallized from hot isopropanol and isolated by filtration in a glovebox. MPN (Sigma-Aldrich, $\geq$ 98 %) was treated in a similar way than n-propyliodide and N-methylimidazole. After the purification MPN was noticed to have changed color from slightly yellowish to fully transparent which indicates that some impurities, probably water, were removed during the purification.

The next step was to purify the components of dye solution. Tert-butanol was used as a solvent during dye preparation. Additionally, both tert-butanol (Sigma-Aldrich) and acetonitrile (Sigma-Aldrich) were used as solvents in the final dye solution. Both solvents were purified in a similar way than isopropanol.

Cis-bis(isothiocyanato)-bis(2,20-bipyridyl-4,40-dicarboxylato)-ruthenium(II)bis-tetrabutylammonium (N719) dye was made of cis-bis(isothiocyanato)-bis(2,20-bipyridyl-4,40-dicarboxylato)-ruthenium(II) (N3) dye that was prepared by Volatec according to the procedure published in [42]. The preparation procedure of N719 was the following: N3 dye that was dissolved in tert-butanol and water was purified by gel filtration on Sephadex LH20 using water as eluent. Main dark-red colored band was collected, and titrated with 0.05 M HNO_3 to pH 4.3. Resulted suspension was stirred for 3 h at room temperature and centrifuged. Precipitate was washed with water and centrifuged again. 2.5 eq of 40 % solution of tert-butanol in water were added to the obtained solid N719 and gel filtration and precipitation steps were repeated once more. Finally, the dye was dried in vacuum. The resulting N719 was pure based on NMR measurements (the inaccuracy of NMR method itself is typically some percents [43]).

3.2 Cell preparation

Cell substrates were 2.5 mm TEC-15 FTO glass. They were washed with washing detergent, de-ionized water, ethanol and acetone and finally UV-treated for 20 minutes. Photoelectrodes were prepared by screen printing TiO_2 paste on top of the glass substrates. The sizes of the active areas of the photoelectrodes were 0.4 cm^2. A $TiCl_4$ treatment according to procedure described in [44] was also performed. Shortly, the photoelectrodes were $TiCl_4$ treated for 20 minutes at 70 °C in $TiCl_4$

Table 1: Compositions of electrolyte batches (A-F). It is marked for each batch if the electrolyte components were pure (P) or unpurified (U).

Batch	I_2	GuSCN	PMII	NMBI	MPN
A	P	P	P	P	U
B	P	P	P	U	P
C	P	P	U	P	P
D	P	U	P	P	P
E	P	U	U	U	U
F	P	P	P	P	P

solution, sintered at 450 °C for 30 minutes, then screen printed with TiO_2 paste, sintered again at 450 °C for 30 minutes, $TiCl_4$ treated once more and finally, sintered at 450 °C for 30 minutes once again. The photoelectrodes consisted of two layers of Dyesol DSL 18NR-T TiO_2 paste and one layer of Dyesol WER2-O TiO_2 paste. The last layer is a light scattering layer that improves cell efficiency by increasing light harvesting efficiency. Photoelectrode thicknesses were approximately 13 μm.

The photoelectrodes were dyed under nitrogen atmosphere for 16 hours in order to prevent them from absorbing water from the air. Dye solution consisted of 0.3 mM N719 in acetonitrile and tert-butanol 1:1 solvent. N719 dye was prepared from N3 dye by Dr. Denys Mavrynsky and was purified as well as the dye solvents as described in chapter 3.1.

The counterelectrodes were made simply by adding 4 μl of 5 mM H_2PtCl_6 in 2-propanol solvent on top of the glass substrates and sintering them at 385 °C for 20 minutes.

Electrolyte consisted of 0.05 M I_2, 0.5 M NMBI, 0.5 M PMII and 0.1 M GuSCN dissolved in MPN. Six batches of electrolytes were made (Table 1): completely purified and completely unpurified electrolytes and also four batches of electrolytes that were otherwise purified but each of them contained one unpurified component. The unpurified components in the partly purified batches were MPN, NMBI, PMII and GuSCN. Iodine was left out of investigations because grade "resublimated" was considered to be already as pure as practically possible. The purification of compounds is described in chapter 3.1. The electrolytes were prepared and stored in argon atmosphere to avoid absorbtion of water from the air.

Entrance of humidity into the cells was avoided by all means during the material preparation and photoelectrode dyeing. In accordance with these proceedings, the

cells were also tried to assemble in dry atmosphere in a glove-box. This did not however succeed because assembling was extremely slow, most of the cells started to leak and even the ones that did not leak, performed weakly due to overheating during the sealing process. Thus for practical reasons, the cells were prepared in air in a normal laboratory room that had temperature of approximately 20 °C and relative humidity of less than 10 % during the cell assembly. The cells were prepared by sealing them with 25 μm Bynel foils.

3.3 Aging tests

Aging tests in this study consist of three main parts: pre- and post-aging measurements, automatic measurements performed during the aging and manual measurements performed on weekly basis during the aging. These measurements include a large variety of different tests described in chapter 2.3 and performed on different measurement devices. Next, the whole aging test procedure is discussed in chronological order.

Firstly, the test cells were prepared by using a method that is described in chapter 3.2. Then the cells were put to light soaking at approximately 0.5 sun illumination for 16 hours to stabilize the cell operation. Typically, cell efficiencies increase during this stabilization soaking and the changes were recorded by measuring IV curves of a couple of cells in each cell group before the light soaking.

Secondly, the pre-aging tests were performed on the cells. Some of the tests were performed on all the cells and some on a couple of cells in each cell group in order to save time. Specifications of the utilized devices are listed in Table 2. Initial tests included the following tests: IV curve measurements and EIS at V_{oc} in the solar simulator (EIS was measured with Zahner potentiostat), IV curve measurements as a function of light intensity with Autolab potentiostat, Raman tests, IPCE and electrolyte transmission measurements. Theoretical basis of the tests has been described in chapter 2.3. The solar simulator has been calibrated with an official calibration solar cell to a state that is equivalent to AM 1.5G illumination spectrum. The spectrum of the halogen lamps that are used in the solar simulator are shown in appendix B. Black tape masks were attached on top of the cells during the IV measurements in order to prevent scattered light from accessing the photoelectrodes from the sides. The masks had square holes that were 1 mm larger than the photoelectrodes from both sides. In impedance measurements, frequency range 10^{-1}-10^{-5} Hz was sweeped back and forth with 10 mV amplitude. Autolab potentiostat is combined with an in-house built white LED light source for measuring IV curves as

Table 2: Devices and the measurements that the devices were utilized for in pre-aging tests.

Device type	Device model	Tests
Solar simulator	In-house built	IV in 1 sun
Potentiostat	Zahner Zennium	EIS at V_{oc}, EIS in dark, IV in dark
Potentiostat	Autolab PGSTAT302 N	IV vs. light intensity
Solar Cell Spectral Response Measurement System	PV Measurements QEX7	IPCE, transmission

a function of varying light intensity up to approximately 0.5 sun equivalent. IPCE tests were performed in DC mode with no bias light. Both IPCE and transmission tests were performed on wavelength range 300-900 nm.

Determination of Raman spectra was also a part of pre-aging tests. Raman spectra were measured by Mr. Sampo Kaukonen from New Energy Technologies group at Aalto University. The measurement device was HORIBA Jobin Yvon LabRam 300 micro-Raman spectrometer equipped with a 514 nm argon laser, and the cells were measured from the photoelectrode side of the cell. A filter (D1) was used in the measurements so that laser power was reduced to 0.124 mW. The grating setting for the whole spectrum measurement was 1800 mm^{-1} for D1 filter. The spot diameter was approximately 0.2 μm leading to laser light intensity of about 10^{11} $\mathrm{W/m}^2$. The Raman spectrometer was calibrated using mono-crystalline silicon. Data acquisition settings were set at an average of 4 cycles of 20 seconds.

Thirdly, the cells were aged. The in-house built light soaking device that was used for aging the cells uses the same lamps as the solar simulator and gives thus 1 sun equivalent illumination. It was confirmed in the beginning of the aging that temperatures of all the cells stayed below 40 °C in light soaking. Additionally, cell temperatures were monitored during the aging at two locations that were considered to be the coolest and warmest spots of the platforms. Based on this record, cell temperatures stayed at $20 - 30\,^{\circ}\mathrm{C}$ during the aging. Because of the large amount of cells in aging the illumination level in light soaking device is not as uniform as in the solar simulator. To be able to compensate the light intensity variations, light intensities of each cell were measured manually every time the cells had been moved or a lamp of the light soaking device had been changed. Illumination of the aging platforms was also monitored automatically by two photodiodes in order to track aging or breakdowns of the lamps. During the aging, automatic IV measurements

Table 3: Devices and the measurements that the devices were utilized for in weekly measurements.

Device type	Device model	Tests
Potentiostat	Zahner Zennium	IV and EIS in dark
Photographing system	In-house built, includes Olympus E-620 camera	Photographs

and EIS measurements at different voltages between short and open circuit voltages of the cells were performed with in-house built Solar Cell Aging Test Unit (SCATU) with similar EIS settings that were used in Zahner potentiostat. The unit makes the actual measurements with Bio-Logic SP-150 potentiostat. Additionally, Agilent 34980A switch and measurement unit is used both for connecting one cell at a time to the potentiostat and for the above-mentioned monitoring of cell temperatures and light intensities during the aging. SCATU performs measurements in cycles for all the cells and takes one measurement approximately in every five minutes, so information about degradation speed of the cell is collected accurately. However, Biologic potentiostat cannot measure EIS of very degraded cells with large impedance as well as Zahner potentiostat [45]. Thus the latter device was still used for impedance measurements at V_{oc} in pre- and post-aging tests.

In addition to automatic SCATU tests, manual tests were performed on weekly basis with devices mentioned in Table 3. These tests included EIS and IV measurements in dark, cell photographing and light intensity logging of each cell. EIS settings were the same than in measurements performed under illumination but tests were repeated at voltage range from 0 V to -0.7 V at intervals of 0.1 V. A detailed description of the photographing system is found in literature [30]. The system utilizes LEDs to keep the illumination constant. Additionally, the white and color balances of the resulting photographs were calibrated by Lightroom 3 software before the analysis of pixel values.

Fourthly, the post-aging tests were performed after the aging period of 1000 hours. These tests were otherwise the same as pre-aging tests but one test was added: licuid chromatography - mass spectrometry (LC-MS) measurements for a couple of cells in each cell group. Tests were conducted by MSc. Sabine Rendon from Laboratory of Organic Chemistry at Åbo Akademi. The chromatographic separations were performed on a Waters Atlantis T3 analytical column equipped with a guard column of the same brand. The exact mass determinations were performed

on a Bruker electrospray ionization quadrupole-time-of-flight mass analyzer (Q-ToF, micrOTOF-Q, Bruker Daltonics) operating in negative mode. Nitrogen was used as a nebulizing and a drying gas. Capillary voltage was set to +4 kV. The analytes were transferred to the mass analyzer by an Agilent 1200 Series LC system consisting of a binary pump, a vacuum degasser, an autosampler, a column temperature controller (30°C), and a DAD UV detector (Agilent Technologies). LC-MS results of the cells were compared with both the results of pure starting material (dye solution) and reference cells that had not been aged under illumination. The results were not compared to pre-aging measurements of each cell because LC-MS is an destructive analysis method.

3.4 Simple statistical methods in analysis of aging data

The statistical methods chosen to be utilized in this study were Peirce's criterion for the detection of outliers in the data, one-way analysis of variances (ANOVA) combined with paired comparison tests for comparison of average values, and regression analysis for presenting the measured data as a function of a regressor.

The Peirce's criterion is a method used for exclusion of parasitic errors, outliers, from the untreated measurement data, and has been described accurately in literature [46]. The method is designed so that it can applied to several suspicious data points and it adjusts the criterion for excluding a data point to the amount of already excluded data points [46]. In addition to these good qualities, one reason for choosing Peirce's criterion for outlier detection was that the method is simple to use: The fraction of deviation of the measured value from the data mean and the standard deviation of the whole data set is calculated and compared to the look-up table shown in literature [46]. The data point is simply excluded if the calculated value is larger than the value checked from the look-up table.

ANOVA and paired comparison tests were utilized for checking if the differences between the cell groups in the averages of measured parameters were significant. The null hypothesis for ANOVA is that there are no differences between the studied groups at a certain significance level [47]. If the null hypothesis fails, the test is continued by performing a paired comparison test between each two cell groups. The comparison is performed by using a t-test [47]. The null hypothesis for the t-test is, again, that there are no differences in the average values of the two studied groups at a certain confidence level. It is notable that ANOVA combined with paired comparison tests does not produce any knowledge of the amount of difference between the cell groups but only information about the existence of a difference

between the groups.

Regression analysis has been applied for analysis of line plots showing result parameters as a function of light intensity during the aging test. Regression lines and confidence intervals have been calculated by Matlab, a software designed for numerical computation. The utilized Matlab functions are *polyfit* and *polyconf*. *Polyfit* fits a polynomial of the given order for the given data by least squares method [48]. After the fit, function *polyconf* is used for determining the confidence intervals of the fit for new observations at given confidence level [49]. In this thesis, all the performed fits were linear ones.

4 Results

4.1 Cells

There were six cell groups with six cells in each group in the study as has been described in chapter 3.2. The cell groups and the corresponding unpurified electrolyte components are listed in Table 4. Also the cells that were aged are listed in the same table. Cells E1 and F2 were not aged because they were left as reference cells for LC-MS measurements and in the case that more pre-aging measurements would be needed. Additionally, cells D6, E6 and F6 were broken so they were left out of study.

Table 4: The cell groups, corresponding unpurified electrolyte components and cells that were aged in electrolyte purification test series.

Cell group	Unpurified electrolyte component(s)	Aged cells
A	MPN	A1-A6
B	NMBI	B1-B6
C	PMII	C1-C6
D	GuSCN	D1-D5
E	All	E2-E5
F	None	F1, F3-F5

4.2 Aging times and dates

The test series was aged in total for 1000 hours under illumination using the procedure described in chapter 3.2. The total aging period was longer than 1000 hours because the cells were in dark during the weekly measurements and these periods were not calculated as aging in light. The exact aging times and dates and the dates of examined weekly and post-aging measurements are listed in Table 5. The table shows that all the measurements that have been performed on weekly basis during the aging have been analysed at approximately 700 hours of aging instead of the post-aging measurement. This earlier moment was chosen because all the cells had degraded faster than was expected and it was not possible to find differences between the cell groups in many post-aging measurements.

Table 5: The exact aging dates and times, and also the dates of the examined weekly and post-aging measurements of electrolyte puification test series.

	Date	Aging hours
Starting time	21.12.2013	0
SCATU results examination time	20.01.2013	700
Weekly measurements examination time	25.01.2013	720
Ending time	11.2.2013	960

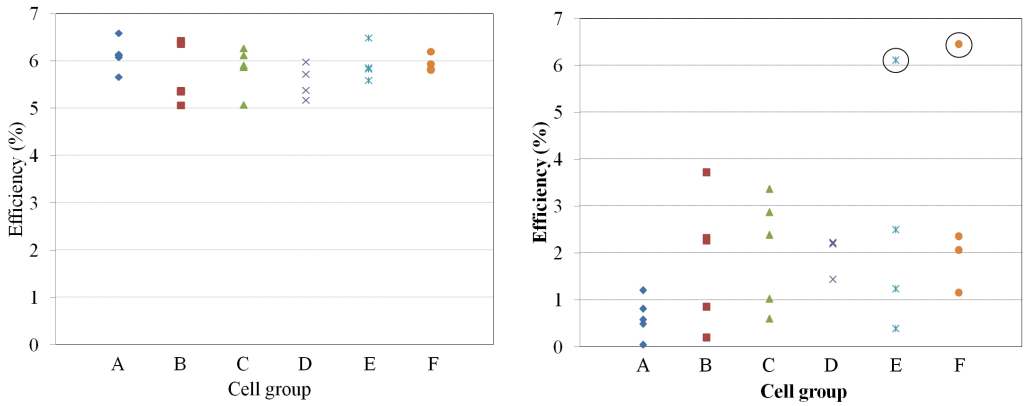

(a) Pre-aging (b) Post-aging

Figure 6: Pre- and post-aging efficiencies of all the measured cells in each cell group. The measurements have been made with a solar simulator. The two circled cells are the reference cells E1 and F2 that have not been exposed to light.

4.3 IV measurement results

The initial efficiencies of the cells measured with the solar simulator are shown in Fig. 6a. Initially, all the groups performed similarly. The initial IV measurements were performed after a light soaking stabilization period of 16 hours and during that time cell efficiencies increased by approximately 1.5 %-units based on the IV measurements that were performed before light soaking (data is not shown). Post-aging results are shown in Fig. 6b. It seems that group A (MPN is unpurified) performs worse than the other groups though the results suffer from so large variations inside the groups that it is difficult to put a reliable ranking of the cell groups. It would be reasonable that the effect of purity of MPN on cell performance would be larger than the effect of other materials as MPN is the solvent of electrolyte. Thus, the volume of MPN in the cell is much larger than the volume of other electrolyte components. It is, however, surprising that group E (totally unpurified) is not performing as weakly as group A.

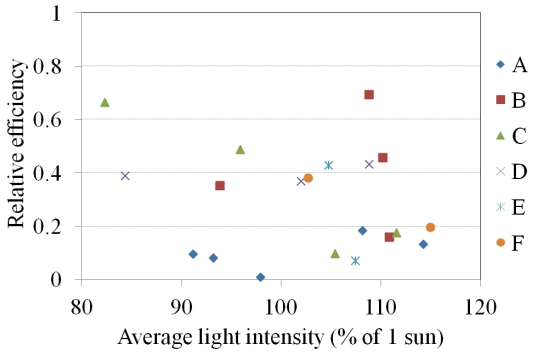

Figure 7: Post-aging efficiencies of all the measured cells in each cell group shown relative to the original efficiency as a function of average light intensity during the aging. The efficiencies have been measured with the solar simulator.

The aging of the cells is generally known to be affected by the light intensity to which the cells are exposed. This test series was the largest one that had been aged in the light soaking device by then. Thus light intensities had varied more than before between the cells. Therefore, one hypothesis for the large deviations of post-aging cell efficiencies was that it resulted from too large light intensity variations during the aging. Cell efficiencies measured with the solar simulator are shown as a function of average light intensity during the aging in Fig. 7. However, this chart does not really support the hypothesis because the dependence between light intensity and cell efficiency in the figure is not clear enough. FF, V_{oc} and I_{sc} were also plotted as a function of average light intensity during the aging but the results were not any clearer. Cell efficiencies and other IV parameters were also plotted as a function of maximum momentary light intensity during the aging (data is not shown). These plots showed similar but not any clearer dependence to light intensity. Thus, the large deviations in the cell efficiencies remain an open question after the analysis of solar simulator results.

The next step is the analysis of SCATU IV results. The raw IV aging data from SCATU is shown in Appendix A. The data implicates that most of the cells have degraded significantly during the aging but group A has degraded faster than the other groups. In the end, the degradation of all the cells has been so significant that it is difficult to distinguish any differences between the cell groups. Thus, SCATU IV data was analyzed at earlier point of time, after 700 hours of aging, in order to reveal the prospective faster aging of some groups compared to the others. The results are shown as a function of average light intensity during the aging in Fig. 8. IV parameters are shown relative to the initial values in order to remove the effect

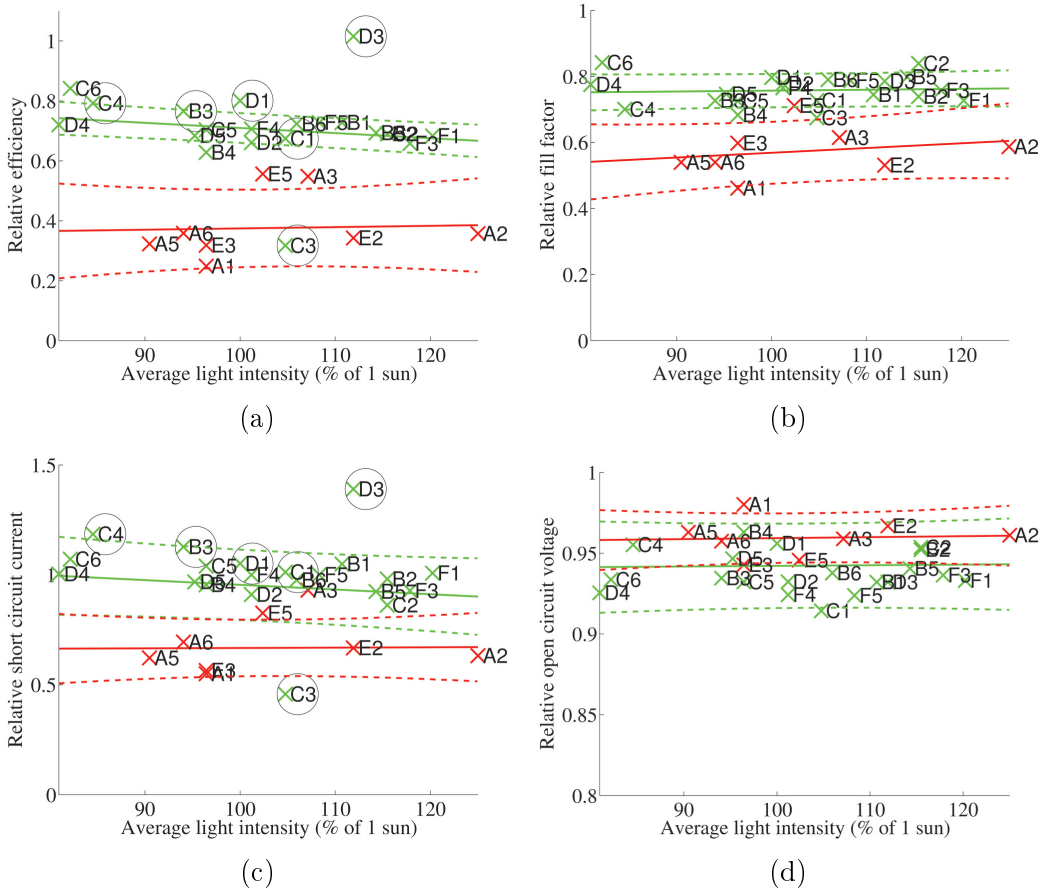

Figure 8: Efficiencies, fill factors, short circuit currents and open circuit voltages of the cells shown relative to initial values after 700 hours of aging. Red color refers to groups A and E (unpurified MPN) and green refers to other cells (purified MPN). Regression lines and 70 % confidence intervals for the results are also included. Cells that are marked by a black circle have been discarded from the regression line calculation because their efficiency and short circuit current data at the examined point of time is inconsistent with the rest of aging data (that is, the data is erroneous at 700 h point of time).

of varying initial performance.

SCATU results in Fig. 8 have relatively large confidence intervals but there is much clearer difference between groups A and E and the other cells than in the post-aging results of the solar simulator. Especially efficiency chart of Fig. 8 shows quite clearly that groups A (unpurified MPN) and E (completely unpurified) perform poorly as compared to the other groups. This fact was also confirmed with regression line fitting. Several regression lines were tested for the data but finally, groups A and E were the only ones that clearly differed from the other groups. Thus the regression lines for groups A and E versus all the other cells are shown in Fig. 8.

Some cells (B3, C1, C4, D1, D3) were discarded from the regression line calculations because aging data from these cells was unreliable at 700 aging hours. This can clearly be seen from the raw data shown in Appendix A: short circuit current and thus also efficiency are inconsistent with the other data, probably because the light intensity to which the cells were exposed has been determined incorrectly at the examined point of time. Additionally, cell C3 was discarded because it seemed to be an outlier, probably because the cell has been contaminated during the cell assembly. The decisions to discard cells were confirmed by Peirce's criterion described in chapter 3.4. With the two groups, cells containing purified and unpurified MPN, cells C3, D3 and E5 were spotted by Peirce's criterion as outliers. Cell E5 was not, however, discarded from the analysis because any reason for the better performance was not found in the cell or in the measurement conditions. Additionally, the exclusion of cell E5 in the analysis would have only made the difference of the groups larger. When the cells were divided in six groups, Peirce's criterion spotted most of the cells suffering from unreliable data at 700 hours moment but gave also false alarms. Thus it seems that Peirce's criterion is most suitable for finding relatively large errors in relatively large cell groups. It must anyway be noticed that the efficiencies of the analyzed cells of Fig. 8 had a notable light intensity dependence whereas Peirce's criterion is designed for detecting random errors in data sets without taking into account any additional parameters. Thus, Peirce's method might perform even better e.g. in the efficiency measurements of fresh cells where additional dependencies to e.g. light intensity or temperature have not yet formed. As a summary for Peirce's criterion, it seems to be an easy and useful tool for evaluating objectively the outliers of the datasets but it must be combined to further inspection of the data and the cells.

Coming back to IV analysis and Fig. 8, η, FF and I_{sc} values are clearly lower in groups A and E as compared to the other groups. V_{oc} has decreased just a little and there are no remarkable differences between the cell groups in case of V_{oc}. Groups A and E have slightly higher voltages when compared to other groups probably because the currents of the cells are lower. Interestingly, other cells possess a weakly decreasing relation of cell performance to light intensity but groups A and E show no or even slightly increasing relation. These IV results indicate that increasing light intensity decreases mostly I_{sc} and the effect is relatively small, approximately 4 %-units in I_{sc} between 90 % and 110 % of 1 sun light intensity in these measurements. However, this effect is not so small that it would need not be tried to minimize during the aging tests.

Finally, the reliability of solar simulator and SCATU IV data was tested by ANOVA test that has been described in chapter 3.4. ANOVA test resulted in a conclusion that solar simulator results were not giving reliable differences between the studied cell groups. With SCATU results, ANOVA did not result in consistent results at first. When cell C3, that was a clear outlier, was removed, ANOVA resulted in the following conclusions: Groups A and E differed from other groups in I_{sc}, V_{oc} and η. Additionally, groups E and F resembled each other in I_{sc} which results from the fact that group F had slightly lower average I_{sc} than groups B-D, probably because F cells had been exposed to quite high light intensities during the aging. FF could not be reliably analyzed because the values were not normally distributed. ANOVA tests were actually made with 95 % confidence level so the conclusion of SCATU results, differing behaviour of groups A and E, is highly reliable.

4.4 Transformation of IV curves during the aging

IV curves of all the cells seemed to transform in a roughly similar way during the aging, in groups A and E (with unpurified MPN) the transformation was just faster than in the other groups. A typical example of transformation of an IV curve is shown in Fig. 9. Three different forms of an IV curve can be seen. At first, the curves are like typical IV curves with quite square appearance. The intermediate level of aging leads to very round IV curve with slightly decreased I_{sc} and V_{oc}. The final level of aging has not been reached by all cells. At this level, series connected resistances (R_{CE}, R_s and R_D) have apparently increased so much that the IV curve has almost transformed to a line that never reaches the saturation level of current and in those cases I_{sc} is actually limited by the series connected resistances. The series connected resistances are analyzed in more detail in chapter 4.7.

4.5 IV measurements as a function of light intensity

The third analyzed measurement is IV curve as a function of light intensity. This test was one of the pre- and post-aging measurements. As explained in chapter 2.3.1, some of the performance limiting factors in the cell can be distinguished from each other by plotting $log(I_{sc})(log(P_{light}))$. This plot can be used to investigate different types of factors affecting I_{sc}, for instance decreased amount of active charge carriers that bends the curve towards I_{lim} at higher light intensities whereas other degradation mechanisms, such as dye degradation, shift the whole curve downwards. Additionally, series resistances in the cell can increase so much that I_{sc} becomes

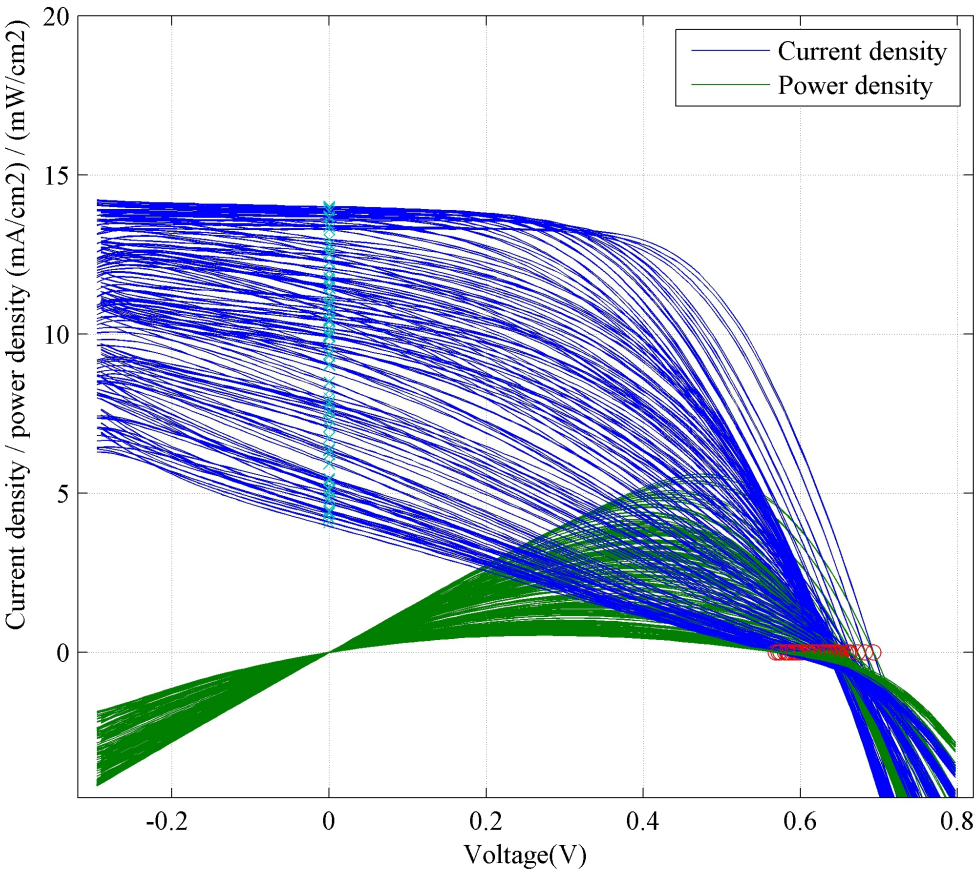

Figure 9: All the IV curves of cell A6 that have been measured during the aging. IV curves are blue and power curves are green. IV curves have a trend of decreasing I_{sc}, V_{oc} and FF during the aging which results in lower output power, as the arrows show.

limited by that. This would also reduce I_{sc} in particular at high light intensities.

The measurements were done for 8 cells that are listed in Table 6. Only cells A5, C2, E2 and F3 showed considerable degradation as compared to the confidence level of the measurement. The results for these cells are shown in Fig. 10. I_{lim} of all these cells has decreased during the aging so much that it affects the cell performance at 1 sun by limiting the output current of the cells at higher light intensities. The whole curves have not shifted downwards during the aging which indicates that the photoelectrode is still working well. In the measured cells, I_{lim} varied between 5-8 mA/cm^2. Cells A5 and E2 were more degraded than C2 and F3. Additionally, the latter two cells are among the three cells that have been exposed to the highest light intensities during the aging in the whole test series 2, while cells A5 and E2 have been exposed to more moderate light intensities.

Table 6: The cells that were used in $log(I_{sc})(log(P_{light}))$ measurements. Also the average light intensities of each cell during the whole 1000 hour aging period are listed.

Cell	A5	B1	C2	D2	E1	E2	F2	F3
I_{ave} (% of 1 sun)	91	109	112	102	0	107	0	115

Thus there are two conclusions of IV curve measurements as a function of light intensity: Unpurified MPN seems to expose cells to larger decrease in I_{lim} during the aging, and that also high light intensity during the aging causes a decrease in I_{lim}. Bearing in mind the relatively large light intensity variations during the aging test, it is recommended that in the future I_{sc} as a function of light intensity is measured for all the cells in a test series in the case that changes in I_{lim} are desired to be detected. In this study, the IV results measured in the LED unit were combined with the IV results of the solar simulator to be able to reach high enough light intensities. Matching the results of the two devices was a bit cumbersome and thus it is recommended that a new, variable lighting unit that could reach 1 sun light intensity (preferably even higher intensities) would be prepared for further limiting current measurements.

used for varying the light intensity reaches just approximately 0.5 sun and this proved to be a slightly too low value for limiting current measurements. In this study, the

4.6 Results of impedance measurement results performed in dark

EIS in dark was one of the weekly measurements and it has been analyzed at the moment of 700 aging hours in accordance with SCATU IV analysis of chapter 4.3. Only groups A (unpurified MPN) and F (purified MPN) were analyzed because IV results of chapter 4.3 showed that the purity of other cell components than electrolyte solvent did not affect the cell lifetimes. Firstly, the equivalent circuit model of EIS was fitted to the measurement results. An example data and fits of both fresh and aged cell are shown in Fig. 11.

The average fitted equivalent circuit model fit parameters R_{PE} and C_{PE}, and electron lifetime in the photoelectrode, τ are shown in Figs. 12a-12c. Photoelectrode resistance R_{PE} has decreased and capacitance C_{PE} has increased slightly during the

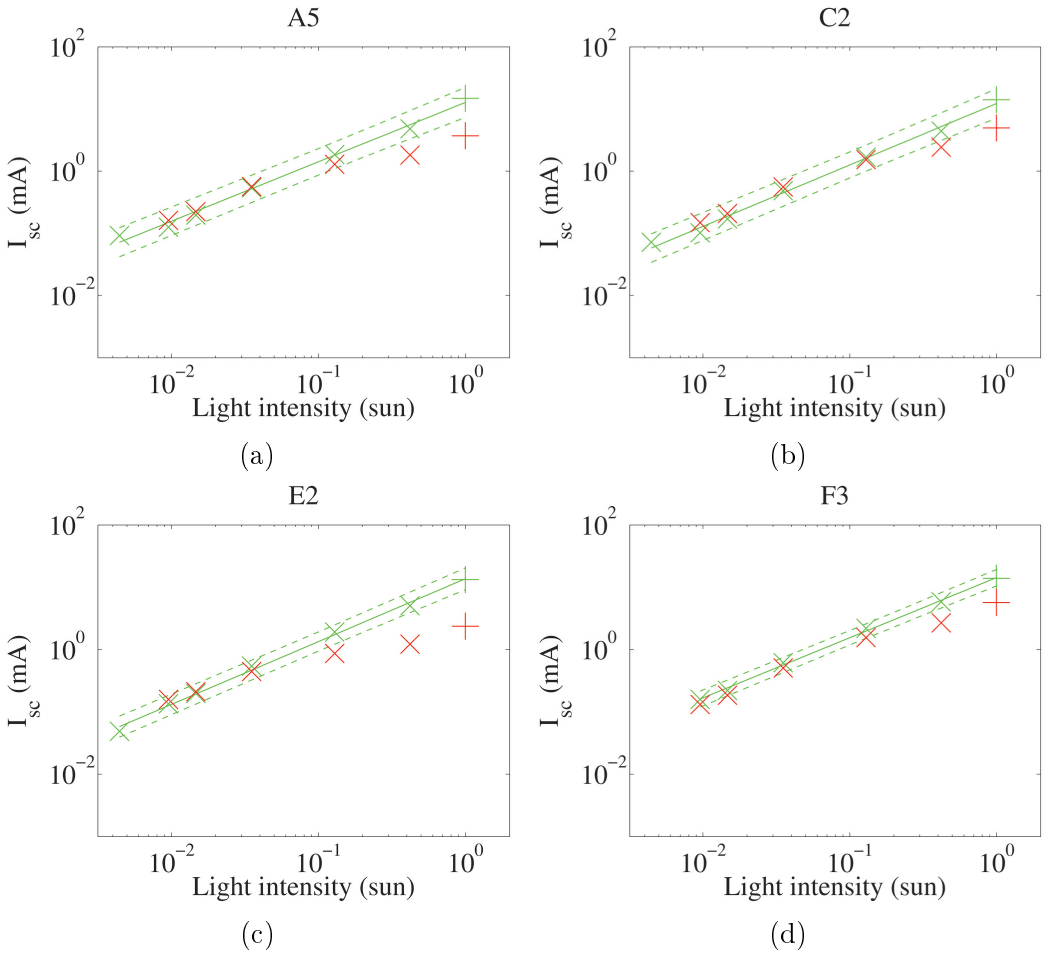

Figure 10: Results for IV curve measurements as a function of light intensity for those cells that showed degradation. Green color indicates pre-aging measurements and red color indicates post-aging measurements. Markers "x" indicate results from cells illuminated with Autolab LED and markers "+" indicate results from cells illuminated with the solar simulator, which explains why the last data point is not perfectly fitted to the curve. Regression lines and 95 % confidence intervals for the pre-aging measurements are also included.

aging in both groups. Like described in chapter 2.3.3, a decrease in R_{PE} indicates that the recombination from TiO_2 to electrolyte has increased and thus cell performance has decreased. τ seems to have improved slightly during the aging at higher voltages and decreased at lower voltages. This is probably not, however, the case. τ in Fig. 12c has been calculated as a product of R_{PE} and C_{PE} (Eq. 10) and thus the errors of both fit parameters accumulate in τ. The large errors at 0.3 V and 0.4 V in C_{PE} arise from the fact that $\log(C_{PE}(V))$ is not linear but has a steep slope at this range. Thus the slight individualistic differences between the cell result in large differences in the values of C_{PE}. The assumption that voltage over the

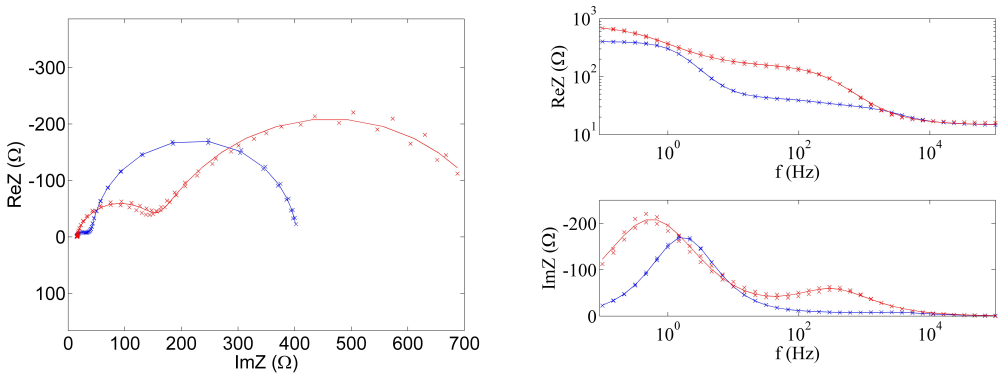

(a) (b)

Figure 11: Example data from impedance measurements performed in dark at -0.6 V. The data points marked by "x" are the actual measurement points and the lines represent the fit made to the measurement result. The data is only shown for cell A6 as the data was very alike in all the cells. The pre-aging data is blue and post-aging data is red. On the left, Nyquist curves are shown. The graph at the right side shows real and imaginary parts of the data as a function of frequence.

photoelectrode is approximately the same as voltage over the solar cell in dark, is a systematic error source in the analysis of EIS in dark results. With larger voltages the assumption does not anymore hold up because the cell current increases and thus resistive losses decrease the photoelectrode voltage. This effect could be roughly compensated by subracting the product of the average cell current (during the impedance measurement) and the total resistance of the cell from the impedance voltage. The total resistance of the cell can be approximated to be the same as the total resistance of the cell read from the Nyquist curve that has resulted from an EIS measured under illumination at open circuit voltage. This compensation would shift the curve especially at higher voltages and could improve the accuracy of estimation of τ. The compensation was not performed during this study because the focus of the study was on the comparison of cell groups and it can be deduced already from the uncompensated data of Fig. 12 that the differences between the cell groups are small even though some aging has happened in both cell groups.

In Fig. 12a, R_{PE} has been plotted in logarithmic scale which results in line graph. It is visible that the constant terms of line equations that can be denoted by $\log(R_{PE,0V})$, have decreased during the aging. The aging was evaluated also quantitatively by calculating the values of $\log(R_{PE,0V})$ (Table 7). The decrease in $\log(R_{PE,0V})$ was 10 - 20 % during the aging for both cell groups, which corresponds a decrease of quite roughly one order of magnitude in R_{PE}. This change is quite significant and it can be partly related to the changes in the shapes of IV curves

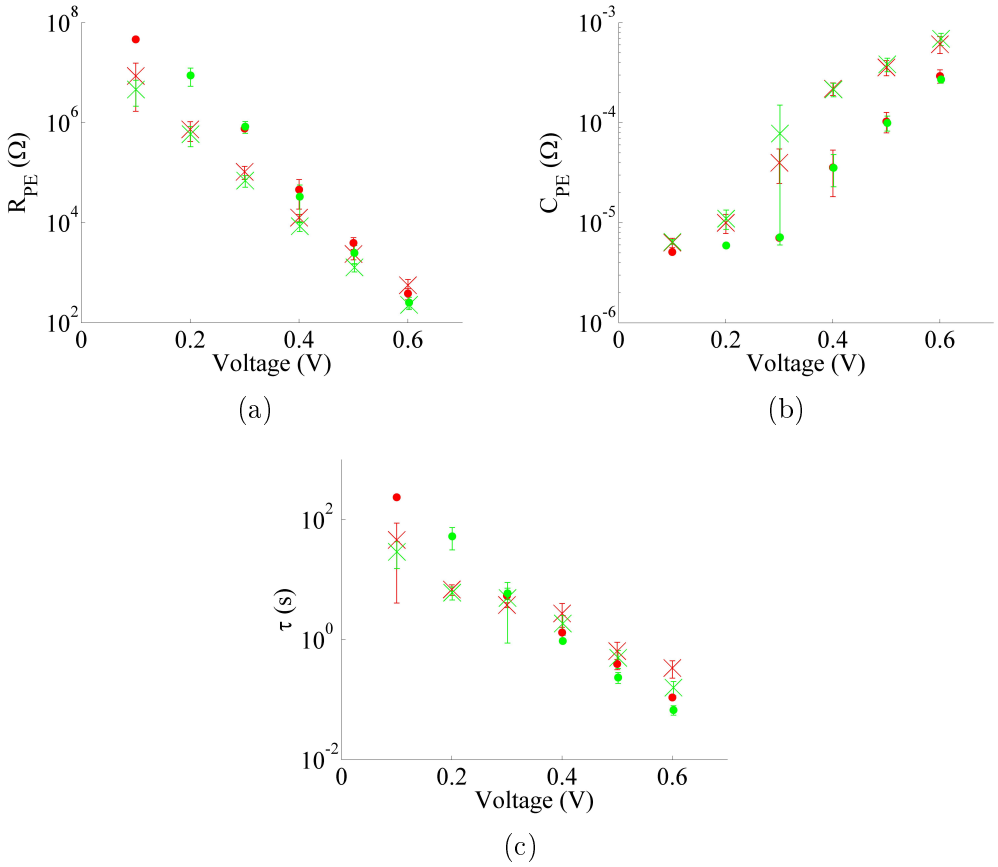

Figure 12: Average photoelectrode resistance R_{PE}, photoelectrode capacitance C_{PE} and electron lifetime τ shown as a function of impedance measurement voltage before and after the aging. Results for group A have been marked by red and results for group F by green. Markers "o" are for pre-aging and markers "x" for post-aging results. The results show standard deviations for the values.

during the aging (chapter 4.4). Based on the types of changes in the IV curves it however seems that increases in the series connected resistive losses investigated in chapter 4.7 would perhaps be more important than changes in R_{PE}. Additionally, the slope of the line in Fig. 12a has changed. This might indicate some changes in the ideality factor regarding the photoelectrode has changed. Interestingly, τ did not decrease during the aging but rather increased to some extent at high voltages (Fig. 12c). Moreover, the estimated electron diffusion length (data not shown) calculated based on the results of EIS in dark measurements had not apparently decreased during the aging, but was about 2.5 times longer than the photoelectrode depth both before and after the aging. This suggests that there were no apparent significant problems or changes during the aging in electron collection efficiency.

There were no significant differences in $\log(R_{PE,0V})$ between cell groups A and

Table 7: The charge transfer resistance between TiO_2 and the electrolyte has decreased during the aging, which is here represented by a decrease in $log(R_{PE,0V})$. The values have been calculated by fitting the EIS in dark results to the DSSC equivalent circuit model, plotting $\log(R_{PE})(V)$ and fitting a regression line to the plot by Microsoft Excel. The analyzed tests were made after 700 hours of aging.

Cell	$log(R_{PE,0V})_{initial}$ (Ω)	$\Delta log(R_{PE,0V})$ (Ω)
A1	20.0 ± 0.4	-2.2 ± 0.9
A2	22.1 ± 0.4	-4.2 ± 1.0
A3	20.1 ± 0.2	-3.8 ± 0.4
A4	23.2 ± 1.3	-3.2 ± 2.1
A5	16.7 ± 0.4	-0.1 ± 0.6
A6	20.5 ± 0.2	-4.0 ± 0.7
F1	20.9 ± 0.5	-3.2 ± 0.8
F3	20.6 ± 0.7	-4.1 ± 0.9
F4	20.1 ± 0.5	-3.9 ± 0.9
F5	20.3 ± 0.8	-3.5 ± 1.2

F even before the aging as can be seen from Table 7. As a conclusion, EIS in dark measurements did not show any remarkable differences between the studied electrolytes before or after the aging nor severe aging. Fig. 13 shows that there is no clear light intensity dependence in $log(R_{PE,0V})$, either.

4.7 Results of impedance measurements performed under illumination

EIS at open circuit voltage was measured as a part of pre- and post-aging tests and also automatically during the aging. EIS V_{oc} has been analyzed at the moment of 700 aging hours. Only groups A and F were analyzed because the IV results of chapter 4.3 indicated that these groups are good representatives of all the cells containing unpurified and purified MPN, respectively. Examples of measurement results of aged cells A6 and F1, and fits to the equivalent circuit model are shown in Fig. 14. The data in Fig. 14 illustrates that cell A6 has degraded drastically compared to cell F1.

The results of the fits of all the analyzed cells are shown in Fig. 15. The bar graph shows that there are no detectable differences between the different electrolytes initially. The differences appear just after the aging. R_{CE} and R_D are clearly higher in group A. Additionally, C_{CE} seems to have increased more in group A than in

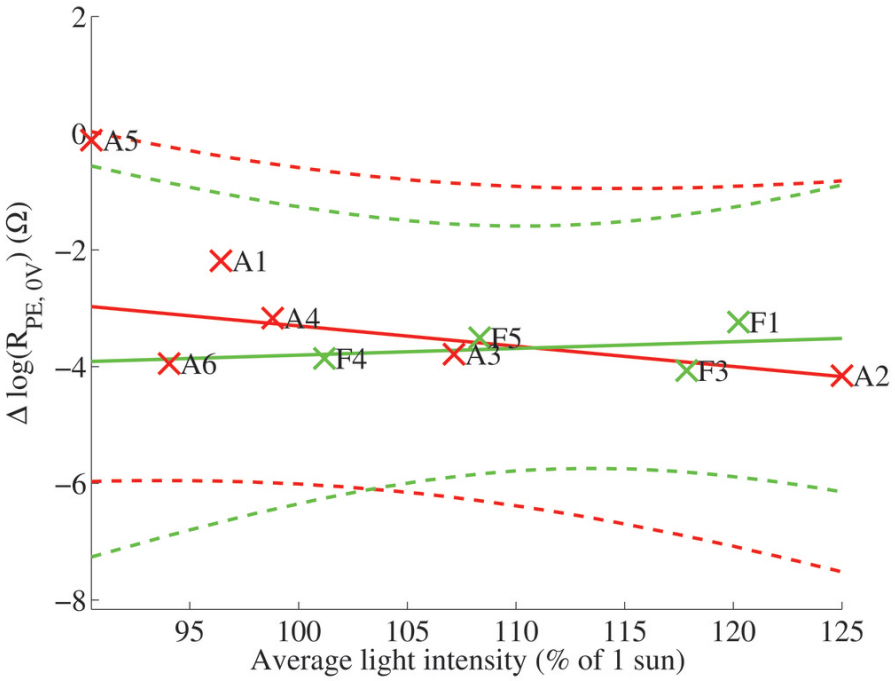

Figure 13: Small changes in the logarithm of the charge transfer resistance at 0 V have occurred after 700 hours of aging. The regression lines and 95 % confidence intervals are also shown in the plot. Red color indicates cells of group A (MPN) and the green color indicates the cells of group F (purified). The values have been calculated by fitting the EIS in dark results to the DSSC equivalent circuit model, plotting $\log(R_{PE})(V)$, fitting a regression line to the plot by Microsoft Excel and finally plotting the constant of the line equation as a function of average light intensity during the aging.

group F. These observations mean that the interface between counter electrode and electrolyte, and also the electrolyte, have degraded during the aging much more in group A than in group F. Based on the R_{CE} data alone it is not possible to say which side of the interface (or both) is responsible for the difference. The stability of R_s during the aging indicates that the cell contacts, especially silver paint, have not degraded during the aging in either cell group. In case of group F, R_{CE} has increased to some amount and R_D has approximately doubled during the aging. The series connected resistances R_s, R_{CE}, and R_D (see chapter 2.3.3) have altogether multiplied several times in group A during the aging whereas in group F the increase has been in the order of tens of percent. This might explain why I_{lim} analyzed in chapter 4.5 has decreased for cells containing unpurified MPN but not for cells containing purified MPN (with exceptions of cells F3 and C2 that had been exposed to high light intensity): in cells containing unpurified MPN series connected resistances have increased so drastically that they have already decreased short circuit currents of

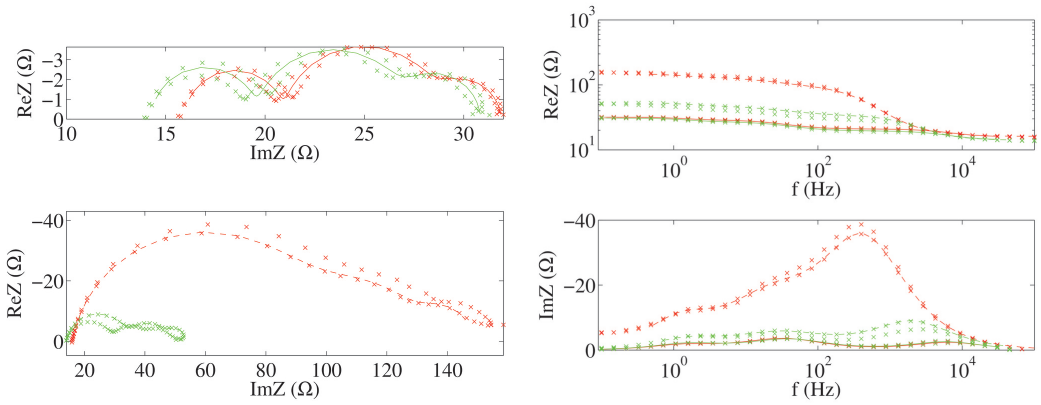

(a) (b)

Figure 14: Example data from impedance measurements performed at open circuit voltage of the cells. The data points marked by "x" are the actual measurement results and the lines represent the fit made to the measurement result. The data is shown for two typical cells, A6 (red) and F1 (green), and it includes both pre-aging (solid line) and post-aging (dashed line) measurements. On the left, Nyquist curves are shown. The graph at the top left shows pre-aging data and the graph at the bottom left shows results after 700 h of aging. The graph at the right side shows real and imaginary parts of the data as a function of frequence.

the cells whereas in cells containing purified MPN the increase in series connected resistances has not been large enough to limit I_{sc}. It has only reformated the IV curve which has led to decrease in FF of the cells.

The same post-aging data that has been shown in Fig. 15 is plotted as a function of average light intensity during the aging in Fig. 16. These graphs illustrate more clearly the difference between the two groups. Firstly, group A has degraded regardless of the applied light intensity. Secondly, standard deviations in group A are much higher than in group F, perhaps depending on the random distribution of the impurities in the unpurified electrolyte solvent.

Based on Fig. 16, R_s, R_D and C_D seem to be relatively independent of the applied light intensity, at least at this intensity scale. Instead, R_{CE} and C_{CE} seem to exhibit light intensity dependence albeit the dependence is opposite to the expected one: the parameter values seem the decrease as light intensity increases. This might implicate that data for more cells would be needed in order to be able to determine reliably the dependence of impedance parameters on light intensity during the aging.

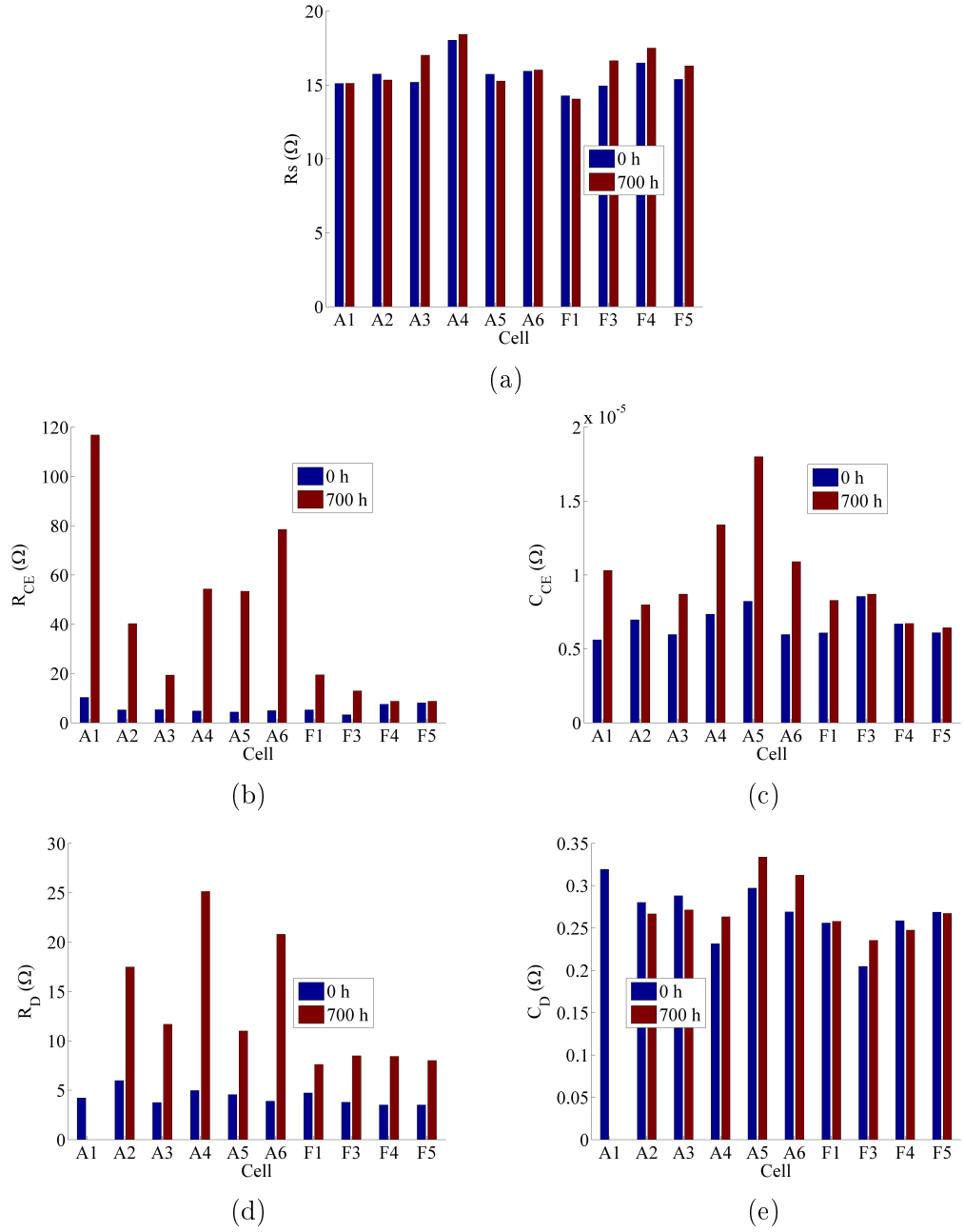

Figure 15: Results of EIS OCV measurements that were performed at the end of and after 700 hours of aging. Obtained parameters are variables of DSSC equivalent circuit model that was fitted to EIS results.

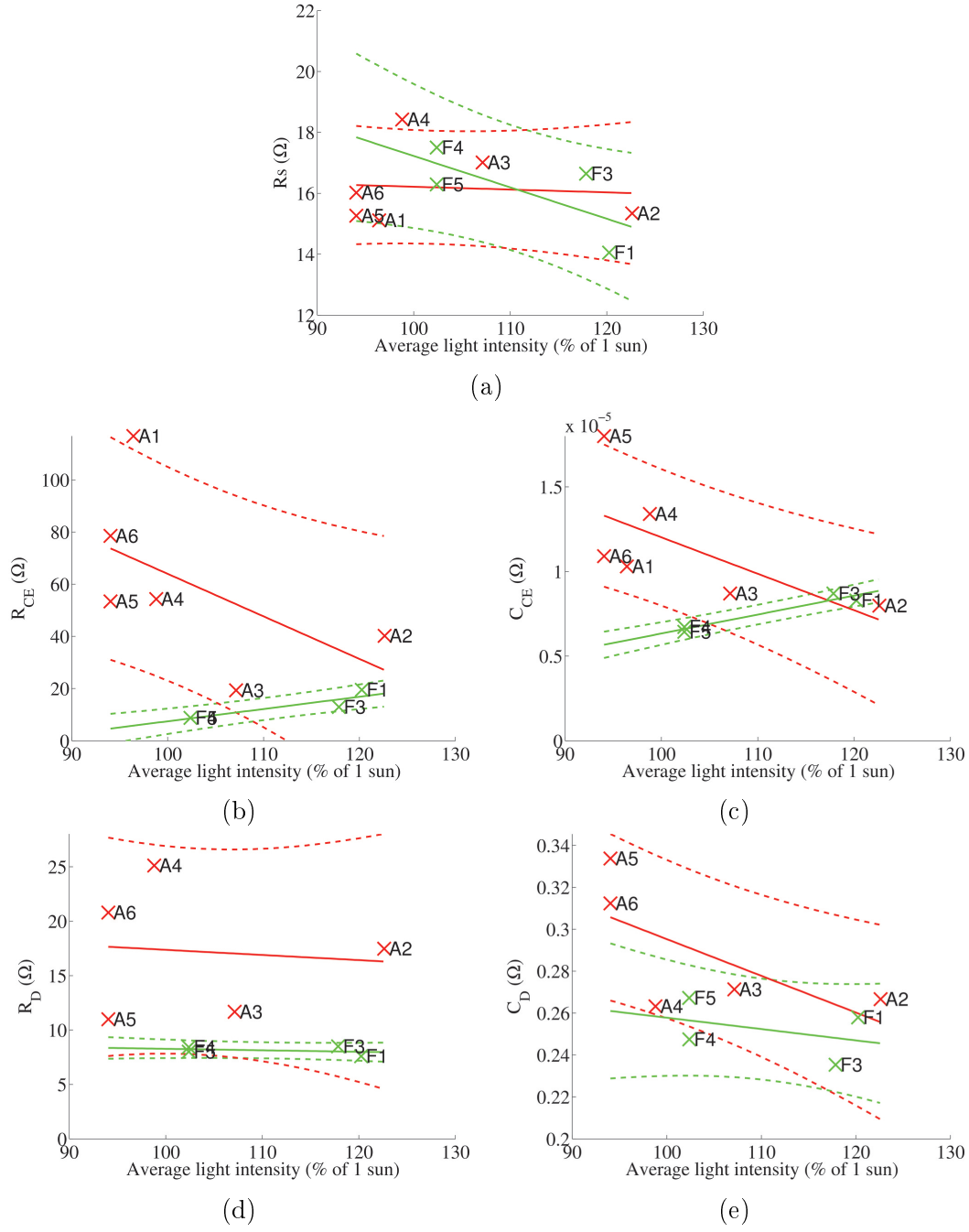

Figure 16: Results of EIS OCV measurements that were performed after 700 hours of aging as a function of average light intensity during the aging. Obtained parameters are variables of DSSC equivalent circuit model that was fitted to EIS results.

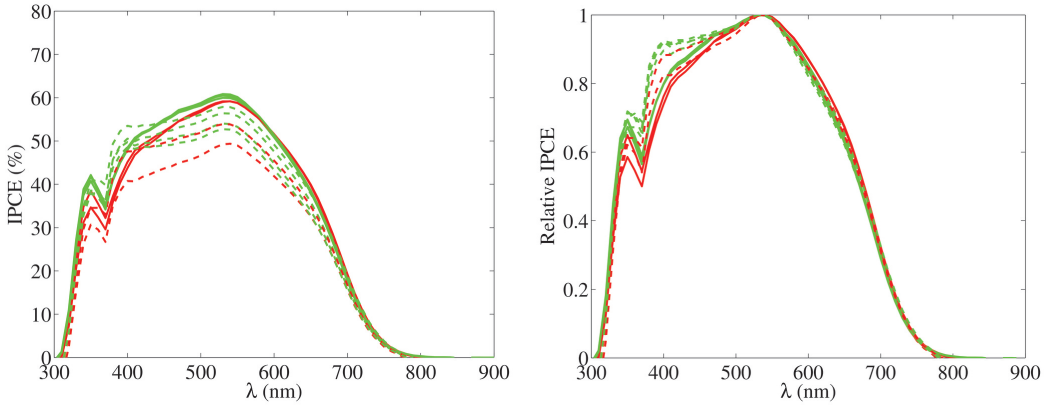

(a) (b)

Figure 17: Results of incident photon to collected electron efficiency (IPCE) measurements in absolute and relative values as a function of light wavelength. Green color indicates cells that contain purified MPN (groups B-D and F) and red color indicates cells with unpurified MPN (groups A and E). One cell for each group has been measured. Solid lines mark the pre-aging measurements and dashed lines mark the post-aging measurements.

4.8 Quantum efficiency measurements

The results of IPCE measurements are shown in Figs. 17 and 18. In the initial measurements cells containing unpurified MPN (A5 and E1) performed slightly worse, i.e. absolute IPCE values of A5 and E1 at wavelengths 320 - 600 nm were a bit lower than the corresponding values of the other cells. Nonetheless it is not certain that this difference would be caused by differences in the dyes and not just by random variation in cell assembly, because there were just two measured cells, A5 and E1, containing unpurified MPN.

Initially, peaks are at the same wavelengths for all the cells. After the aging the original peaks have not moved but there has appeared an extra peak at 400 nm for all the cells aged under illumination. This peak has very likely appeared because the electrolyte has bleached and e.g. iodine in it absorbs less light at the shorter wavelengths [50] allowing dye absorb more light in this wavelength area. It is also noteworthy that the new peak does not appear in the IPCE curves of reference cells E1 and F2 that have been stored in dark and do not apparently have bleached. Thus, the electrolyte bleaching seems to be a photoinduced effect.

It has been explained in chapter 2.3.2 that decrease in η_{IPCE} can result from decrease in four main factors: η_{LH} that is light harvesting efficiency of the dye, η_{INJ} that is electron injection efficiency from the dye to TiO_2, η_{COL} that is electron collection efficiency of the injected electron to the external circuit and η_{REG} that is

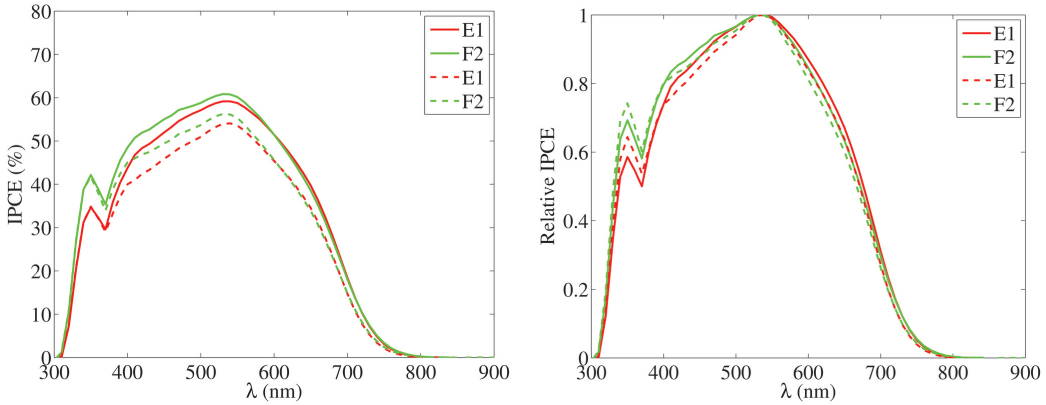

(a) (b)

Figure 18: Results of incident photon to collected electron efficiency (IPCE) measurements in absolute and relative values as a function of light wavelength for reference cells that were not aged in light. Green color indicates cell F2 and red color indicates cell E1. Solid lines mark the pre-aging measurements and dashed lines mark the post-aging measurements.

dye regeneration efficiency. η_{INJ} is independent of wavelength, whereas η_{COL} and η_{LH} are dependent on wavelength. The effect of η_{REG} can not be separated from the effect of η_{INJ} based on this measurement. It can be interpreted from IPCE results that initially, cells with unpurified MPN might have had slightly lower η_{INJ} or η_{REG} since there is an overall decrease in the IPCE rather than a wavelength dependent one. η_{INJ} or η_{REG} also decrease during the aging, but not drastically. Changes in η_{COL} and η_{LH} seem to be very small apart from the extra peak that has appeared because of bleaching of the electrolyte which has improved η_{LH} at those wavelengths. Altogether, IPCE results show that dye and photoelectrodes in the studied cells operate relatively well and strongly degraded cells have aged mainly because of some other reason.

Electrolyte transmission results are shown in Figs. 19 and 20. The results are quite similar for all the cells. Transmission at the shorter wavelengths where electrolyte components, e.g. iodine, absorb light [50], is higher after the aging than before it. This observation verifies the conclusion drawn already from IPCE measurements: electrolyte in all the cells has bleached during the aging.

The dip in some graphs just below 600 nm is a local error caused by the measurement device. Deviations in the results may be caused by the fact that there was quite a small area in each cell that contained electrolyte but no photo electrode. This area included also the electrolyte filling hole. Thus it was difficult to fix the beam of the measurement device to such a point of the cell that it contained just electrolyte.

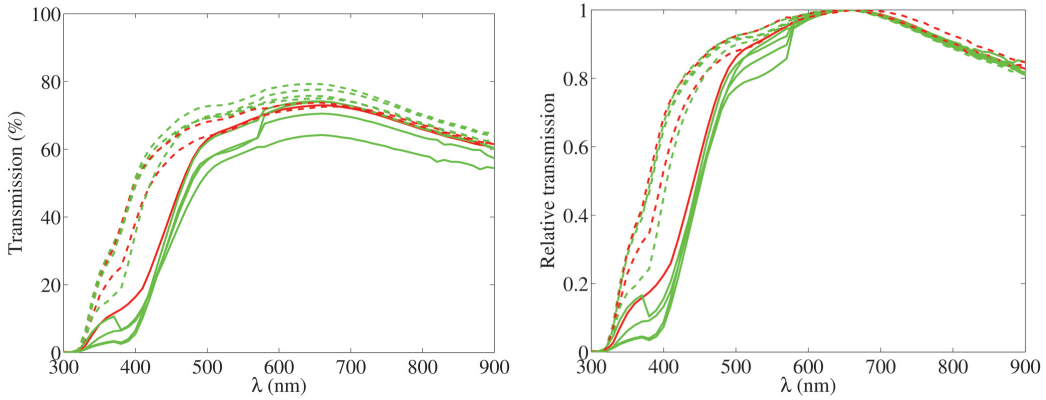

(a) (b)

Figure 19: Results of electrolyte transmission measurements in absolute and relative values as a function of light wavelength. Green color indicates cells that contain purified MPN (groups B-D and F) and red color indicates cells with unpurified MPN (groups A and E). One cell for each group has been measured. Solid lines mark the pre-aging measurements and dashed lines mark the post-aging measurements.

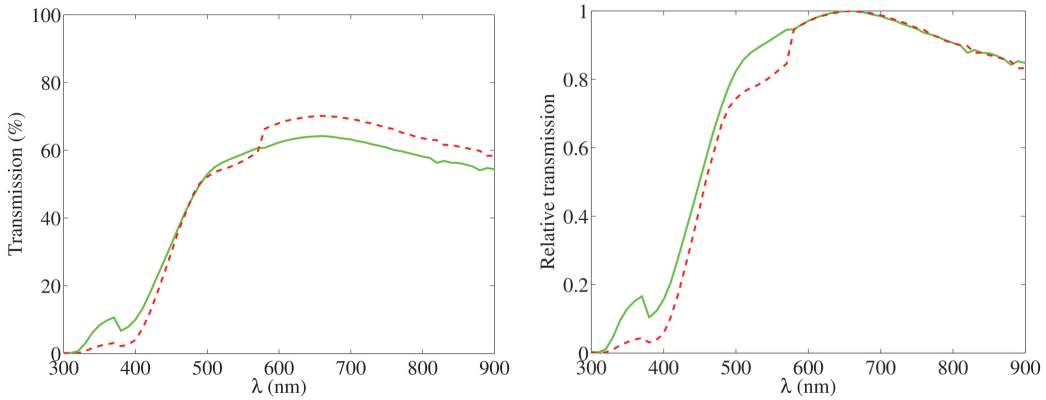

(a) (b)

Figure 20: Results of electrolyte transmission measurements in absolute and relative values as a function of light wavelength for reference cells that were kept in dark during the aging test. Green solid line indicates pre-aging measurement of cell F2 and red dashed line indicates the post-aging measurement of cell E1. Unfortunately, the pre-aging measurement for cell E1 and post-aging measurement for cell F2 failed.

A radical example of the difficulty in the cell placement to the measurement device is that data from both cells E1 and F2 had to be left out of investigation because the data seemed like the measurement beam had accidentally been targeted completely on bare glass instead of electrolyte. Fig. 20 contains just pre-aging data of E1 and post-aging data of F2, but it can be seen that bleaching has not occurred at least in cell F2 during the storage in dark. Observation by eyesight also confirmed that both

reference cells had a similar, unbleached color after the storage in dark. This observation in turn supports the conclusion drawn already from the IPCE measurements: bleaching seems to be a photoinduxed effect.

4.9 Liquid chromatography - mass spectroscopy measurements

LC-MS measurements can be used for analysing changes in the dye (see chapter 2.3.4). One cell for each cell group was analyzed and all the cells were analyzed only after the aging because LC-MS is a destructive measurement technique. Thus, the aged cells were compared to the reference cells E1 and F2 that had been kept in dark during the aging test, and to the test results of pure dye. The results of LC-MS measurements supported the conclusions made from IPCE tests: all the aged cells were found to have degraded to some extent through ligand substitution reactions but apparently there were no differences in the degradation between the cell groups. An example of the resulting LC-MS data is shown in Fig. 21 and Table 8. The amount of degradation products can be determined roughly in LC-MS but determination of the actual amounts of the dye complexes is not possible by LC-MS.

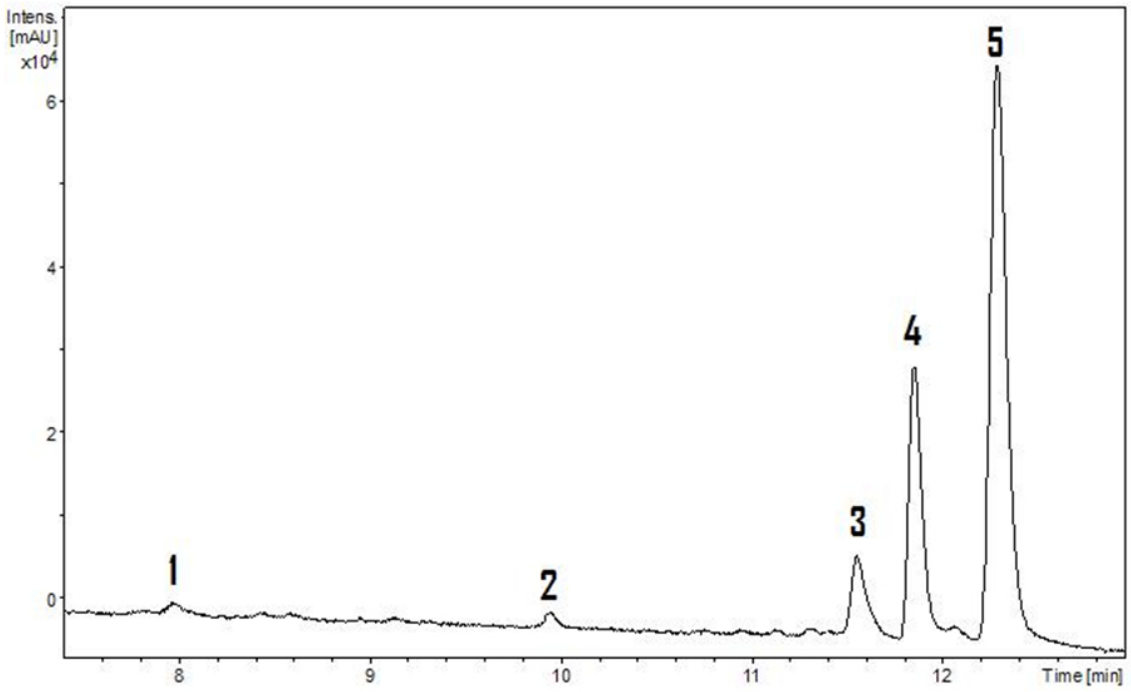

Figure 21: A sample UV-chromatogram from one of the aged cells that has been measured with LC-MS method (see Table 8 for peak identifications).

The major impurity in the aged dye is [RuL_2(NCS)(MBI)], a complex resulting from ligand exchange between the dye and NMBI that is an electrolyte com-

Table 8: Identifications of the peaks in the UV-chromatogram of Fig. 21.

Peak	m/z	Ruthenium complex	Description
1	662.99	[RuL2(NCS)(H2O)]	Minor impurity formed in the cell even in dark.
2	731.03	[RuL2(NCS)(MPN)]	Minor impurity formed in the cell even in dark.
3	704.96	[RuL2(NCS)(SCN)]	Impurity present in fresh self-made dye.
4	778.04	[RuL2(NCS)(MBI)]	Major, photo-induced impurity.
5	704.96	[RuL2(NCS)2] or N3 (fully protonated N719)	Dye.

ponent. Interestingly, this impurity was not present in the reference cells which indicates that $[RuL_2(NCS)(MBI)]$ is a photoinduced impurity. $[RuL_2(NCS)(SCN)]$ is an isomer of N719 dye that is not as effective in electron injection as N719. It is often removed from the dye to increase cell efficiency but in this study the focus was on differences between the electrolytes and thus the isomer was not removed. $[RuL_2(NCS)(MPN)]$ and $[RuL_2(NCS)(H_2O)]$ were minor degradation products in the dye and they were present in both aged and reference cells but not in the fresh dye. Thus LC-MS suggests that the amount of $[RuL_2(NCS)(H_2O)]$ in the dye is not dependent of the amount of water in the cell (supposing that unpurified electrolyte solvent contained water as an impurity). It is, however, possible that there actually were larger portions of water complexes in the dyes than LC-MS suggests because $[RuL_2(NCS)(H_2O)]$ was unstable in the solution that was used for the extraction of the dye. $[RuL_2(NCS)(MBI)]$ is approximately two times less efficient dye than N719 [51] but the effectiveness of $[RuL_2(NCS)(MPN)]$ as a dye has apparently not been studied. Interestingly, the degradation products listed in Table 8 have not apparently been reported to have formed during low temperature aging but only during high temperature aging [24, 51].

As a conclusion, based on LC-MS measurements it seems that dye degradation has happened during the aging to some extent but not so much that it would explain the decrease in cell efficiencies. The analysis of IPCE results in chapter 4.8 lead to this same result. Appearance of $[RuL_2(NCS)(MBI)]$ only in the cells aged in light is an interesting observation that could be worth further studies.

4.10 Raman spectroscopy

Raman spectroscopy is used for identifying molecules by their resonance vibrational frequencies and observing the changes in chemical bonds (see chapter 2.3.5 for Raman theory). One aged cell for each cell group was measured. The measured Raman spectra that have been divided by the intensity of the TiO_2 peak (145 cm^{-1}) in the spectrum, are shown in Fig. 22. The analysis was decided to be performed in relative means rather than by comparing absolute peak intensities because the overall spectra intensities seemed to have approximately halved during the aging, which could mean that the measurement conditions had not remained constant between the pre- and post-aging measurements. Additionally, the peak intensities were compared by heights (after having performed a linear baseline fit) rather than by areas because the peak shapes remained quite similar. This is, however, one error factor in the Raman analysis. It can be observed from Fig. 22 that no new peaks have apparently formed and the initial peaks have seemingly not moved in the spectra during the aging test.

The intensities of tri-iodide and dye peaks of each measured cell in pre- and post-aging tests are shown relative to TiO_2 peak intensity in Tables 9 and 10. The results are a bit surprising because the dye and tri-iodide peaks seem to have gained strength during the aging. This would mean that the concentrations of the dye and tri-iodide have actually increased during the aging test, which does not seem reasonable. The increase is however not large (apart from cells B6 and F1) and is probably related to the same changes in experimental setup that lead to the decrease in overall spectra intensities in all the measured cells. Cell B6 that differs from the other cells by strongly increased relative tri-iodide peak, was detected to have leaked during the last days of the aging test by examining the cell photographing results. The electrolyte leakage is probably the reason for the seemingly increased tri-iodide concentration as this significantly alters the optical properties of the solar cell, affecting also Raman results. The result of cell F1 is suspected to be a result of a slightly imprecise focus during the Raman test because it should not be possible that the amount of dye would increase during the aging as drastically as the test result indicates.

In Table 11, the initial TiO_2, I_3^- and dye peaks are compared to the post-aging values. Table 11 shows the already mentioned decrease in Raman spectra intensities because the average peak ratios are clearly over two. This might indicate that the overall change in Raman intensities explains the altered results for cells for cells of series B, C, and E, meaning that there is no major apparent changes in the Raman

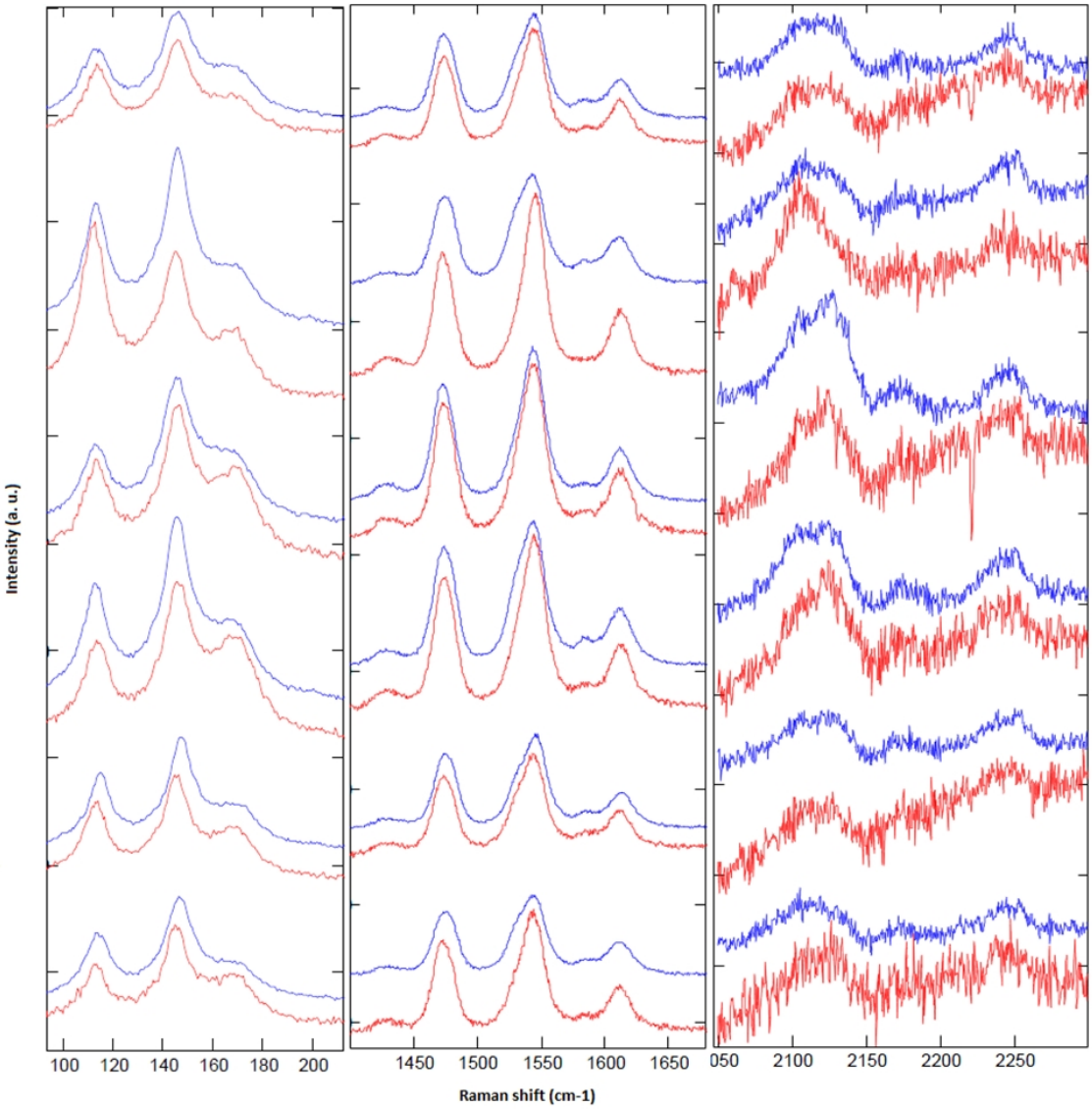

Figure 22: Raman results for all the test cells measured with D1 filter. Cells are cells are shown in alphabetical group order from top to bottom. The pre-aging results are marked by blue color and post-aging results by red color.

results of these cells after the aging. In Table 11, cells A1/A6 and F1 also differ from the average value, A1/A6 by less decreased and F1 by more decreased overall peak intensity. Additionally, cell E1 seems to have a bit lower peak intensity. The result for F1 might be a result of the already proposed imprecise focus during the measurement. The observations about differing Raman results for cells A1/A6 and E1 are intriguing because during the previously analyzed tests in this study, it has become clear that the cell groups A and E containing unpurified electrolyte differ from the other cells by having aged faster.

Table 9: The intensities of I_3^- peak (113 cm^{-1}) of each cell shown relative to the intensity of TiO_2 peak (145 cm^{-1}).

	A1/A6	B6	C1	D1	E5	F1
Pre-aging	0.79	0.80	0.77	0.78	0.81	0.80
Post-aging	0.87	1.09	0.82	0.80	0.86	0.79

Table 10: The integrated intensities of N719 peaks (1400-1700 cm^{-1}) of each cell shown relative to the intensity of TiO_2 peak (145 cm^{-1}) and normalized by the highest ratio value (post-aging of F).

	A6/A1	B6	C1	D1	E5	F1
Pre-aging	0.91	0.67	0.73	0.78	0.75	0.71
Post-aging	0.92	0.79	0.89	0.82	0.82	1.00

The decreased intensity of tri-iodide peak has, however, been linked to the decrease in tri-iodide concentration, at least at high aging temperatures, in literature [52]. Thus the results of Raman seem to suggest that cells A1/A6 and E1 have degraded less than the other cells. It is possible that the result presented here, implicating that the peak intensities could increase more in more degraded cells in some occasions, results from a real phenomenon. Some examples of possible candidates for a such phenomenon are that the changes in the optical properties of the molecules affect the light absorption, or that the electronic structure of the molecules have changed so that the Raman peaks have not moved significantly but instead the intensities of the peaks have changed. At the moment, the result can however also be explained by the fact that in group A, a different cell was measured in pre- and post-aging results, and by denoting that the slightly lower results for cell E5 have resulted from the overall variations in the measurement. Thus, any reason for the observation that peak intensities seem to have decreased less in cells containing unpurified MPN, can not reliably given based on these Raman measurements. More measurements would be needed for a reliable analysis: firstly, to ensure that the Raman results shown here are not distorted by the changed measurement setup, and secondly, to be able to confirm that the results have not arisen from the individual variations between the cells instead of variations between the groups. For future tests, the measurements of reference cells kept in dark at low temperature during the aging are also recommended in order to track the possible changes in the

Table 11: The ratios of TiO_2, dye and I_3^- peak intensities (see Tables 9 and 10) at pre- and post-aging measurements for each cell group. Additionally, the average changes for all the measured cells have been shown.

Peak	A1/A6	B6	C1	D1	E5	F1	
TiO_2	1.58	2.72	2.56	2.31	1.99	4.64	2.63
I_3^-	1.44	1.99	2.43	2.24	1.88	4.72	2.45
Dye	1.56	2.29	2.11	2.17	1.82	3.29	2.21

measurement setup more precisely.

As a conclusion for the Raman results, no differences between the cell groups could not be reported by a full confidence. This results from the probable changes in the measurement setup between the two testing times and from the small amount of studied cells. Thus, more studies regarding the utilization of Raman tests in analysis of cell aging are recommended.

4.11 Cell photographing

Cell photographing can be utilized for tracking the iodine concentration of the electrolyte during the aging if the measurements are performed with a technique described in chapter 2.3.6. The photographing results for the electrolytes of the cells are shown in Fig. 23. In the resulting figure, the cells have been divided in two groups: cells containing unpurified MPN (cell groups A and E) or purified MPN (cell groups B-D and F). This way of presenting the data was chosen because cell groups A and E were the only groups differing from the other groups.

The red and green pixel values in Fig. 23 remain stable in both presented groups during the whole aging period. This indicates that there has not occurred significant dye desorption to the electrolyte during the aging. Blue pixel values of Fig. 23 are changing at the beginning of the aging and stabilize to quite constant level at the latter half of the aging period. The increase in the blue pixel values is clearly faster in cells containing unpurified MPN during the first couple of hundred hours of the aging. These observations indicate that the yellowish color of the electrolyte (caused by iodine) bleaches in both groups during the aging, yet the bleaching is much faster in cells that contain unpurified MPN.

Probably, the stabilization of blue pixel values at the final half of the aging does not mean that the bleaching of the electrolytes has ended. Instead it is more likely that the iodine concentration reaches the lower limit of the accurate observation

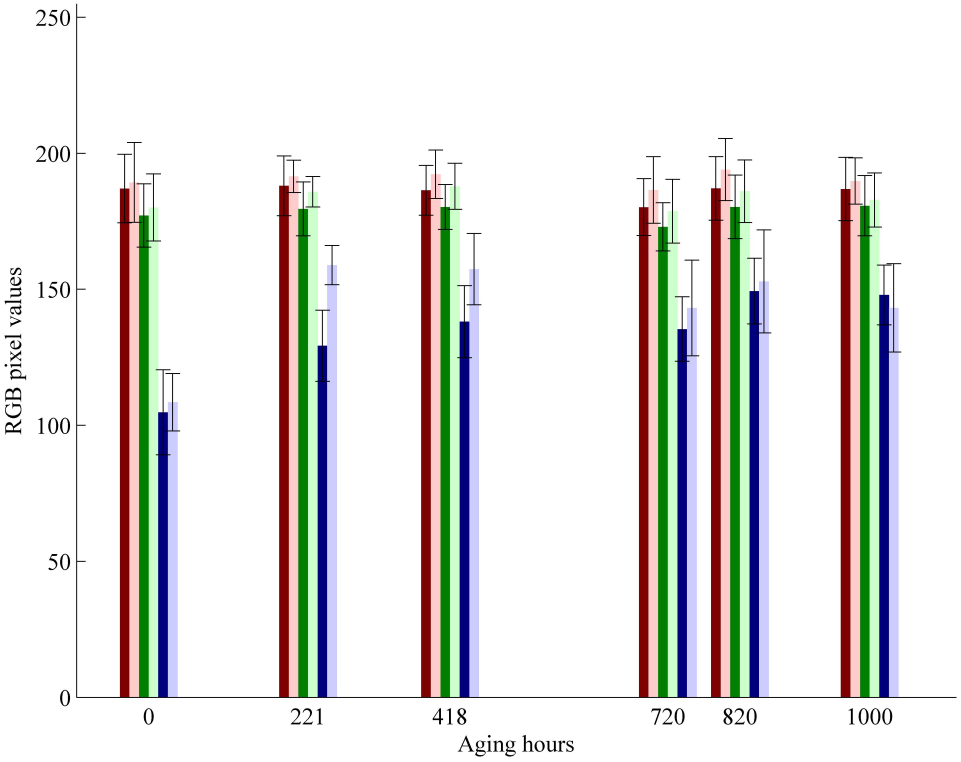

Figure 23: The average RGB values as a function of aging hours. Also the standard deviations of the values are shown. Red, green and blue bars indicate red, green and blue pixel values, correspondingly. Bars that consider cells containing purified MPN (groups B-D and F) are dark colored and bars that consider cells containing unpurified MPN (groups A and E) are light colored.

area of photographing technique and thus the changes are no more recorded. This assumption gets support from the fact that blue pixel values analyzed on areas close to cell electrolyte but containing just bare TCO glass were in average 165±20 pixels for a few cells that were checked. As the other electrolyte components, apart from iodine and PMII, are colorless, bleaching means that the blue pixel value of the electrolyte approaches the blue pixel value of the bare glass. It can also be noticed that all the pixel values at 720 h point are lower than the other bars, meaning that the photographs were darker at this point of time. This might be caused by LED lamps which batteries were running low in the photographing system but not so low that lower light intensity was apparent directly by eyesight. The batteries were changed by the next measurement. Additional problem was caused by epoxy glue: the cells had been glued quite heavily in order to prevent electrolyte leakage during the aging but unfortunately the counter electrode side of the cells became

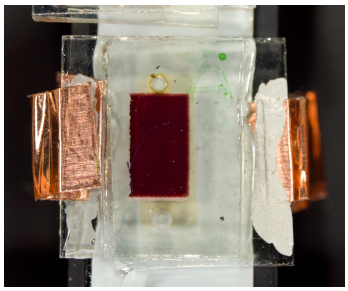

Figure 24: Photograph of cell D4 that has been taken after 418 hours of aging.

uneven and created more shadows and reflections to the photographs. This increased standard deviations of the photographing results. An example about the shadowing is shown in Fig. 24. Thus it is advisable for further tests to use plenty of epoxy glue but dry the cells in such position that the running marks of the glue form to the photo electrode sides of the cells.

4.11.1 Connection of ultraviolet light and electrolyte bleaching

Fast aging of all the cell groups in this study, even group F that contained only purified electrolyte components, has become evident in the previous chapters but it was not expected beforehand. It has become clear already in previous chapters that the photoelectrodes of the cells did not degrade drastically and thus the reasons for fast aging had to be searched elsewhere. Bleaching of all the cell groups during the aging offered an important hint for the analysis of the reason to unexpectedly fast aging of the cells. It has been explained in chapter 2.2 that one suspected reason for electrolyte bleaching has been UV exposure. Thus the illumination spectrum of the light soaking lamps was evaluated and compared to the AM 1.5G illumination spectrum. The resulting graphs are in Appendix B and they show that the amount of UV illumination, one fifth of the UV illumination in AM 1.5G spectrum, is actually so large that it might have affected the cell degradation. The remaining question is, why passed 1000 hours aging tests have been performed with the same light soaking device before [53–55]. This subject was decided to study alongside further photographing result analysis by a comparison test that has been is described in chapter 4.11.2.

4.11.2 Estimation of iodine concentration in the cells during the aging

The resolution of iodine concentration estimation by cell photographing has been calculated to be $7.35 \cdot 10^{-4}$ M per blue pixel within 0.025-0.1 M iodine in article [30].

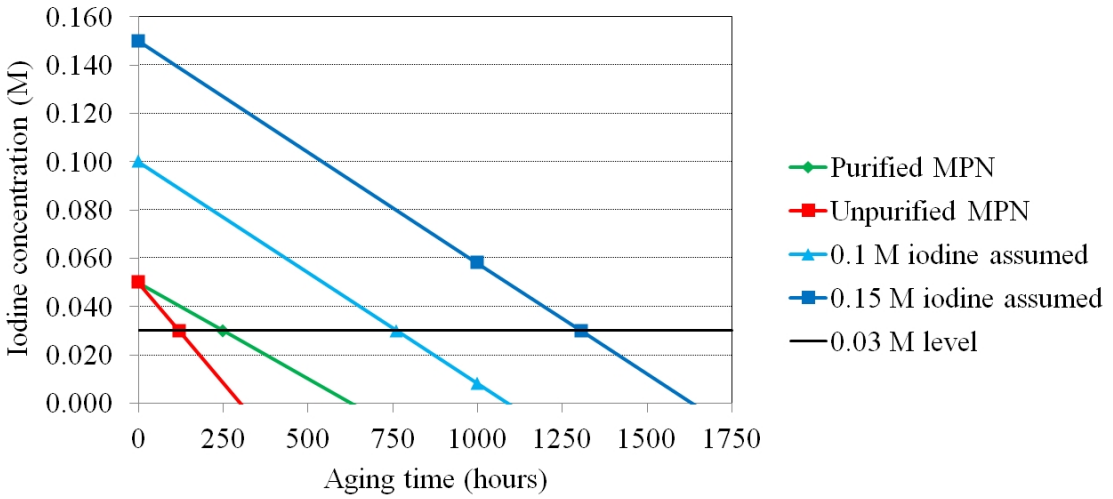

Figure 25: The estimated decrease speed of iodine consentration during the aging. The estimate has been made on the basis of the average cell photographing results and literature [30]. Red and green lines present the cells measured in this thesis. Blue lines present the assumed degradation pace for electrolytes containing 0.10 M and 0.15 M iodine. The commercial electrolyte used in [30,53–55] has been estimated to have iodine concentration in range of 0.10-0.15 M based on electrolyte color.

Based on this assumption and the change in blue pixel values during the first 221 hours of aging (Fig. 23), the estimated decrease in iodine concentration as a function of aging hours has been plotted in Fig. 25. Additionally, the 0.03 M iodine level has been marked in the graph because it has been detected to be the approximate limit below which the low iodine concentration starts to affect the output current of the cell [56]. At 0.02 M the limiting current of the cell is already smaller than I_{sc} of the cell [56]. The red and green lines in the figure represent the cells of this study. In this kind of plot the drastic difference in the bleaching speeds of cells containing purified and unpurified MPN is even more clearly visible than in Fig. 23: cells with unpurified MPN cross 0.03 M line after 120 hours of aging and cells with purified MPN just after 250 hours of aging. One suggestion for the reason of different bleaching speeds of the cells containing purified and unpurified MPN is that unpurified MPN contains more water that reacts with TiO_2 when exposed to UV light.

A straightforward thought arising from red and green lines in Fig. 25 is that would the cell performance remain stable for a longer time if just more iodine would be added to the electrolyte. The experimental confirmation of this question was not in the scope of this thesis, but some calculations were done based on aging data presented by Asghar et al [30]. The most remarkable difference between Asghar's

cells and the cells aged in this study is that Asghar's cells contained commercial Dyesol HSE-EL electrolyte which has been used in cells that have passed 1000 hours aging tests [53–55]. Additionally, Asghar's cells had been aged under UV lamps that emitted four times more UV light than the aging lamps used in this study (see appendix B). Thus, the rate of the change in blue pixel values of these cells (data presented in article [30]) was multiplied by four, and the slope of change in iodine concentration of the cells was calculated in the similar way than previously. Remarkably, the slope was basically the same as in the cells of this study containing purified MPN. This suggests that the commercial electrolyte known for stability bleaches at the same rate as electrolyte containing purified MPN. The same slope also supports the hypothesis of cell degradation caused by UV that has been presented in chapter 4.11.1 because the cells of article [30] are mainly UV-degraded.

The exact iodine concentration of the commercial electrolyte is unknown but based on electrolyte color it can be estimated to be significantly larger than 0.05 M concentration used in this thesis. As informed guesses, the slope of change in iodine concentration calculated from the photographing data of the article was combined with the initial iodine concentration estimates of 0.1 M and 0.15 M. The resulting lines are shown in Fig. 25 marked with blue color. The lines of 0.1 M and 0.15 M electrolytes cross the 0.03 M limit just after 760 and 1300 hours of aging, respectively.

This leads to two deductions: Firstly, increase in iodine concentration of electrolyte containing purified MPN might lead directly to stability of cell performance during 1000 hours aging test. This would explain why the cells degraded quickly in this study while earlier similar stability studies have passed the 1000 hours test. Secondly, even the amount of UV that seems minor is probably a significant factor in cell stability tests and thus it should be reported accurately in research works considering cell stability.

4.11.3 Comparison of photographing results to IV aging data

The estimated aging durations after which the decrease in iodine concentration starts to limit cell current were presented in chapter 4.11.2. This estimation can be compared the IV aging data of the cells that is presented in appendix A. Apart from cells A3 and E3, all the cells in groups A and E follow the prediction of Fig. 25 amazingly well: short circuit currents of the cells start to decrease just after 120 hours of aging.

However, for the cells with purified MPN this drop in I_{sc} is not as clear and some of the cells seem to have even practically constant I_{sc} during the aging test.

This difference between photograph-based prediction and actual IV data can be interpreted from two different perspectives: either it is caused by measurement errors, or I_{sc} is affected also by other factors than mere iodine concentration. Naturally, it is also possible that the both perspectives are partly correct.

Firstly, the error perspective is presented. Assuming that the slope of the change in blue pixel values is reliable, perhaps the most probable explanation for the difference is based on spatial distribution of the iodine in the cell. It has been detected in ongoing studies by Mr. Sami Jouttijärvi that at least in short circuited circumstances iodine diffuses to the cell area that contains also the dyed photoelectrode. In this case, the electrolyte outside the photoelectrode would look more transparent, and that is why concentration of iodine and I_{sc} of some of the cells would be larger than cell photographing suggests.

From the second perspective, in the photographing analysis currently only iodine is assumed to contribute to I_{lim}. There could also exist some additional charge carrier in the electrolyte, e.g. a reaction product of iodine and electrolyte impurities, that maintains I_{lim} and thus also I_{sc}. One proposition for the transparent charge carriers is a reaction product of hydroxyl groups (OH^-) and tri-iodide [22]. Addition of same amount of NaOH as iodine to electrolyte has been tested for intentional bleaching of electrolyte in order to improve cell efficiency [56]. This attempt did not work very well because I_{sc} of the cell decreased and R_s increased resulting in low FF and η [56]. This description of IV curves of intentionally bleached actually fits quite well to the aged IV curves in this study that have been described in chapter 4.4. As a speculation, OH^- groups could be introduced to the cell e.g. because of UV-induced reactions between water and TiO_2.

Both hypotheses could perhaps be verified by combining two experimental techniques: photographing the cells containing a TiO_2 scattering layer also on the counter electrode side, and IV measurements in dark. The scattering layer is white in color so the potential spatial distribution of the electrolyte would be noticed. IV measurements in dark are a traditional way of determination of I_{lim} and thus the electrolyte concentration predictions of cell photographing could be compared to IV in dark measurements. It has actually already been detected that I_{lim} calculated from the IV in dark measurements is higher than the iodine concentration calculated from cell photographing results predicts [30]. However, counter electrode side photographing has not yet been performed. Additionally, if it will be confirmed that there appears some transparent charge carriers in the cell, further investigations about the composition of these carriers will be needed.

5 Summary

In this study three main questions were studied: Firstly, could purification of electrolyte components affect the initial cell performance? Secondly, could purification of electrolyte components increase the cell lifetime? The third question, arisen during the study, was that what is the cause of the unexpectedly fast degradation of all the test cells in the aging test.

The answer to the first research problem is clear. Initial cell performance does not seem to be affected by the purification of electrolyte components. No differences were found either in the initial efficiencies of the cells nor in any of the numerous other tests performed in this study.

The second research problem is also solved. Based on this study, cell lifetime indeed increases as a result of purification of electrolyte solvent (methoxypropionitrile in this case). The purification of the other electrolyte components did not lead to apparent improvements in the cell lifetime. Based on the performed tests, the cell degradation results from similar mechanisms in the cells containing purified and unpurified solvent but degradation rate is clearly faster in the cells containing unpurified solvent. The photoelectrodes of the cells seem to have degraded only slightly during the aging but evidently, the electrolytes have degraded massively through visually detectable bleaching. Additionally, counter electrode degradation is possible as the effects of degradation in the electrolyte and at the counter electrode can not be fully separated from each other based on the tests performed in this study. Because of bleaching, the amount of charge carriers in the cells has decreased leading to a decrease in the limiting currents of the cells. In most cells, the decrease has been large enough to affect also the short circuit currents of the cells. The progressive bleaching has increased also the series connected resistances in the cells leading to a decrease in fill factors of the cells. This effect is manifested especially dramatically in rapidly degrading cells containing unpurified solvent, as the resistances have increased so much that the IV curves of the cells have turned to mere descending lines.

A very plausible explanation to the third problem, regarding to the fast aging of the cells, has also been found. It was detected that the lamps used in the aging system emitted a small portion of UV light that has been related to electrolyte bleaching. The bleaching rate of the cells that contained purified solvent was compared to another study [30] that was performed with iodine-based electrolyte that is known to be stable. When the amount of UV of the lamps used in the latter study was proportioned to the amount of UV of the lamps in this study, the rates

of bleaching in the cells were discovered to be basically the same. This means that the fast bleaching of the electrolyte in this study was very likely caused by UV but progressed much faster in the cells containing unpurified electrolyte solvent. It is possible that in the presence of UV, TiO_2 reacted with some impurity of the solvent, most likely water, and that the electrolyte containing unpurified solvent bleached faster because it contained more of this impurity.

There was also a secondary objective for this study; the determination of optimal way of performing long aging studies. The methods used in this study offer a good framework for long-term aging tests as all the applied procedures and performed tests were afterwards assessed to have been useful. This conclusion is not actually the one that had initially been hoped for because performing a large variety of tests for large cell series is very laborious. The advantage gained in performation of partly overlapping tests is however that the tests support each other if the differences between the cell groups are not very clear. Reduction of the workload by leaving a part of the cells out of manual tests is not recommended, either, because each time some of the cells had intentionally not been measured during this study, it was later detected that the result analysis would have benefited from additional data. The amount of work in cell analysis can instead be decreased by paying special attention to the very careful minimization of variations in the measurement conditions during the aging test. E.g. large variations in light intensity during the aging lead to extra work in the form of result analysis that must be performed as a function of light intensity. Based on this study, the amount of five working test cells for each cell group is sufficient when statistical methods are utilized in result analysis. Larger amount of test cells is, however, recommended because this would increase the tolerance of the agint test to unexpected misfortunes, e.g. cell leakages, and increase the reliablity of the results.

As a conclusion of electrolyte purification studies, the purification of electrolyte solvent in cell stability studies is recommended. Additionally, the actual UV exposure of the aged cells seems to be an important factor in interpretation of research works regarding cell stability. Thus, the amount of UV in the spectrum of the aging lamps and the potential UV filters should always be reported in cell stability studies in order to enable the comparison of separate studies. The condenced advices regarding the planning of long-term aging studies are the following ones: tests that overlap in the area of the obtained information should be used, the inevitably varying measurement conditions should be recorded carefully, statistical methods should be applied to the data analysis, and the amount of test cells should be large.

References

[1] A. Goodrich, P. Hacke, Q. Wang, B. Sopori, R. Margolis, T. L. James, and M. Woodhouse, "A wafer-based monocrystalline silicon photovoltaics road map: Utilizing known technology improvement opportunities for further reductions in manufacturing costs," *Solar Energy Materials and Solar Cells*, vol. 114, no. 0, pp. 110 – 135, 2013.

[2] A. Stoppato, "Life cycle assessment of photovoltaic electricity generation," *Energy*, vol. 33, no. 2, pp. 224 – 232, 2008. 19th International Conference on Efficiency, Cost, Optimization, Simulation and Environmental Impact of Energy Systems ECOS 2006.

[3] J. Burschka, N. Pellet, S.-J. Moon, R. Humphry-Baker, P. Gao, M. K. Nazeeruddin, and M. Grätzel, "Sequential deposition as a route to high-performance perovskite-sensitized solar cells," *Nature*, vol. 499, no. 7458, pp. 316–319, 2013.

[4] N. Jiang, T. Sumitomo, T. Lee, A. Pellaroque, O. Bellon, D. Milliken, and H. Desilvestro, "High temperature stability of dye solar cells," *Solar Energy Materials and Solar Cells*, 2013. In press, corrected proof.

[5] M. Toivola, J. Halme, L. Peltokorpi, and P. Lund, "Investigation of temperature and aging effects in nanostructured dye solar cells studied by electrochemical impedance spectroscopy," *International Journal of Photoenergy*, vol. 2009, 2009.

[6] H. Pettersson and T. Gruszecki, "Long-term stability of low-power dye-sensitised solar cells prepared by industrial methods," *Solar Energy Materials and Solar Cells*, vol. 70, no. 2, pp. 203 – 212, 2001.

[7] H. Greijer Agrell, J. Lindgren, and A. Hagfeldt, "Degradation mechanisms in a dye-sensitized solar cell studied by UV-VIS and IR spectroscopy," *Solar Energy*, vol. 75, no. 2, pp. 169 – 180, 2003.

[8] P. Sommeling, M. Späth, H. Smit, N. Bakker, and J. Kroon, "Long-term stability testing of dye-sensitized solar cells," *Journal of Photochemistry and Photobiology A: Chemistry*, vol. 164, no. 1-3, pp. 137–144, 2004. Proceedings of the Dye Solar Cell Osaka ICP-21 Pre-symposium. Dedicated to Professor Shozo Yanagida on the occasion of his retirement.

[9] H.-L. Lu, T. F.-R. Shen, S.-T. Huang, Y.-L. Tung, and T. C.-K. Yang, "The degradation of dye sensitized solar cell in the presence of water isotopes," *Solar Energy Materials and Solar Cells*, vol. 95, no. 7, pp. 1624 – 1629, 2011.

[10] S. Ito, T. N. Murakami, P. Comte, P. Liska, C. Grätzel, M. K. Nazeeruddin, and M. Grätzel, "Fabrication of thin film dye sensitized solar cells with solar to electric power conversion efficiency over 10%," *Thin Solid Films*, vol. 516, no. 14, pp. 4613 – 4619, 2008. 6th International Conference on Coatings on Glass and Plastics (ICCG6)- Advanced Coatings for Large-Area or High-Volume Products.

[11] T. KITAMURA, K. OKADA, H. MATSUI, and N. TANABE, "Durability of dye-sensitized solar cells and modules," *Journal of solar energy engineering*, vol. 132, no. 2, 2010.

[12] European Commission, Joint Research Centre, Institute for Energy, Renewable Energy Unit, "Photovoltaic geographical information system (PVGIS)." http://re.jrc.ec.europa.eu/pvgis/, 09 2013.

[13] M. I. Asghar, K. Miettunen, J. Halme, P. Vahermaa, M. Toivola, K. Aitola, and P. Lund, "Review of stability for advanced dye solar cells," *Energy Environ. Sci.*, vol. 3, pp. 418–426, 2010.

[14] B. Macht, M. Turrion, A. Barkschat, P. Salvador, K. Ellmer, and H. Tributsch, "Patterns of efficiency and degradation in dye sensitization solar cells measured with imaging techniques," *Solar Energy Materials and Solar Cells*, vol. 73, no. 2, pp. 163 – 173, 2002.

[15] K. Zhu, S.-R. Jang, and A. J. Frank, "Effects of water intrusion on the charge-carrier dynamics, performance, and stability of dye-sensitized solar cells," *Energy Environ. Sci.*, vol. 5, pp. 9492–9495, 2012.

[16] J. Halme, P. Vahermaa, K. Miettunen, and P. Lund, "Device physics of dye solar cells," *Advanced Materials*, vol. 22, no. 35, pp. E210–E234, 2010.

[17] K. Hara and H. Arakawa, "Dye-sensitized solar cells," in *Handbook of Photovoltaic Science and Engineering* (S. S. Hegedus and A. Luque, eds.), pp. 663–700, John Wiley & Sons, Ltd, 2005.

[18] R. Kern, N. Van der Burg, G. Chmiel, J. Ferber, G. Hasenhindl, A. Hinsch, R. Kinderman, J. Kroon, A. Meyer, T. Meyer, R. Niepmann, J. van Roosmalen,

C. Schill, P. Sommeling, M. Späth, and I. Uhlendorf, "Long term stability of dye-sensitized solar cells for large area power applications," *Optoelectronics review*, vol. 8, no. 4, pp. 284–288, 2000.

[19] M. Grätzel, "Mesoscopic solar cells for electricity and hydrogen production from sunlight," *Chemistry Letters*, vol. 34, no. 1, pp. 8–13, 2005.

[20] W. J. Lee, E. Ramasamy, D. Y. Lee, and J. S. Song, "Efficient dye-sensitized solar cells with catalytic multiwall carbon nanotube counter electrodes," *ACS Applied Materials & Interfaces*, vol. 1, no. 6, pp. 1145–1149, 2009. PMID: 20355903.

[21] E. Figgemeier and A. Hagfeldt, "Are dye-sensitized nano-structured solar cells stable? an overview of device testing and component analyses," *International Journal of Photoenergy*, vol. 6, no. 3, pp. 127–140, 2004.

[22] N. Papageorgiou, W. Maier, and M. Grätzel, "An iodine/triiodide reduction electrocatalyst for aqueous and organic media," *Journal of the electrochemical Society*, vol. 144, no. 3, pp. 876–884, 1997.

[23] M. Ikegami, J. Suzuki, K. Teshima, M. Kawaraya, and T. Miyasaka, "Improvement in durability of flexible plastic dye-sensitized solar cell modules," *Solar Energy Materials and Solar Cells*, vol. 93, no. 6-7, pp. 836–839, 2009. 17th International Photovoltaic Science and Engineering Conference.

[24] H. T. Nguyen, H. M. Ta, and T. Lund, "Thermal thiocyanate ligand substitution kinetics of the solar cell dye N719 by acetonitrile, 3-methoxypropionitrile, and 4-tert-butylpyridine," *Solar Energy Materials and Solar Cells*, vol. 91, no. 20, pp. 1934 – 1942, 2007.

[25] P. T. Nguyen, R. Degn, H. T. Nguyen, and T. Lund, "Thiocyanate ligand substitution kinetics of the solar cell dye z-907 by 3-methoxypropionitrile and 4-tert-butylpyridine at elevated temperatures," *Solar Energy Materials and Solar Cells*, vol. 93, no. 11, pp. 1939 – 1945, 2009.

[26] A. R. Andersen, J. Halme, T. Lund, M. I. Asghar, P. T. Nguyen, K. Miettunen, E. Kemppainen, and O. Albrektsen, "Charge transport and photocurrent generation characteristics in dye solar cells containing thermally degraded n719 dye molecules," *The Journal of Physical Chemistry C*, vol. 115, no. 31, pp. 15598–15606, 2011.

[27] A. Hauch and A. Georg, "Diffusion in the electrolyte and charge-transfer reaction at the platinum electrode in dye-sensitized solar cells," *Electrochimica Acta*, vol. 46, no. 22, pp. 3457 – 3466, 2001.

[28] M. Toivola, L. Peltokorpi, J. Halme, and P. Lund, "Regenerative effects by temperature variations in dye-sensitized solar cells," *Solar Energy Materials and Solar Cells*, vol. 91, no. 18, pp. 1733 – 1742, 2007.

[29] M. Carnie, D. Bryant, T. Watson, and D. Worsley, "Photocatalytic oxidation of triiodide in uva-exposed dye-sensitized solar cells," *International Journal of Photoenergy*, vol. 2012, 2012.

[30] M. I. Asghar, K. Miettunen, S. Mastroianni, J. Halme, H. Vahlman, and P. Lund, "In situ image processing method to investigate performance and stability of dye solar cells," *Solar Energy*, vol. 86, no. 1, pp. 331 – 338, 2012.

[31] A. Hinsch, J. Kroon, R. Kern, I. Uhlendorf, J. Holzbock, A. Meyer, and J. Ferber, "Long-term stability of dye-sensitised solar cells," *Progress in Photovoltaics: Research and Applications*, vol. 9, no. 6, pp. 425–438, 2001.

[32] C. Law, S. C. Pathirana, X. Li, A. Y. Anderson, P. R. F. Barnes, A. Listorti, T. H. Ghaddar, and B. C. O'Regan, "Water-based electrolytes for dye-sensitized solar cells," *Advanced Materials*, vol. 22, no. 40, pp. 4505–4509, 2010.

[33] J. Nelson and M. Ratner, *The physics of solar cells.* Imperial College Press, 2004.

[34] R. Budhiraja, *Separation chemistry.* New Age International (P) Limited, Publishers, 2004.

[35] R. Anderson, D. Bendell, and P. Groundwater, *Organic Spectroscopic Analysis.* Royal Society of Chemistry, 2004.

[36] I. V. Chernushevich, A. V. Loboda, and B. A. Thomson, "An introduction to quadrupole–time-of-flight mass spectrometry," *Journal of Mass Spectrometry*, vol. 36, no. 8, pp. 849–865, 2001.

[37] H. Ibach and H. Lüth, *Solid-state physics: an introduction to principles of material science.* Springer, Berlin, 2nd ed., 2003.

[38] I. Asghar, S. Kaukonen, L. Antila, J. Halme, E. Rikkinen, P. Lund, and J. Korppi-Tommola, "Using characteristic raman spectra to improve understanding of stability of dye solar cells," September 2013. to be submitted.

[39] K. Miettunen, I. Asghar, S. Mastroianni, J. Halme, P. R. Barnes, E. Rikkinen, B. C. OŔegan, and P. Lund, "Effect of molecular filtering and electrolyte composition on the spatial variation in performance of dye solar cells," *Journal of Electroanalytical Chemistry*, vol. 664, pp. 63–72, 2012.

[40] D. F. Shriver, *The Manipulation of Air Sensitive Compounds*, vol. 1969. McGraw-Hill: New York, 2nd ed., required.

[41] D. S. McGuinness, W. Mueller, P. Wasserscheid, K. J. Cavell, B. W. Skelton, A. H. White, and U. Englert, "Nickel(ii) heterocyclic carbene complexes as catalysts for olefin dimerization in an imidazolium chloroaluminate ionic liquid," *Organometallics*, vol. 21, no. 1, pp. 175–181, 2002.

[42] M. K. Nazeeruddin, S. M. Zakeeruddin, R. Humphry-Baker, M. Jirousek, P. Liska, N. Vlachopoulos, V. Shklover, C.-H. Fischer, and M. Grätzel, "Acid-base equilibria of (2,2́-bipyridyl-4,4́-dicarboxylic acid)ruthenium(ii) complexes and the effect of protonation on charge-transfer sensitization of nanocrystalline titania," *Inorganic Chemistry*, vol. 38, no. 26, pp. 6298–6305, 1999.

[43] A. Derome, *Modern NMR techniques for chemistry research*. Pergamon, Jan 1987.

[44] S. Ito, P. Liska, P. Comte, R. Charvet, P. Pechy, U. Bach, L. Schmidt-Mende, S. M. Zakeeruddin, A. Kay, M. K. Nazeeruddin, and M. Grätzel, "Control of dark current in photoelectrochemical (tio2/i–i3-) and dye-sensitized solar cells," *Chem. Commun.*, pp. 4351–4353, 2005.

[45] A. Tiihonen, "Preparation of dye solar cell aging test unit," Bachelor's thesis, Aalto University, Faculty of Information and Natural Sciences, Degree programme in Engineering Physics and Mathematics, 2011.

[46] S. M. Ross, "Peirceś criterion for the elimination of suspect experimental data," *Journal of Engineering Technology*, vol. 20, no. 2, pp. 38–41, 2003.

[47] I. Mellin, *Todennäköisyyslaskenta*. Teknillinen korkeakoulu, 2006.

[48] "Documentation (polyfit)." http://www.mathworks.se/help/matlab/ref/polyfit.html, 09 2013.

[49] "Documentation (polyconf)." http://www.mathworks.se/help/matlab/ref/polyconf.html, 09 2013.

[50] C. Wu, Y. Gong, S. Han, T. Jin, B. Chi, J. Pu, and L. Jian, "Electrochemical characterization of a novel iodine-free electrolyte for dye-sensitized solar cell," *Electrochimica Acta*, vol. 71, no. 0, pp. 33 – 38, 2012.

[51] P. T. Nguyen, B. X. T. Lam, A. R. Andersen, P. E. Hansen, and T. Lund, "Photovoltaic performance and characteristics of dye-sensitized solar cells prepared with the n719 thermal degradation products [ru(lh)2(ncs)(4-tert-butylpyridine)][n(bu)4] and [ru(lh)2(ncs)(1-methylbenzimidazole)][n(bu)4]," *European Journal of Inorganic Chemistry*, vol. 2011, no. 16, pp. 2533–2539, 2011.

[52] A. G. Kontos, T. Stergiopoulos, V. Likodimos, D. Milliken, H. Desilvesto, G. Tulloch, and P. Falaras, "Long-term thermal stability of liquid dye solar cells," *The Journal of Physical Chemistry C*, vol. 117, no. 17, pp. 8636–8646, 2013.

[53] K. Miettunen, X. Ruan, T. Saukkonen, J. Halme, M. Toivola, H. Guangsheng, and P. Lund, "Stability of dye solar cells with photoelectrode on metal substrates," *Journal of The Electrochemical Society*, vol. 157, no. 6, pp. B814–B819, 2010.

[54] K. Miettunen, I. Asghar, X. Ruan, J. Halme, T. Saukkonen, and P. Lund, "Stabilization of metal counter electrodes for dye solar cells," *Journal of Electroanalytical Chemistry*, vol. 653, no. 1-2, pp. 93–99, 2011.

[55] K. Miettunen, T. Saukkonen, X. Li, C. Law, Y. K. Sheng, J. Halme, A. Tiihonen, P. R. F. Barnes, T. Ghaddar, I. Asghar, P. Lund, and B. C. OŔegan, "Do counter electrodes on metal substrates work with cobalt complex based electrolyte in dye sensitized solar cells?," *Journal of The Electrochemical Society*, vol. 160, no. 2, pp. H132–H137, 2013.

[56] K. Miettunen, "Loss mechanisms and optimization of dye-sensitized solar cells deposited on stainless steel substrates," Master's thesis, Helsinki University of Technology, Department of Engineering Physics and Mathematics, 2006.

A Relative IV data during the aging

IV aging data that has been measured with SCATU for all the aged cells. Data of cell A4 has been left out because the measurement channel was broken and data was erroneous.

In SCATU, light intensity varies during the aging test because of lamp aging and breakdowns. These variations are visible in the data as small variations in short circuit current, fill factor and efficiency. The variations have already been partly compensated by dividing the cell current by the actual relative light intensity of the cell.

Additionally, it must be mentioned that IV results of solar simulator and SCATU vary slightly. Variations exist because of two reasons. Firstly, SCATU light intensity differs from solar simulator light intensity, which is very close to 1 sun. The already mentioned simple light intensity compensation by dividing the current by relative light intensity does not rectify fill factor of the cell, and thus efficiency is a bit different measured with SCATU and solar simulator. Secondly, cells are connected directly to the solar simulator but by using a separate cell platform to SCATU. This leads to increased cell resistance in SCATU which decreases the measured efficiency.

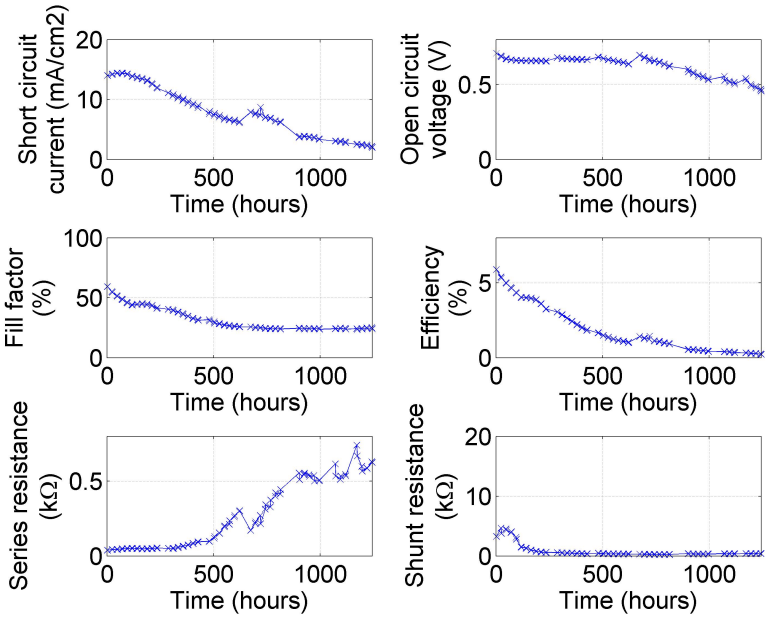

Figure A1: Cell A1

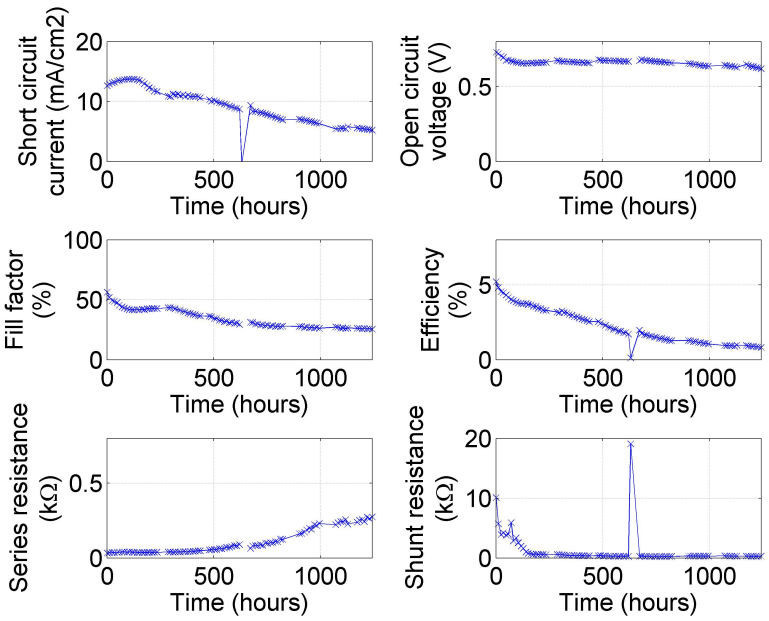

Figure A2: Cell A2

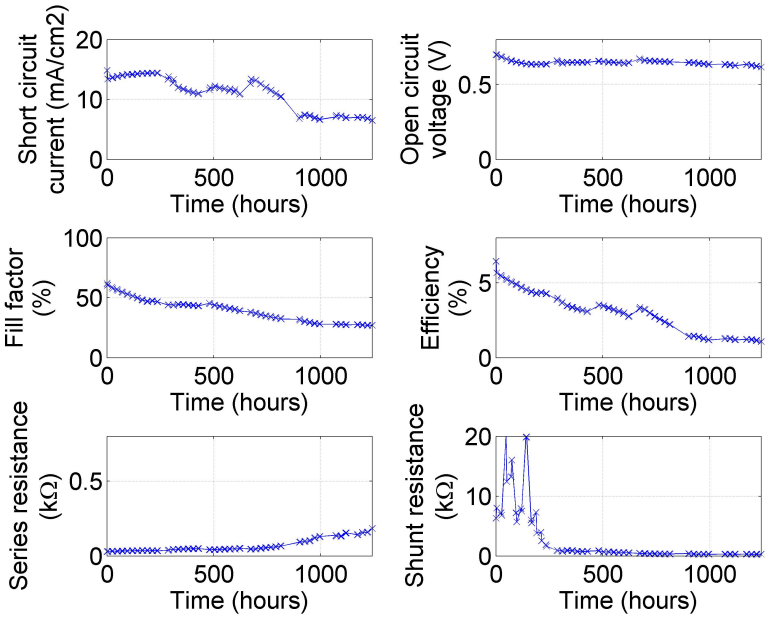

Figure A3: Cell A3

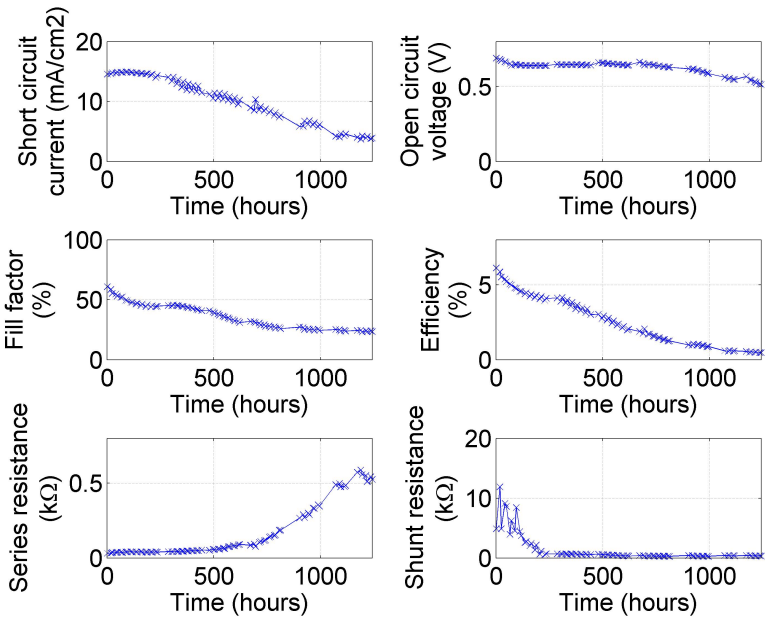

Figure A4: Cell A5

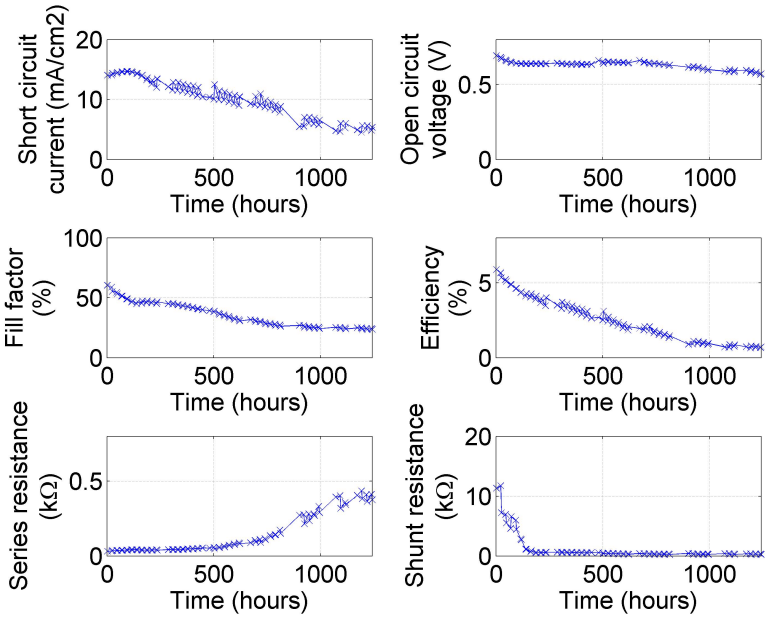

Figure A5: Cell A6

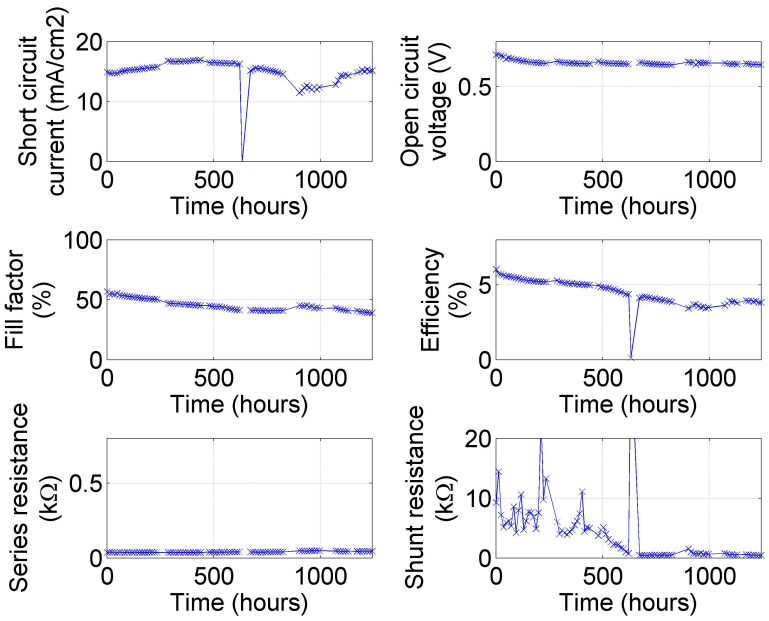

Figure A6: Cell B1

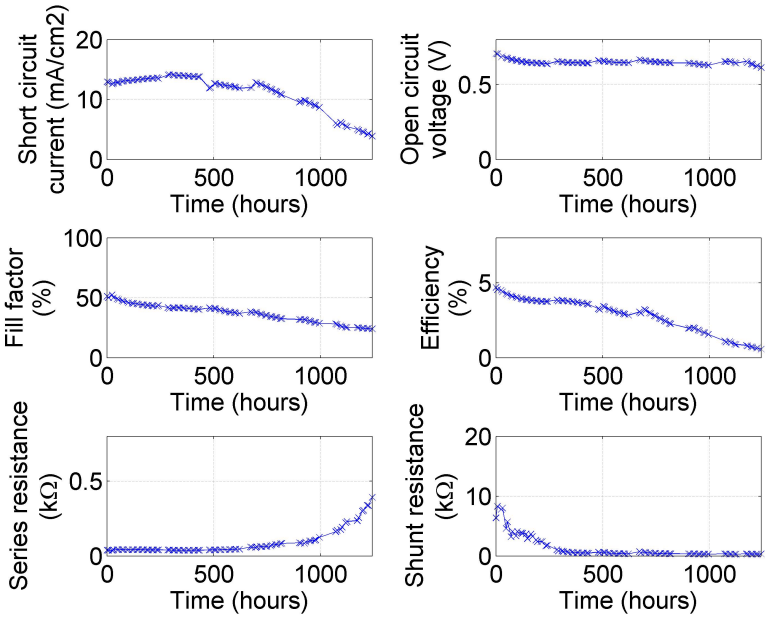

Figure A7: Cell B2

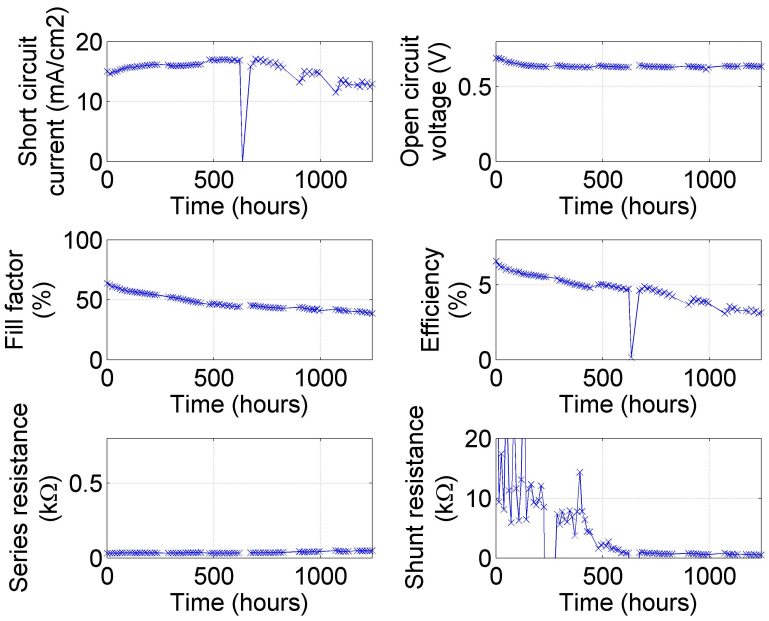

Figure A8: Cell B3

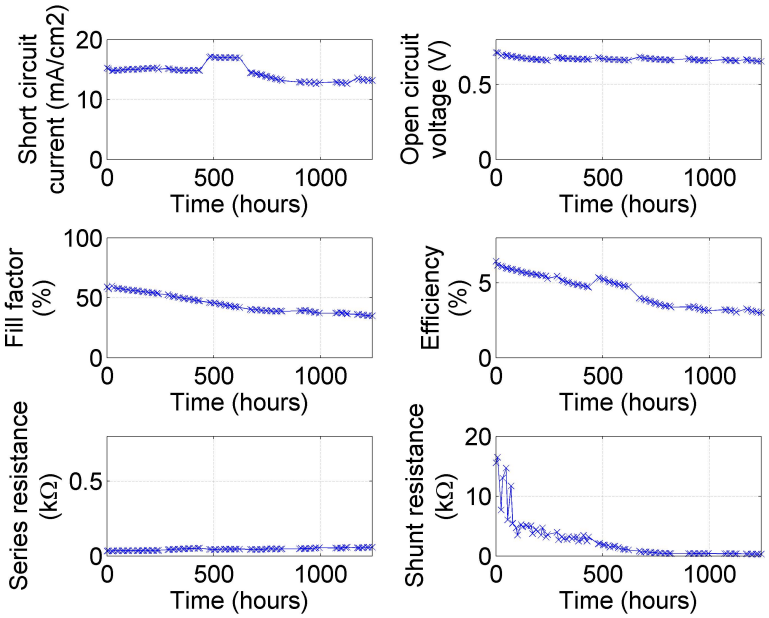

Figure A9: Cell B4

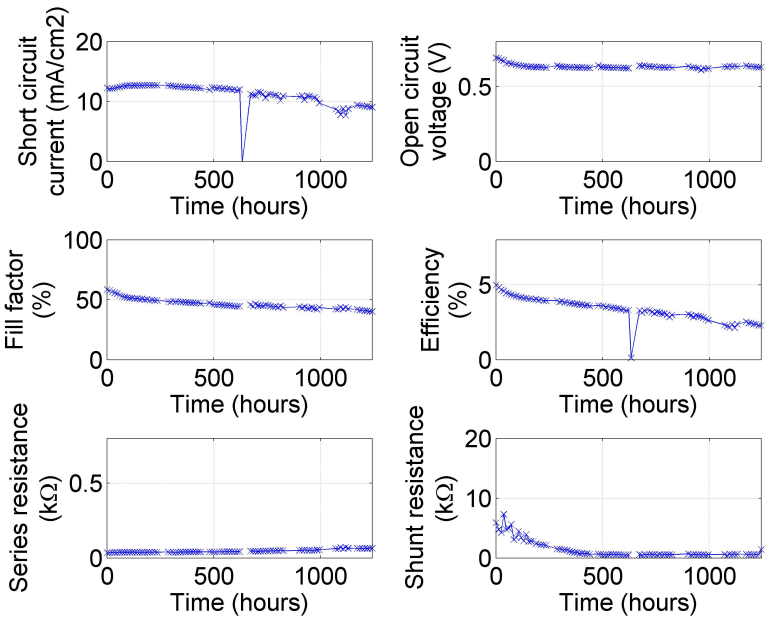

Figure A10: Cell B5

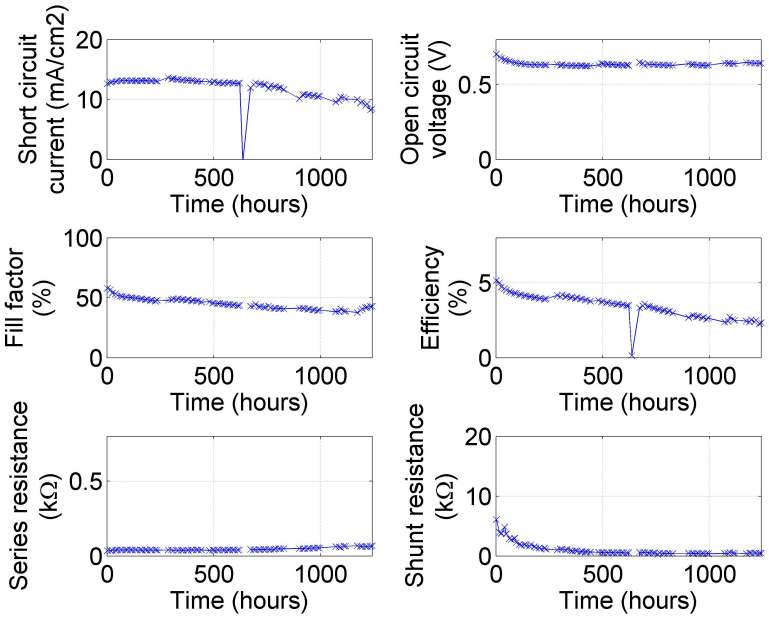

Figure A11: Cell B6

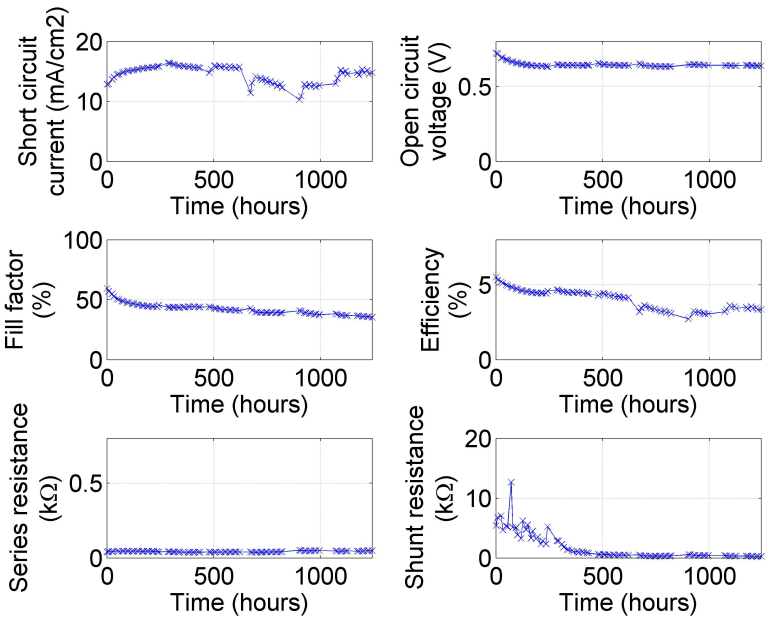

Figure A12: Cell C1

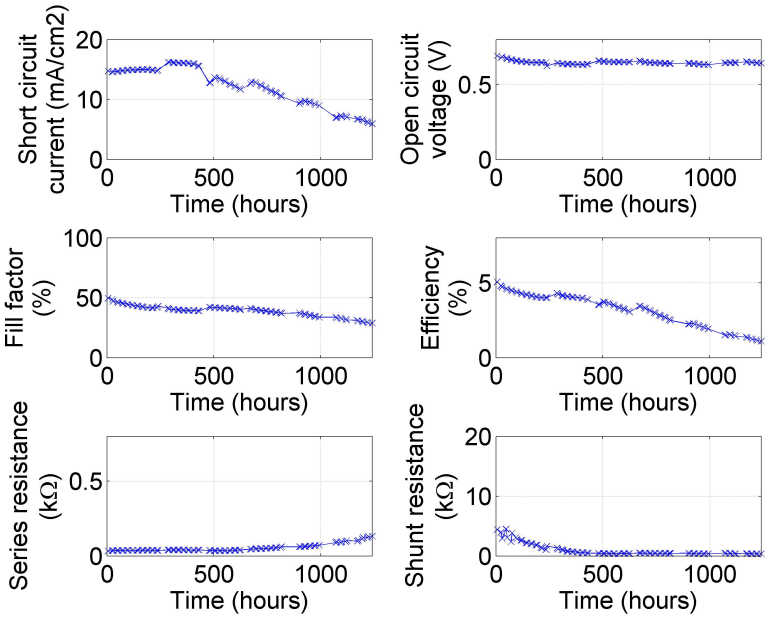

Figure A13: Cell C2

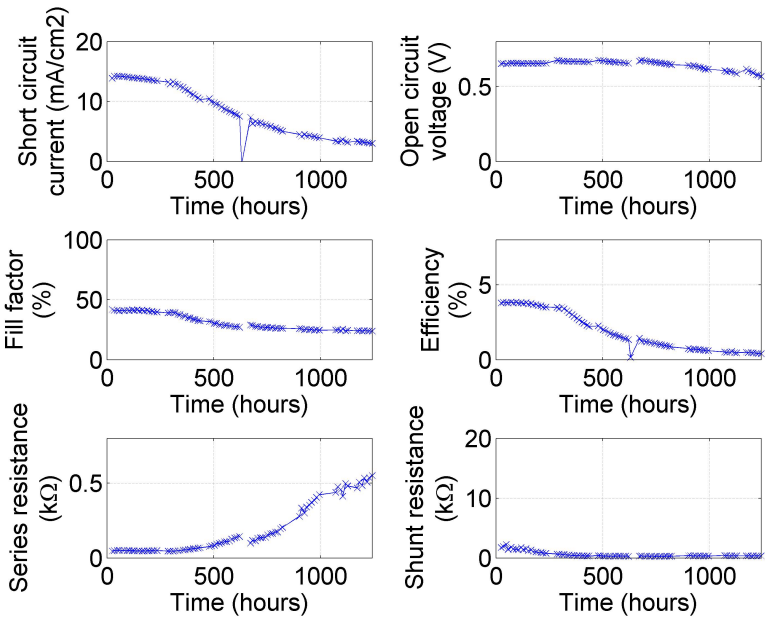

Figure A14: Cell C3

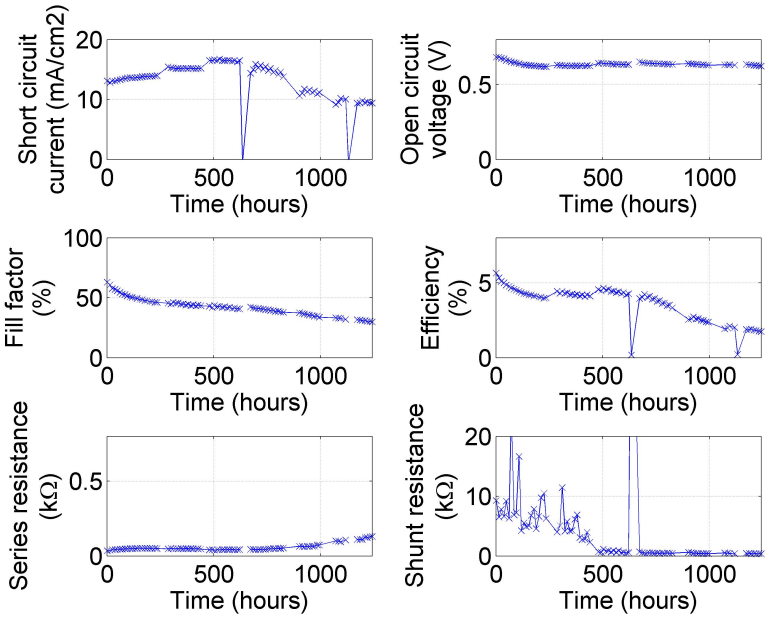

Figure A15: Cell C4

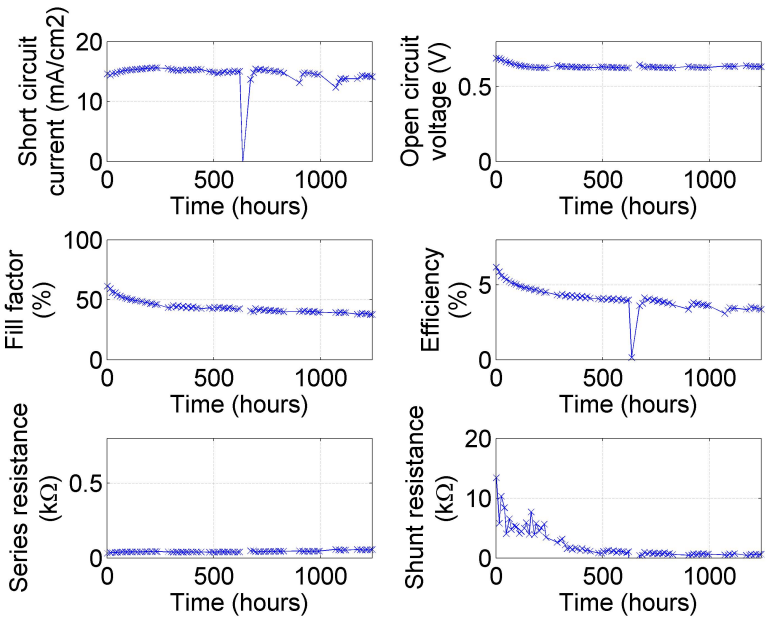

Figure A16: Cell C5

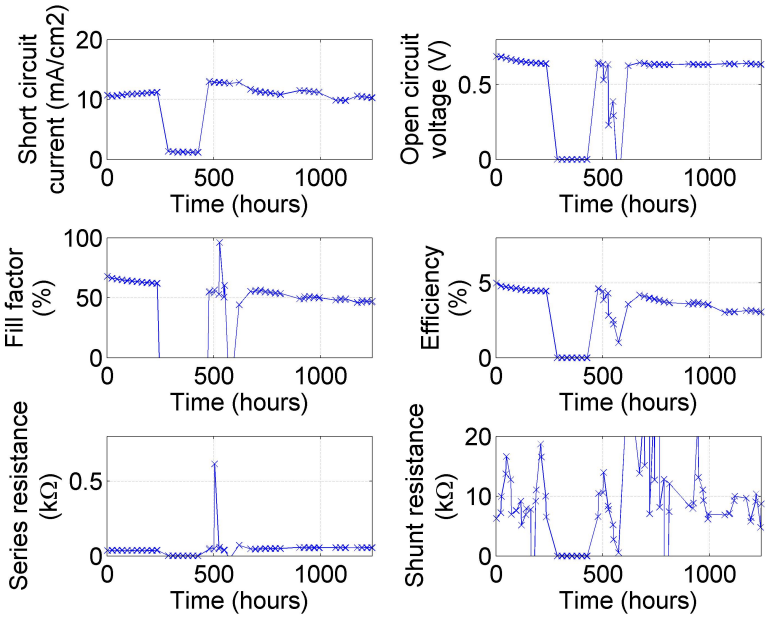

Figure A17: Cell C6

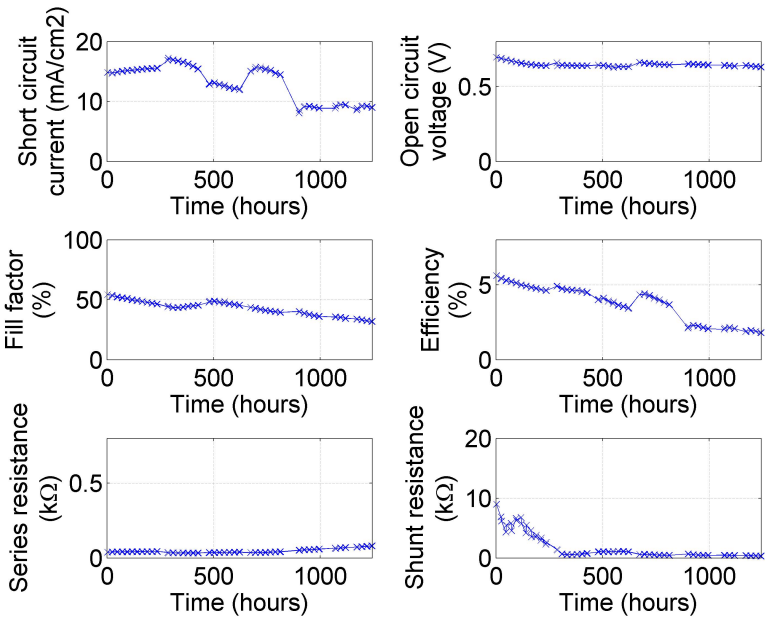

Figure A18: Cell D1

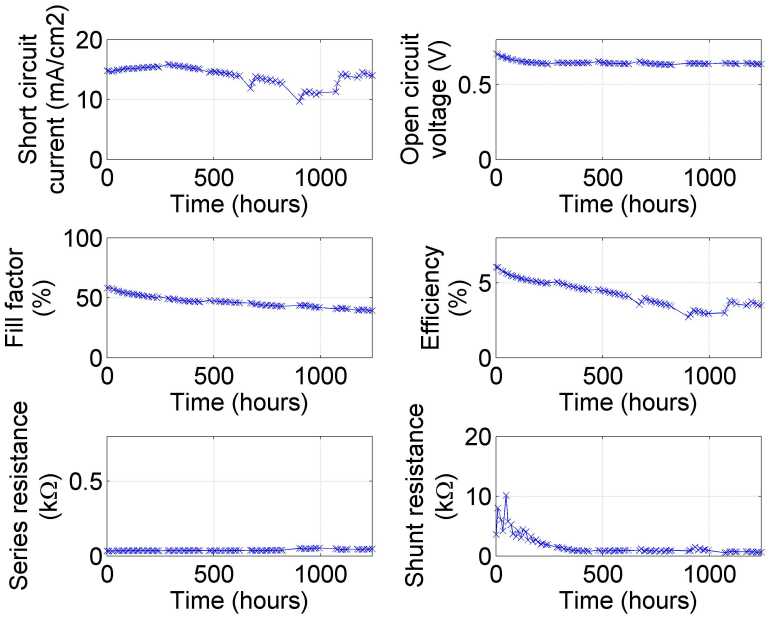

Figure A19: Cell D2

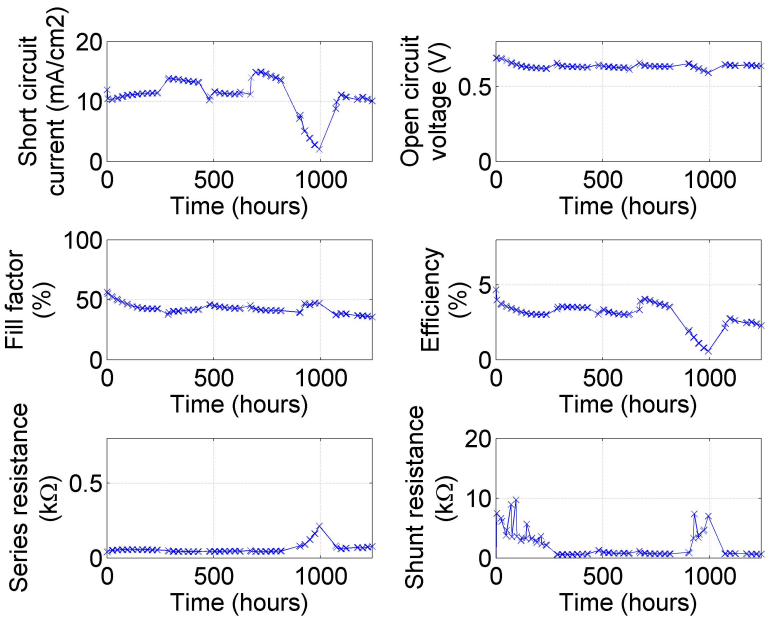

Figure A20: Cell D3

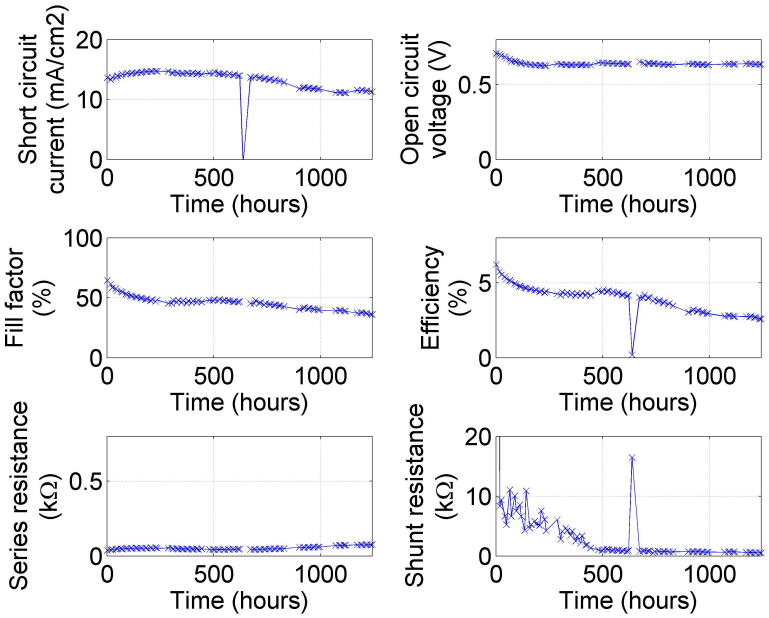

Figure A21: Cell D4

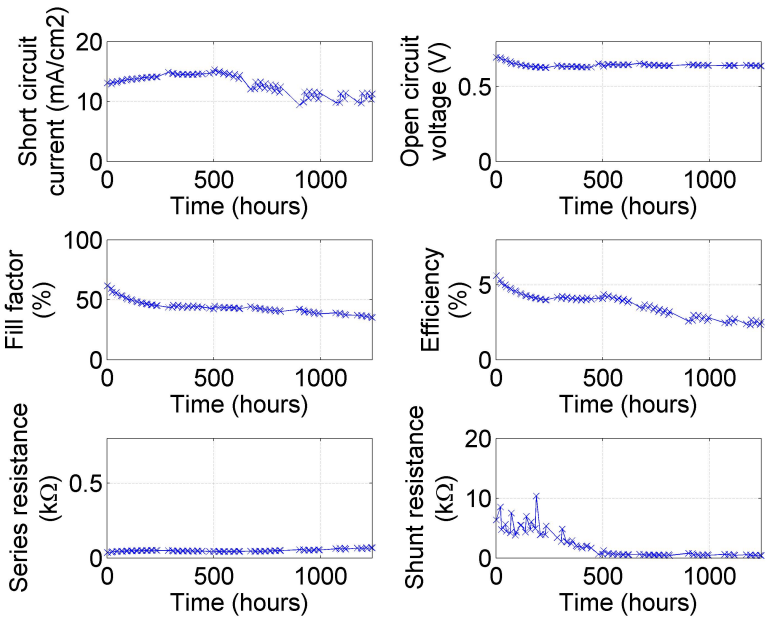

Figure A22: Cell D5

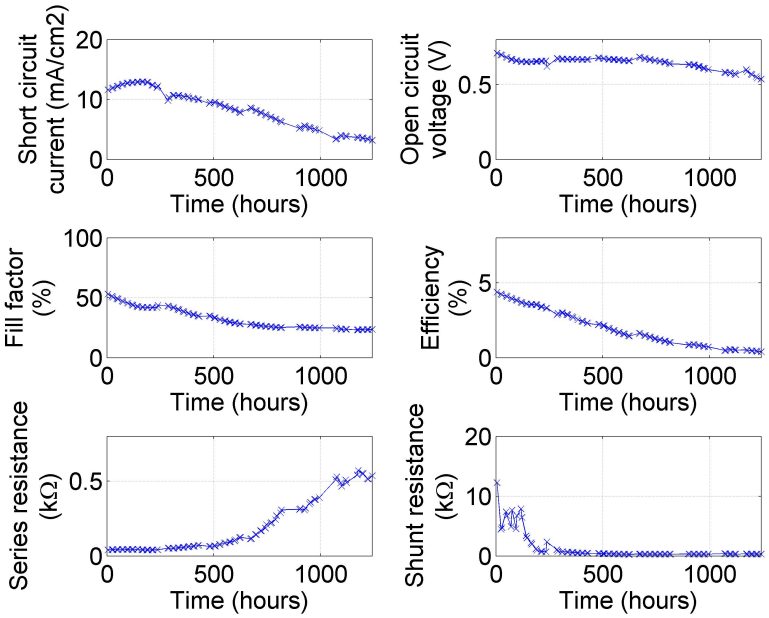

Figure A23: Cell E2

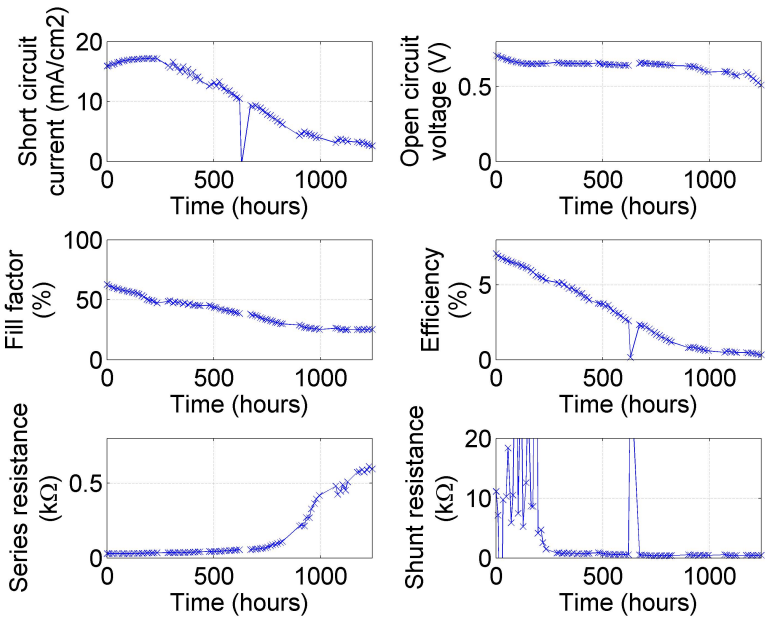

Figure A24: Cell E3

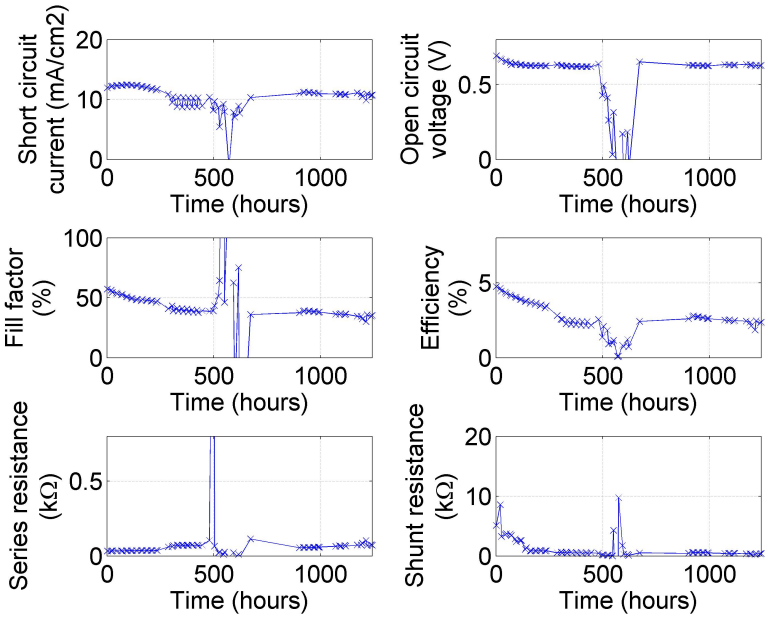

Figure A25: Cell E4

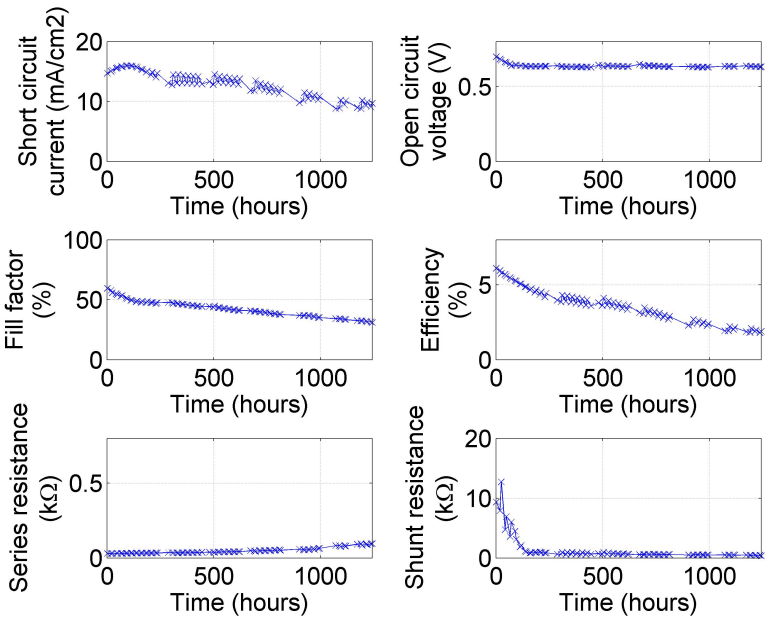

Figure A26: Cell E5

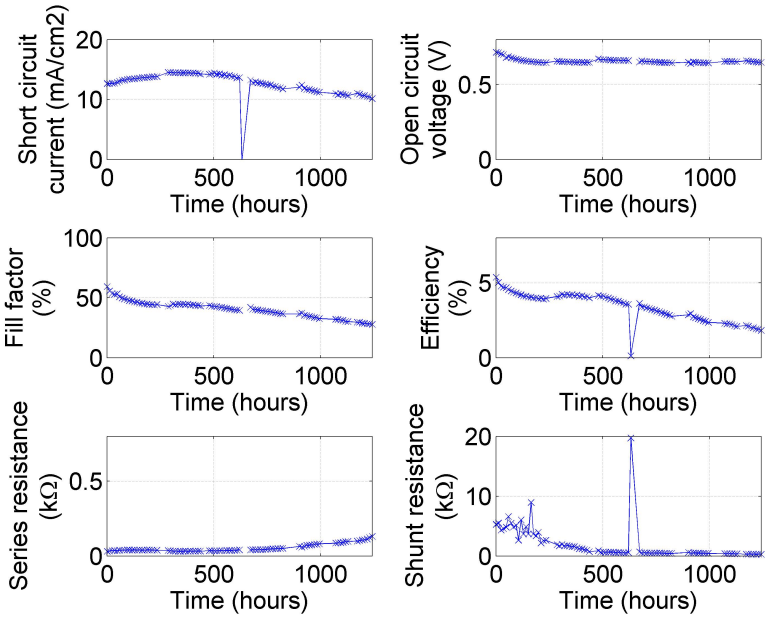

Figure A27: Cell F1

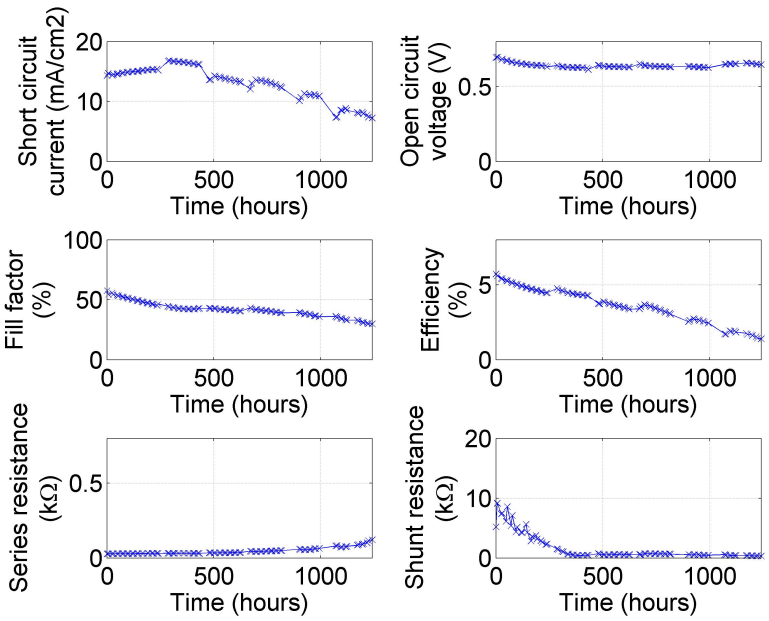

Figure A28: Cell F3

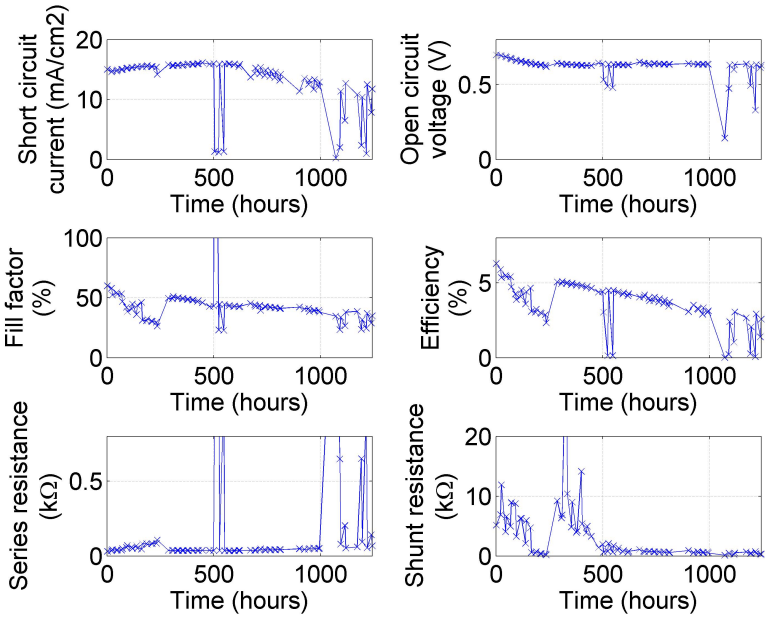

Figure A29: Cell F4

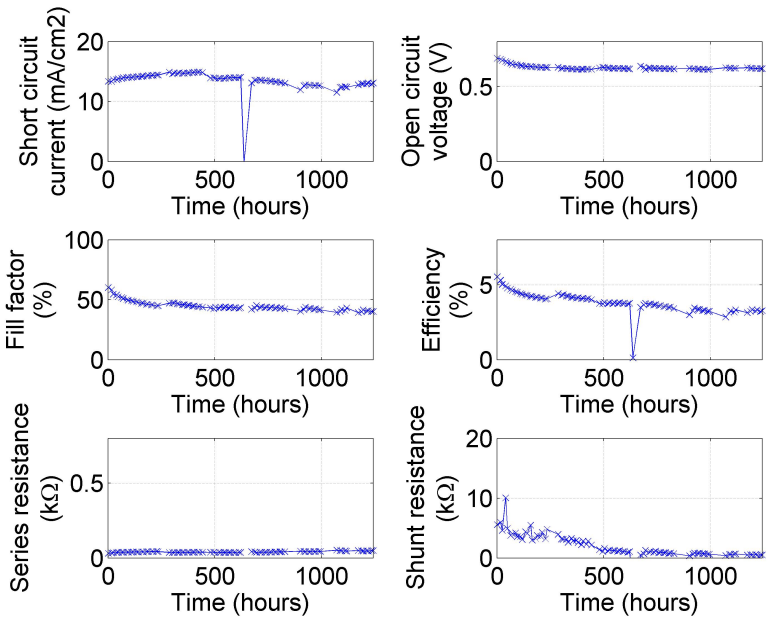

Figure A30: Cell F5

B Illumination spectra of AM 1.5G and light soaking lamps

Figures B1 and B2 illustrate the photon flux of sun and Philips 13117 lamps of the solar simulator, correspondingly, and the photon flux absorbed by TiO_2, as a function of light wavelength. The measured TiO_2 film thickness has been 6,2 μm and bandgap of TiO_2 is assumed to be 3.2 eV (appr. 387 nm). Absorption of TiO_2 below 387 nm has been calculated to correspond to a source current density of 0.049 mA/cm^2 in solar simulator and 0.27 mA/cm^2 in sunlight. The measurement data regarding transmittance of TCO glass and absorption of TiO_2 has been measured by Antti Ruuskanen and calculations have been performed by MSc. Erno Kemppainen from New Energy Technologies Group at Aalto University. Additionally, the amount of UV illumination in solar simulator lamps is approximately one fifth of the UV illumination in AM 1.5G spectrum.

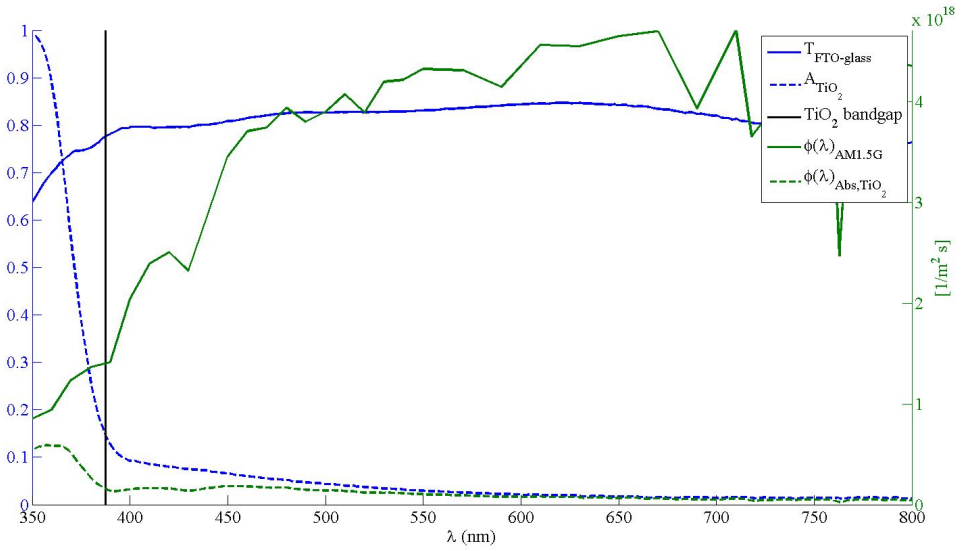

Figure B1: Transmittance of FTO glass ($T_{FTO-glass}$), absorbance of titanium dioxide (A_{TiO_2}), photon flux of sun ($\phi_{AM1.5G}$) and photon flux absorbed by titanium dioxide (ϕ_{Abs,TiO_2}) as a function of light wavelength. Also the bandgap of titanium dioxide is marked to the graph.

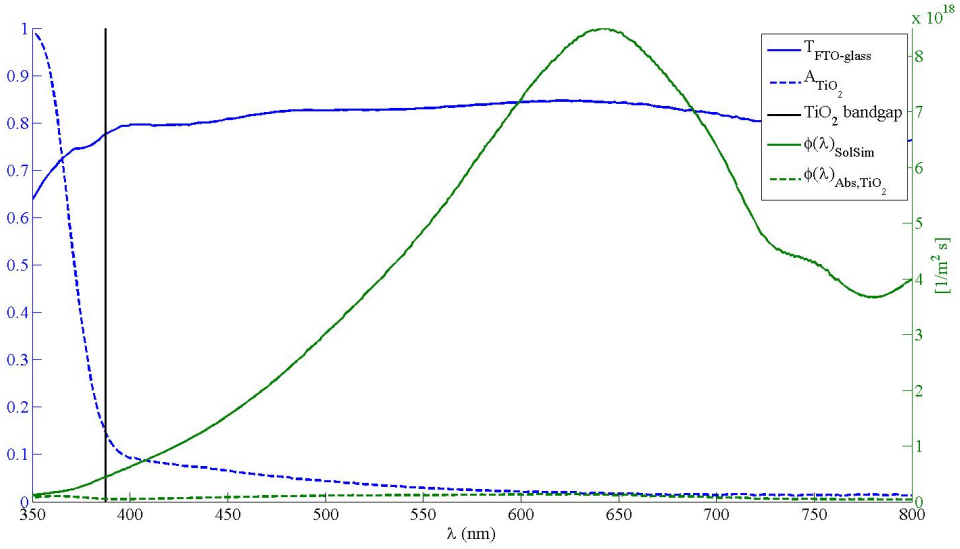

Figure B2: Transmittance of FTO glass ($T_{FTO-glass}$), absorbance of titanium dioxide (A_{TiO_2}), photon flux of solar simulator (ϕ_{SolSim}) and photon flux absorbed by titanium dioxide (ϕ_{Abs,TiO_2}) as a function of light wavelength. Also the bandgap of titanium dioxide is marked to the graph.